BINARY METAL OXIDE AND POLYMER BASED LIQUID REPELLENT SELF-CLEANING SURFACES

ANAND GANESH VENKATESAN

NATIONAL UNIVERSITY OF SINGAPORE

2014

BINARY METAL OXIDE AND POLYMER BASED LIQUID REPELLENT SELF-CLEANING SURFACES

ANAND GANESH VENKATESAN

(B. Eng.) Anna University, Chennai - India.

A THESIS SUBMITTED

FOR THE DEGREE OF DOCTOR OF PHILOSOPHY

DEPARTMENT OF MECHANICAL ENGINEERING

NATIONAL UNIVERSITY OF SINGAPORE

2014

DECLARATION

I hereby declare that this thesis is my original work and it has been written by me in its entirety. I have duly acknowledged all the sources of information which have been used in the thesis.

This thesis has also not been submitted for any degree in any university previously.

Anand Ganesh Venkatesan **10th June 2014**

ACKNOWLEDGEMENTS

In the first place I would like to express my heartfelt gratitude to Professor Seeram Ramakrishna for his supervision, advice, guidance from the very early stage of this research and also for providing me an excellent atmosphere for doing the research. His continuous encouragement in various ways inspired me and enriched my growth as a research student.

It is a pleasure to thank my advisor and friend Professor A. Sreekumaran Nair for his incessant support, patience, encouragement and his willingness to share his thoughts with me, which was very fruitful for shaping up my ideas and research.

I am grateful to Dr. Saifullah for his support and guidance in this research. His knowledge and involvement in research has triggered and nurtured my intellectual maturity that I will benefit from, for a long time to come.

I will forever be thankful to Dr. Sundaramurthy, Dr. Radhakrishnan Sridhar, Dr. Murugan, Dr. Venugopal and Dr. Molamma for teaching me new scientific concepts and polymer chemistry. The knowledge that I imparted from them helped me to formulate new ideas and assisted me to advance further in my research.

Many thanks to Dr. Timothy Michael Walsh for his excellent guidance and valuable advice in scientific discussions and furthermore, spending his time in showing and explaining the entire process involved in the fabrication and installations of huge solar modules.

I would like to dedicate this thesis to my beloved parents and my lovely brother. Without my parents' blessings and moral support, I don't think I could have completed my PhD Studies. Thank you mom and dad!!! I love you and am forever indebted to you for giving me life and your love.

I would like to convey special thanks to my friends Saman, Hemant, Naveen and Rajeswari for their continuous encouragement and support in my experiments and useful technical discussions that helped me to shape my research in a better way.

I gratefully acknowledge PhD Research Scholarship from National University of Singapore for financially supporting my entire PhD Studies.

My time at Singapore was made enjoyable in large part due to my roomies who became a part of my life. I am grateful to all my roomies (Satheesh, Rohit, Suresh, Vinoth, Prasanna and Jagadeesh) for their moral support in difficult times of my life.

Lastly, I would like to thank the Almighty for giving me wonderful parents, teachers and friends. They all made my life very pleasant and enjoyable.

LIST OF PUBLICATIONS

1. Direct electrospraying of lubricating material to fabricate robust and highly transparent omniphobic surfaces.

   V. Anand Ganesh, Saman Safari Dinachali, Radhakrishnan Sridhar, Hemant Kumar Raut, Aleksander Góra, Avinash Baji, A. Sreekumaran Nair and Seeram Ramakrishna. Submitted to *Advanced Materials Interfaces*.

2. Robust Superamphiphobic Film from Electrospun TiO_2 Nanostructures.

   V. Anand Ganesh, Saman Safari Dinachali, A. Sreekumaran Nair and Seeram Ramakrishna. *ACS Applied Materials & Interfaces*, 2013, 5, 1527-1532.

3. Electrospun SiO_2 nanofibers as a template to fabricate a robust and transparent superamphiphobic coating.

   V. Anand Ganesh, Saman Safari Dinachali, Hemant Kumar Raut, Timothy Michael Walsh, A. Sreekumaran Nair and Seeram Ramakrishna. *RSC Advances*, 2013, 3, 3819-3824.

4. Superhydrophobic fluorinated POSS-PVDF-HFP nanocomposite coating on glass by electrospinning.

   V. Anand Ganesh, A. Sreekumaran Nair, Hemant Kumar Raut, Tristan Tsai Yuan Tan, Chaobin He, Jianwei Xu and Seeram Ramakrishna. *Journal of Materials Chemistry*, 2012, 22, 18479-18485.

5. Photo-catalytic Superhydrophilic TiO_2 Coating on Glass by Electrospinning.

   V. Anand Ganesh, A. Sreekumaran Nair, Hemant Kumar Raut, Timothy Michael Walsh and Seeram Ramakrishna. *RSC Advances,* 2012, 2, 2067-2072.

6. A review on self-cleaning coatings.

   V. Anand Ganesh, Hemant Kumar Raut, A. Sreekumaran Nair and Seeram Ramakrishna. *Journal of Materials Chemistry*, 2011, 21, 16304-16322.

7. Anti-reflective coatings: A critical, in-depth review.

   Hemant Kumar Raut, **V. Anand Ganesh,** A. Sreekumaran Nair and Seeram Ramakrishna. *Energy & Environmental Science,* 2011, 4, 3779-3804.

8. Robust and durable polyhedral oligomeric silsesquioxane-based anti-reflective nanostructures with broadband quasi-omnidirectional properties.

   Hemant Kumar Raut, Saman Safari Dinachali, Ai Yu He, **V. Anand Ganesh,** M.S.M. Saifullah, Jaslyn Law and Seeram Ramakrishna. *Energy & Environmental Science,* 2013, 6, 1929-1937.

9. Porous SiO_2 Anti-reflective Coatings on Large-area Substrates by Electrospinning and their Applications to Solar Modules.

   Hemant Kumar Raut, A. Sreekumaran Nair, Saman Safari Dinachali, **V. Anand Ganesh,** Timothy Michael Walsh and Seeram Ramakrishna. *Solar Energy Materials and Solar Cells,* 2013, 11, 9-15.

10. Fabrication of highly uniform and porous MgF_2 anti-reflective coatings by polymer-based sol-gel processing on large-area glass substrates.

    Hemant Kumar Raut, Saman Safari Dinachali, Kwadwo Ansah Antwi, **V. Anand Ganesh** and Seeram Ramakrishna. *Nanotechnology*, 2013, 24, 505201.

TABLE OF CONTENTS

SUMMARY

The self-cleaning effect is related to the contact angle - the angle formed at the three-phase boundary (liquid/solid/vapor) between the surface of a liquid drop deposited on the surface of a solid. The principle behind this technology is derived from the behavior of water droplets on the surface of lotus leaves ("Lotus Leaf Effect"). Self-cleaning coatings are broadly classified into two major categories: hydrophilic and hydrophobic. Both of the categories clean themselves by the action of water. In a hydrophilic coating (water contact angle < 90º), water is made to spread (i.e., 'sheeting' of water) over the surfaces, which carries away the dirt and other impurities, while in the hydrophobic technique (water contact angle > 90º), the water droplets slide and roll over the surfaces thereby cleaning them. However, the hydrophilic coatings using suitable metal oxides have an additional property of chemically breaking down the complex dirt deposits by a sunlight-assisted cleaning mechanism. Both hydrophilic and hydrophobic surfaces involve the application of nanostructures (metal oxide/polymer) to achieve the self-cleaning phenomenon.

Recent reports state that by applying new-age functional self-cleaning coatings on architectural glasses, windows, automobiles and household applications can collectively contribute to a global market share of about 3.8 billion USD by 2017. However, with the growing industrial demands and the constant need for eco-friendliness, the present research in self-cleaning coating technology is primarily focusing on the development of highly durable and sustainable coatings that can reduce the consumption of resources and

environmental impacts. Nonetheless, implementation of conventional coating technologies may lead to increase in design complexity and cost. The scalability of the techniques has also been a challenge.

In this dissertation, simple, cost-effective and scalable nanostructures fabrication techniques, *viz. Electrospinning/Electrospraying*, have been investigated to develop durable, environment friendly, transparent, high performance liquid repellent (Hydrophobic/Superhydrophobic, Amphiphobic/Superamphiphobic coatings) self-cleaning coatings. To achieve this objective, suitable metal oxide and polymer based electrospun/electrosprayed surfaces have been developed and the self-cleaning attributes along with the optical and mechanical properties of the fabricated surfaces were thoroughly studied. Furthermore, the mechanism leading to the surface morphology and surface modifications that are performed to enhance the self-cleaning performance parameters have also been studied and analyzed.

The final outcome of the thesis is to draw a comparison between various liquid repellent (Superhydrophobic, Amphiphobic, Superamphiphobic) self-cleaning surfaces fabricated in this research work and to identify the best suited approach to achieve a robust, transparent, high performance liquid repellent self-cleaning coatings on glass surface by employing electrospinning/electrospraying techniques.

LIST OF TABLES

Chapter 2

Chapter 3

Chapter 4

Chapter 5

Chapter 6

Chapter 7

LIST OF SCHEMES

Chapter 3

Chapter 4

Chapter 5

Chapter 6

LIST OF FIGURES

Chapter 1

Chapter 2

Chapter 3

Chapter 4

Chapter 5

Chapter 6

LIST OF ABBREVIATIONS

CA	Contact Angle
CAH	Contact Angle Hysteresis
SA	Sliding / Slipping Angle
RA	Rolling Angle
PFPE	Perfluoropolyether
FTS	(tridecafluoro-1,1,2,2-tetrahydrooctyl)-1-trichlorosilane
PVDF	Poly(vinylidene fluoride)
POSS	Polyhedral oligomeric silsesquioxanes
PVP	Polyvinylpyrrolidone
PVAc	Polyvinyl acetate
SEM	Scanning Electron Microscopy
AFM	Atomic Force Microscopy
XRD	X-Ray Diffraction
TGA	Thermal Gravimetric Analysis
FTIR	Fourier Transform Infrared Spectroscopy
NMR	Nuclear Magnetic Resonance spectroscopy

Chapter 1

Introduction

1. Introduction

1. Background and motivation

For several years, the glass industry has been trying to solve a problem which affects every building, skyscrapers, automobiles, solar panels and other architectural structures in the world. The problem can be stated as "How to preserve the essential attributes of glass, such as optical transparency and external esthetics without constant and costly maintenance?" In addition to the aesthetic issues, it is a well-known phenomenon that if glass is not cleaned regularly, then over a period of time the glass can weather, which makes it almost impossible to restore its original properties. In extreme circumstances this can lead to the glass needing replacement. The process of cleaning glass is tedious and time consuming. Furthermore, it can also lead to safety and environmental issues.

Several approaches have been made in recent years to fight dirt and dust accumulation on the glasses of solar panels, buildings and automobiles. The invention of self-cleaning coatings was a real breakthrough in the glass sector. Lots of research is underway in self-cleaning technology not only to enhance the quality of the coatings but also to improve durability and optical quality.

The economic benefits achieved because of the application of these innovative functional coatings are phenomenal. Recent reports state that by applying new-age functional self-cleaning coatings on architectural glasses, windows, automobiles and household applications can collectively contribute to a global market share of about 3.8 billion USD by 2017 [1,2]. Furthermore, the convenience in maintaining the aesthetic values of the architectural structures and the cost saving potential offered by the application of self-cleaning coatings resulted in a continuous increase in demand for smart glasses/windows (glasses/windows with functional capabilities like self-cleaning).

Architectural structures and windows manufactured with self-cleaning coated glasses could open up a new dimension in architectural industry and could also lead to a potential market investment. It is projected that the market for smart windows will grow substantially over the next few years, becoming a billion-dollar market by 2015 and then more than doubling by 2018 (Figure 1.1).

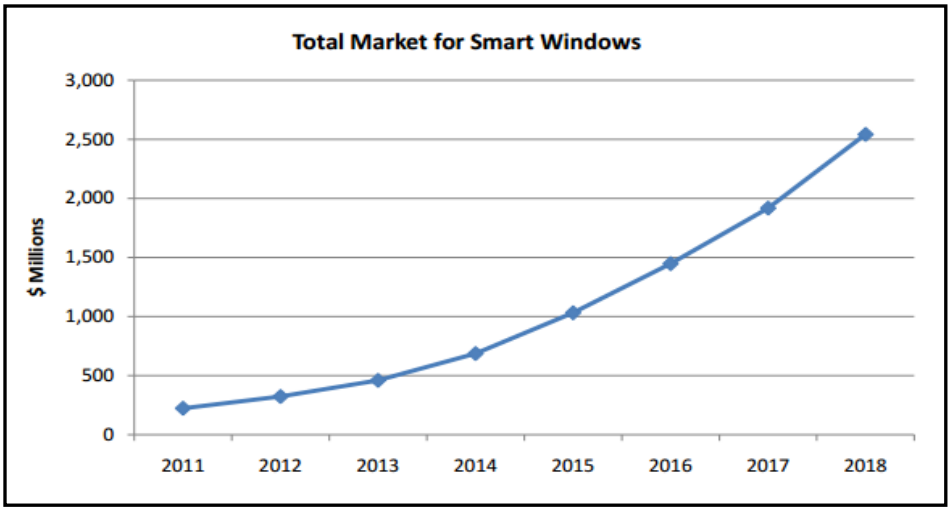

Figure 1.1: Projections on global market for Smart Windows. (Source: "Substantial Growth Anticipated for Smart Windows Market" - A NanoMarkets White Paper)

Hence, we believe that the research on fabrication of cost-effective, transparent and durable self-cleaning coatings on glass will have substantial impact in the growing architectural/automobile coatings and smart windows market.

The phenomenon of self-cleaning is achieved by the deposition of metal oxides/polymer nanostructures on the glass surface. Various conventional techniques like vapor deposition (Chemical vapour deposition/Physical vapour deposition) [3-5], sputtering [6-9], sol-gel [10,11] etc. have been adopted in recent years to fabricate such coatings on a glass surface. However, these techniques face certain limitations. Sol-gel technique has volatile components and therefore it is difficult to control the thickness of the deposited film over large areas. Sputtering, which is basically a batch process, is time consuming as well as costly [12]. CVD is a continuous processing method in which precursor compounds in the gas phase react and deposit on glass surface. Though the process parameters can be accurately controlled, it is still an expensive technique [13]. It is worthwhile adding that all these techniques face the challenges of scalability.

This research work primarily focuses on developing transparent, liquid repellent self-cleaning coatings (*viz.* Hydrophobic/Superhydrophobic coatings, Amphiphobic/Superamphiphobic coatings) on glass surface by employing simple, versatile, cost-effective and scalable nanostructures' fabrication techniques, *Electrospinning/Electrospraying* [14].

2. Scope and research objective

Although there are extensive research literatures with regard to developing different self-cleaning surfaces, it is relatively sparse with regard to surface durability, adhesion with the glass surface, optical properties and large area applications.

The scope of the thesis is to employ electrospinning/electrospraying techniques as a platform to fabricate liquid repellent self-cleaning surfaces (Hydrophobic/Superhydrophobic, Amphiphobic/Superamphiphobic coatings) on glass substrate with robustness and optical transparency. Furthermore, the thesis also focuses on studying and analyzing the surface morphology and surface modifications that are performed to enhance the self-cleaning performance parameters with good optical properties.

The specific objectives of this research are as follows:

- Investigate binary metal oxides and polymer based material systems that are suitable for the fabrication of liquid repellent self-cleaning surfaces by electrospinning/electrospraying.
- Fabricate highly robust and transparent self-cleaning surfaces on glass substrate by electrospinning/electrospraying techniques and analyze their optical properties and self-cleaning capabilities.
- Experimentally investigate the adhesion and mechanical durability of the coatings on glass substrate and look for improvement in performance by adopting surface modification approaches.

3. Dissertation outline

- In Chapter 2, a comprehensive literature study on diverse materials and techniques that are employed to fabricate different types of self-cleaning coatings are discussed. Furthermore, this chapter also talks about numerous functions and potential applications of self-cleaning coatings.
- In Chapter 3, a transparent superhydrophobic coating on glass substrate is produced by electrospinning of fluorinated POSS-PVDF-HFP (POSS - Polyhedral oligomeric silsesquioxanes; PVDF-HFP - Poly(vinylidene fluoride-co-hexafluoro propylene)) nanocomposites. The fabricated superhydrophobic surface exhibited continuous, uniform non-beaded nanofibers with very high water contact angle (WCA > 155º) and low sliding angle (SA < 5º).
- In Chapter 4, electrospraying approach has been employed to fabricate robust, highly transparent and slippery amphiphobic surface using lubricating material (PFPE, Perfluoropolyether). The transmittance of the coating was around 91% and the surface contact angles achieved using conc. NaOH (sodium hydroxide, γ = 85 mN/m), water (γ = 72.1 mN/m), conc. H_2SO_4 (sulfuric acid, γ = 55.1 mN/m), and acetone (γ = 23.1 mN/m) were measured to be 119º, 116º, 99.5º and 40.8º, respectively.

- Chapter 5 elucidates a simple and scalable procedure to fabricate robust superamphiphobic surface on glass substrate from electrospun porous rice shaped TiO_2 nanostructures. The surface contact angle achieved using

water (γ = 72.1 mN/m) and hexadecane (γ = 27.5 mN/m) were 166º ± 0.9 and 138.5º ± 1, respectively. The contact angle hysteresis for a droplet of water and hexadecane were measured to be 2º and 12º, respectively.

- Chapter 6 will discuss about how electrospun nanofibers can be used as a template to develop a robust and transparent superamphiphobic coatings on glass. The template is produced using SiO_2 nanofibers and the fabricated surface exhibited very high surface contact angles (161º and 146.5º) for water (γ = 72.1 mN/m) and hexadecane (γ = 27.5 mN/m), respectively.

- The dissertation closes with Chapter 7 in which conclusions of the research findings, ideas and recommendations for future research are discussed.

4. Key research contributions

- It is extremely difficult to achieve a stable, homogenous coating of lubricating materials (Example: PFPE) on a smooth/flat surface due to the poor adhesion of the lubricating material with the surface (glass/silicon). In this research, we have devised a new chemical approach to fabricate a smooth, stable, homogenous coating of PFPE on a flat substrate. The fabricated coating is robust and highly transparent and exhibited exceptional amphiphobic property. (Kindly refer Chapter 4)
- In this research, we have formulated a novel chemical approach to develop robust and transparent binary metal oxide based superamphiphobic coatings without implementing any complex surface designs, surface over hangs and re-entrant geometry. (Kindly refer Chapter 5 and 6)

Chapter 2

Literature review

2. Literature review on Self-cleaning coatings

1. Introduction

Many technologies existing in today's world have been derived from nature. Self-cleaning technology is one amongst them. Many surfaces in nature exhibit self-cleaning properties. The wings of butterflies [15] and the leaves of plants, such as cabbage and lotus, are a few examples. Because of the extensive range of applications, from window glass cleaning, solar panel cleaning and cements to textiles, this technology received a great deal of attention during the late 20^{th} century and now numerous research works are going on around the world to develop highly efficient and durable self-cleaning surfaces with enhanced optical properties. Apart from the wide range of applications, this technology also offers various benefits, which include reduction in the maintenance cost, elimination of manual effort and also reduction in the time spent in cleaning work.

Self-cleaning coatings are broadly classified into two major categories: hydrophilic and hydrophobic. Both of the categories clean themselves by the action of water. In a hydrophilic coating, the water is made to spread (sheeting of water) over the surfaces, which carries away the dirt and other impurities, whereas in the hydrophobic technique, the water droplets slide and roll over the surfaces thereby cleaning them. However, the hydrophilic coatings using suitable metal oxides have an additional property of chemically breaking down the complex dirt

deposits by sunlight-assisted cleaning mechanism. The literature review will discuss the materials, processes, mechanisms and characterization involved in the self-cleaning coatings. Furthermore, the review will highlight the challenges still to be met along with recent innovations in this direction.

2. Self-cleaning effect

The self-cleaning phenomenon is related to the surface contact angle. It is the angle formed at the three phase boundary (solid/liquid/vapor) between the surfaces of the liquid drop to the surface of the solid. In general, if the contact angle is < 90º, the solid surface is termed as a hydrophilic surface. When the contact angle (CA) is > 90º, the surface is defined as a hydrophobic surface. Similarly, a surface with a water contact angle approaching zero is classified as superhydrophilic and a surface with a contact angle > 150º is usually categorized as superhydrophobic (Figure 2.1).

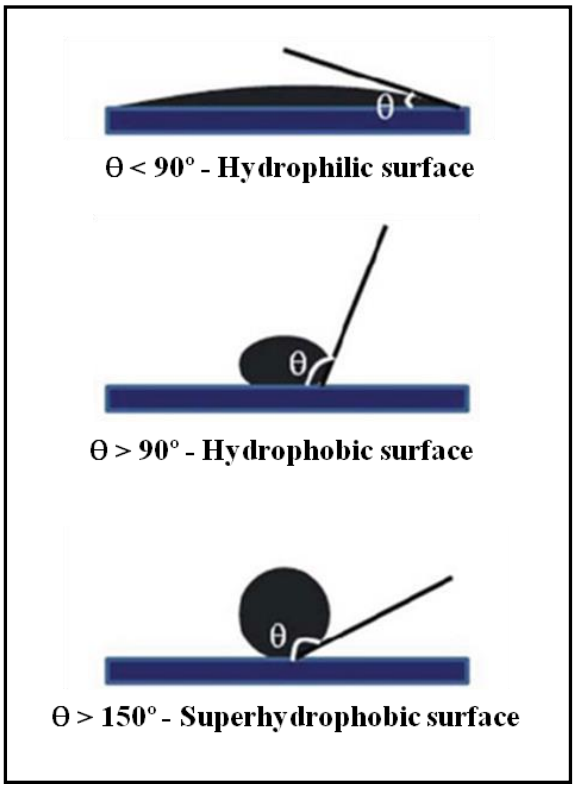

Figure 2.1: A schematic representation of hydrophilic, hydrophobic and superhydrophobic surfaces. (Reproduced with permission from Reference 162).

3. Wetting theories

The theoretical description about the wettability of the surface was first explained using Young's equation. When a water droplet is placed on a flat surface, the contact angle made by the droplet with the surface is given by:

$$Cos\ \theta = \frac{(\gamma_{SV} - \gamma_S)}{\gamma_{LV}} \qquad ------(1)$$

where γ_{SV}, γ_{SL} and γ_{LV} refer to the interfacial tensions of the solid-vapor, solid-liquid, and liquid-vapor phases, respectively.

The contact angle obtained using Young's equation is the result of thermodynamic equilibrium of the free energy at the interface of solid, liquid and vapor [16]. Wenzel modified Young's equation and proposed a new theory with an assumption that the liquid follows the roughness of the surface (Figure 2.2) [17]. At thermodynamic equilibrium, the relationship between the apparent contact angle and the roughness factor of the given surface will be linear and can be expressed as follows.

$$Cos\ \theta_W = r\ Cos\ \theta \qquad ------ (2)$$

where θ_W is the apparent contact angle of the given surface and r represents the roughness factor and θ denotes to Young's angle. Roughness factor (r) is defined as follows.

$$r = \frac{actual\ surface\ area}{projected\ surface\ area} \qquad ------ (3)$$

Hence, for a surface with roughness factor $r > 1$, then by Wenzel's prediction, for a hydrophilic surface: $\theta_W < \theta < 90^o$ and for a hydrophobic surface $\theta_W > \theta > 90^o$. Surface roughness can improve hydrophobicity as well as hydrophilicity depending on the nature of the surface [16]. For surfaces with increased roughness, air pockets get trapped between the roughness causing nanostructures and the water droplet, resulting in the formation of a composite (solid-liquid-vapor) interface, leading to the suspension of water droplet on top of the nanostructures (Cassie-Baxter model; Figure 2.2) [18]. Because of the suspension of water droplet on top of the nanostructures, the apparent contact angle will be the sum of contributions of different phases as shown in equation 4.

$$Cos\ \theta_c = f_1\ Cos\ \theta_1 + f_2\ Cos\ \theta_2 \quad ------ (4)$$

where θ_c is the apparent contact angle, f_1 and f_2 are the surface fraction of phase 1 (solid) and phase 2 (air) , respectively.

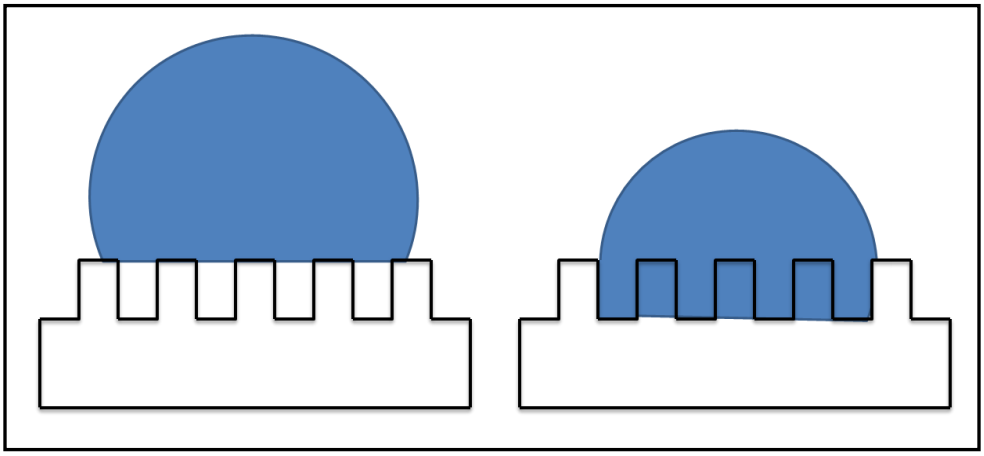

Figure 2.2: Interaction of liquid droplet on a rough surface. Cassie-Baxter's state (left); Wenzel's state (right).

In summary, both the wetting theories can only qualitatively predict the contact angle made on a rough surface. Hence lots of research works are being carried out to understand the concept of surface wettability.

3.1. Roughness parameters

Roughness of the surface cannot be characterized precisely with a single roughness parameter. Instead a set of roughness parameters are defined, *viz*. 2D and 3D roughness parameters. 2D parameters (marked with the letter "R") can characterize surface profiles and are widely used in different applications. However, these parameters may not provide full information on the three-dimensional surfaces. Parameters that can characterize surface topographies are referred as 3D parameters (marked with the letter "S"). Some of the 3D parameters have their 2D counterparts; others are specifically developed for 3D surfaces [16]. Table 2.1 gives the summary of 3D parameters and their 2D counterparts as stated by the ISO 25178. The notations used in the table are explained below.

S_a – arithmetic mean height of the surface; S_q (and its 2D counterpart) – standard deviation of height; R_p and R_v – maximum height of the summit and maximum depth of the valleys, respectively; R_z – peak to peak value and R_{10z} – mean height value of 5 local maxima and local minima.

The ratio between the interfacial and projected area (S_{dr}) gives the additional surface area contributed by the texture. This parameter is widely used in wettability studies as it helps in computing the roughness ratio (roughness factor, *r*) [Equation (1)].

$$r = 1 + S_{dr}/100 \quad \text{----- (1)}$$

Table 2.1: Some typical 2D and 3D roughness parameters.

Symbol	Name	Equations	Description
R_a, S_a	Arithmetic average	$S_a = \frac{1}{MN}\sum_{j=1}^{N}\sum_{i=1}^{M}\lvert\eta(x_i, y_j)\rvert$	Average of |z|
R_q, S_q	Root mean square (RMS) roughness	$S_q = \sqrt{\frac{1}{MN}\sum_{j=1}^{N}\sum_{i=1}^{M}\eta^2(x_i, y_j)}$	Standard deviation of z
R_p, S_p	Maximum height of peaks	$S_p = MAX\,(\eta_p)$	Max z
R_v, S_v	Maximum depth of valleys	$S_v = MIN\,(\eta_v)$	Min z
R_z, S_z	Maximum height of the surface	$S_z = (\lvert S_p\rvert + \lvert S_v\rvert)$	Max z – Min z
R_{10z}, S_{10z}	Ten point height	$S_{10z} = \frac{\sum_{i=1}^{5}\lvert\eta_{pi}\rvert + \sum_{i=1}^{5}\lvert\eta_{vi}\rvert}{5}$	Average of five highest local maxima and five deepest local minima
S_{dr}	Area factor	$S_{dr} = \frac{(Textured\ surface\ area) - (Cross\ sectional\ area)}{Cross\ sectional\ area} * 100\ \%$ $= \frac{\sum_{j=1}^{N-1}\sum_{i=1}^{M-1} A_{i,j} - (M-1)(N-1)\Delta x\Delta y}{(M-1)(N-1)\Delta x\Delta y} * 100\ \%$	Ratio between the interfacial and projected areas

Using these surface roughness parameters, several new surface topographies have been developed recently and wettability studies are being carried out.

4. Hydrophobic and superhydrophobic coatings

4.1. Nature's lead

Nature is the source of inspiration for many researchers around the world to develop aesthetic self-cleaning functional systems. The lotus flower is referred as the symbol of purity in Asian religions. Ward *et al*. [19] first observed the self-cleaning phenomenon and described the fact that, although the lotus leaf rises from muddy water, it is clean and remain untouched by dirt and other pollutants. The mystery behind this mechanism was unfolded after the invention of the scanning electron microscope (SEM) in mid 1960s [20]. Studies conducted using SEM revealed that the surfaces, which appear to be macroscopically smooth, exhibit microscopic roughness on different scale lengths [21-23]. These surfaces, along with the presence of epicuticular wax crystalloids, make the leaves superhydrophobic. These findings led the way for the fabrication of various biomimetic superhydrophobic surfaces inspired by nature. The results of the research work conducted by Guo *et al*. [24] disclosed that there are two major types of surface microstructures in plant leaves with superhydrophobicity: (i) hierarchical micro and nanostructures, (ii) unitary micro-line structures. This revelation paved way for the development of several synthetic methods to mimic the natural superhydrophobic surfaces.

4.1.1. Plant leaves with hierarchical structures

Figure 2.3 shows SEM images of hierarchical structures present in three different plant leaves. Figure 2.3 a and b are SEM images of lotus leaf at low and high magnifications, which show the uniformly textured surface with 3-10 mm sized flanges and valleys tinted with a 700-100 nm sized wax-like material (Figure 2.3 a). A lot of nanorod-like structures with an average diameter of about 50 nm is randomly distributed on the subsurface layer (Figure 2.3 b).

This textured surface helps the lotus leaf to exhibit superhydrophobic property. The water contact angle observed was around 162º (inset of Figure 2.3 b) [24,25]. Figure 2.3 c and d show the SEM images of rice leaf. The top surface of the leaf possess the papillae with an average diameter of about 5-8 mm and they are arranged in one-dimensional order (Figure 2.3 c). The sub layer of the surface consists of innumerable nanopins that are proportionally well distributed to enhance the air trapping mechanism in the surface (Figure 2.3 d). The water contact angle (WCA) exhibited by this surface is 157º (inset of Figure 2.3 d).

Like lotus and rice leaves, taro leaf also shows superhydrophobicity (Figure 2.3 e and f). Compared to the above two plant leaves, taro leaf possesses distinct microstructures (10 mm) that are distributed in their corresponding nest like caves (Figure 2.3 e). A higher magnification SEM image (Figure 2.3 f) shows the presence of harmoniously distributed nanopins on its surface along with the formed microstructure. The WCA observed in this leaf is around 159º (inset of Figure 2.3 f).

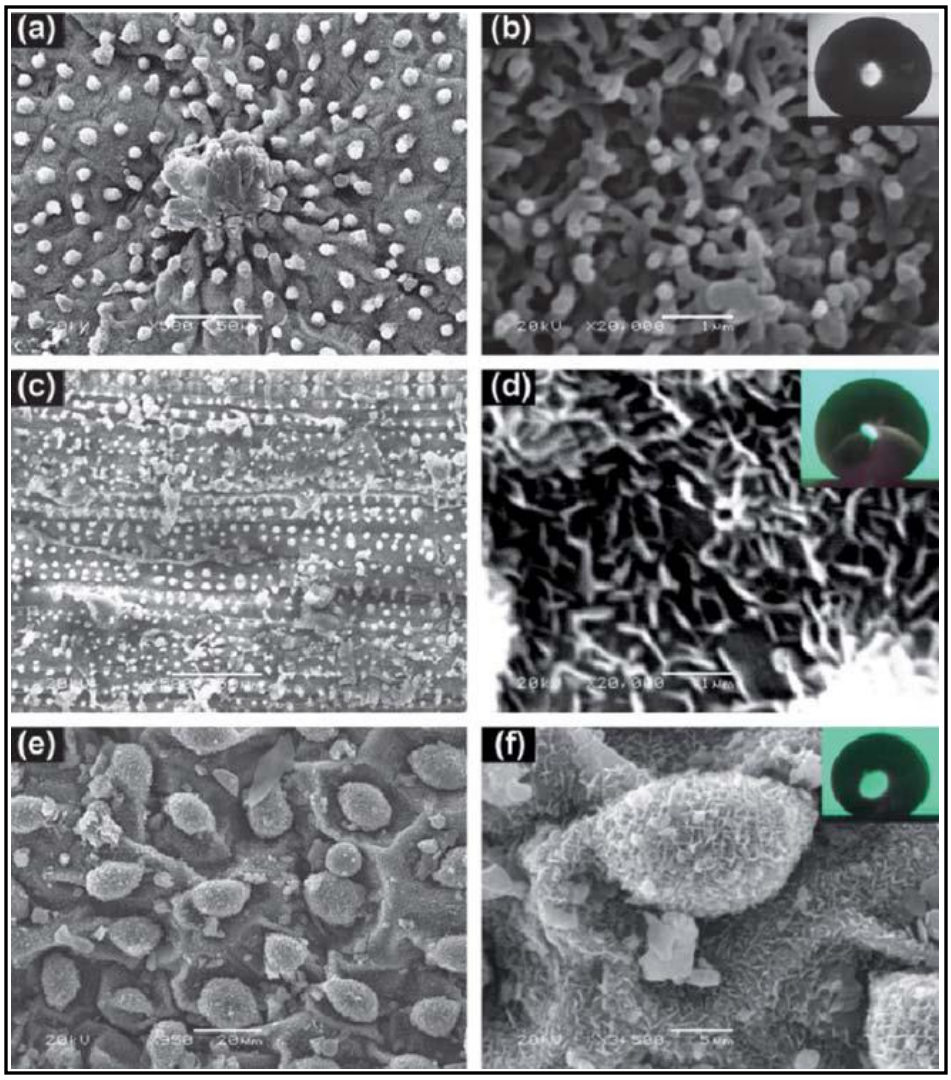

Figure 2.3: SEM images of natural superhydrophobic surfaces with hierarchical structures. (a) and (b) are the SEM images of lotus leaf with low and high magnifications, respectively, and the inset of (b) is a water CA on it with a value of about 162º; (c) and (d) are the SEM images of rice leaf with low and high magnifications, respectively, and the inset of (d) is a water CA on it with a value of about 157º; (e) and (f) are the SEM image of taro leaf with low and high magnifications, respectively, and the inset of (f) is the water CA on it with a value of about 159º. (Reproduced with permission from Reference 24).

4.1.2. Plant leaves with unitary structure

Figure 2.4 shows the SEM images of unitary structures exhibited by different plant leaves. In the rear face of Ramee leaf (Figure 2.4 a), uniformly distributed slick fibers with diameter 1 to 2 μm can be seen forming a unitary structure which is different from the surface with hierarchical structures of the aforementioned plant leaves [24]. This unique structure is also found on the surfaces of Chinese watermelon shown in Figure 2.4 c and d. Surprisingly the surface morphologies of Ramee leaf and Chinese water melon are similar and both exhibits a WCA of ~ 159º. This discovery clearly explains that the hierarchical structure is not the only necessary condition to exhibit superhydrophobicity.

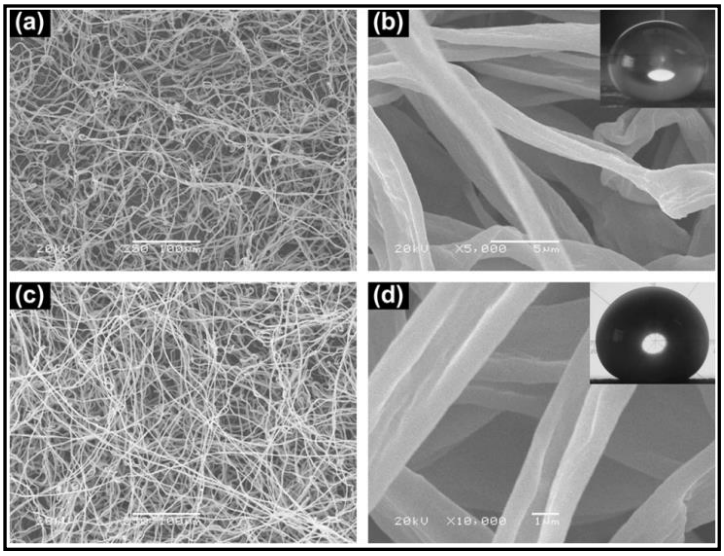

Figure 2.4: SEM images of natural superhydrophobic surfaces with unitary structure. (a) and (b) are the SEM images of Ramee rear face with low and high magnifications, respectively, and the inset of (b) is a water CA on it with a value of about 164º; (c) and (d) are the SEM images of Chinese watermelon surface with low and high magnifications, respectively, and the inset of (d) is the water CA on it with a value of about 159º. (Reproduced with permission from Reference 24).

4.2. Materials and mechanisms to produce hydrophobic and superhydrophobic coatings

Inspired by the superhydrophobic properties exhibited by nature, researchers around the world started working on developing technologies to produce surfaces with extremely low surface energies and also to control the morphology of the surface on a micron and nanometer scale. This idea of controlling surface morphology opens up many possibilities for developing a variety of engineered surfaces. Techniques to produce hydrophobic and superhydrophobic surfaces can be broadly classified into two categories: a) making a rough surface using a low surface energy material; b) modifying a rough surface with a material of low surface energy.

4.2.1. Roughening the surface of low surface energy material

4.2.1.1. Silicones: Polydimethylsiloxane (PDMS) belongs to a group of organosilicon compounds, commonly known as silicones. The intrinsic deformability and hydrophobic properties of PDMS makes it a highly suitable material for producing superhydrophobic surfaces. Various methods are practiced to produce superhydrophobic surfaces using PDMS. For example, Khorasani *et al.* [26] did surface modification on PDMS using a CO_2 pulsed laser as an excitation source to introduce peroxide groups onto the PDMS surface. These peroxides are capable of initiating graft polymerization of 2-hydroxyethyl methacrylate (HEMA) onto the PDMS. The water contact angle (WCA) of the treated PDMS was measured to be 175º. The reason for such an increase in WCA was due to the porosity and chain ordering on the surface of PDMS.

Jin *et al.* [27] used a PDMS elastomer containing micro and nanocomposite structures to produce superhydrophobic surfaces. They employed laser etching to induce roughness on the PDMS surface. The surface produced by this technique exhibited WCA as high as 160º and sliding angle lower than 5º.

4.2.1.2. Fluorocarbons: Fluorinated polymers are attracting lots of interest these days because of their extremely low surface energies. Roughening these polymers will result in superhydrophobic surfaces. Zhang *et al.* [28] achieved superhydrophobicity by stretching a Teflon (polytetrafluoroethylene) film. The superhydrophobic property achieved is due to the presence of fibrous crystals with large fractions of void space on the surface. Morra *et al.* [29] produced a rough surface on Teflon by treating it with oxygen plasma. The WCA obtained by this technique was 168º. Because of the limited solubility, many fluorinated materials have not been used directly but linked with other rough materials to make superhydrophobic surfaces.

4.2.1.3. Organic materials: Although silicones and fluorocarbons were extensively used to produce superhydrophobic surfaces, recent research has shown that hydrophobicity can be obtained using paraffinic hydrocarbons as well.

Lu *et al.* [30] proposed a simple and inexpensive method for forming a superhydrophobic coating using ‘‘low-density polyethylene’’ (LDPE). In this method, a highly porous superhydrophobic surface of polyethylene (PE) was produced by controlling the crystallization time and nucleation rate (Figure 2.5 a). A WCA of about 173º was obtained by this method. Jiang *et al.* [31] showed that

a superhydrophobic film can be obtained by electrostatic spinning and spraying of polystyrene (PS) solution in dimethylformamide (DMF). The surface obtained was composed of porous microparticles and nanofibers (Figure 2.5 b).

Recent research work has shown that alkylketene [32], polycarbonate [33] and polyamide [34] also exhibit superhydrophobic properties.

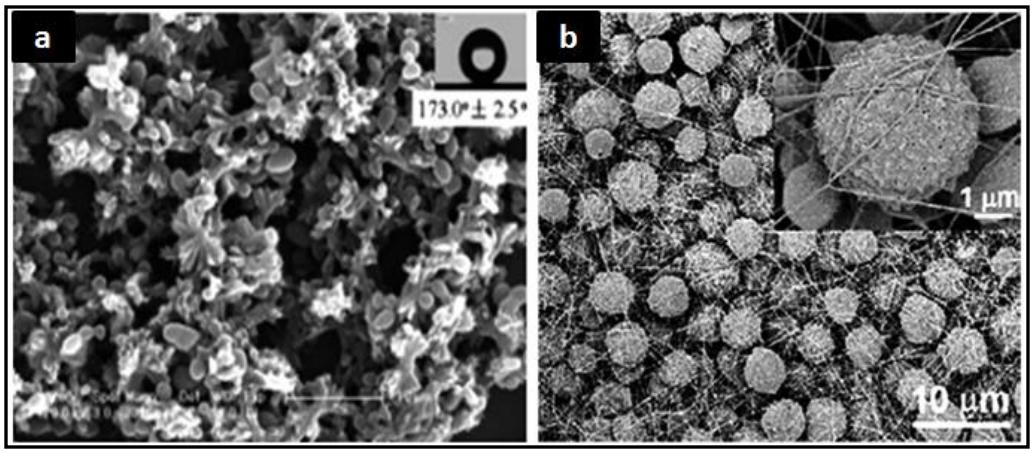

Figure 2.5: (a) SEM image of the flower-like crystal structure of PE. (b) SEM image of the PS surface produced by electrostatic spinning and spraying. (Reproduced with permission from References 30 and 31).

4.2.1.4. Inorganic materials: Superhydrophobic properties have been exhibited by a few inorganic materials as well. Recent research work conducted on oxides such as ZnO and TiO_2 resulted in the production of films with reversibly switchable wettability. Feng *et al.* [35] synthesized ZnO nanorods by a two-step solution method. XRD study showed that the ZnO nanorod films were superhydrophobic due to the low surface energy of the (001) plane of the nanorods on the surface of the film. When the film is exposed to UV radiation, electron-hole pairs were produced resulting in the adsorption of hydroxyl group on the ZnO surface. Consequently, the superhydrophobic property of the film is

converted to superhydrophilic. Dark storage of the UV irradiated film for a week made it superhydrophobic again.

4.2.2. Making a rough surface and modifying the surface with material of low surface energy

This section primarily focuses on various techniques reported in the past few years to fabricate rough surfaces and subsequently modifying the surface chemistry to produce superhydrophobic membranes.

4.2.2.1. Wet chemical reaction and hydrothermal reaction: Wet chemical reaction is a straightforward technique that can effectively control the dimensionality and morphology of the nanostructures (nanoparticles, nanowires and mesoporous inorganics) produced [36-38]. This method was widely used in the fabrication of biomimetic superhydrophobic surfaces on metal substrates like copper, aluminium and steel. Wang *et al*. [39] used chemical composition method to produce a superhydrophobic surface on copper substrate. The substrate was immersed into n-tetradecanoic acid solution for about a week, which resulted in surface modification of the substrate, which then exhibited superhydrophobicity. Qu *et al*. [40] employed a surface roughness technique by etching polycrystalline metals with acidic or basic solution of fluoroalkylsilane. After treating with fluoroalkylsilane, the etched surfaces exhibited superhydrophobicity (Figure 2.6 a and b).

Superhydrophobic surfaces on nickel substrates were created by employing a wet chemical process in which monoalkylphosponic acid reacts with Ni to produce flowery microstructures constituting a continuous slipcover [41].

A stable superhydrophobic surface is produced on a copper substrate by using oxalic acid as a reaction reagent and then chemical modification is done using poly(dimethysiloxane) vinyl terminated (PDMSVT) (Figure 2.6 c) [42].

A layer of interconnected $Cu(OH)_2$ nanowires was generated on a Cu plate by immersing it into the mixture of NaOH and $K_2S_2O_8$ solution. After chemical modification with dodecanoic acid, the surface exhibited superhydrophobicity (Figure 2.6 d) [43]. Liang *et al*. [44] fabricated a biomimetic superhydrophobic surface on magnesium alloy by micro-arc oxidation pre-treatment and chemically modifying the surface with PDMSVT with spin coating.

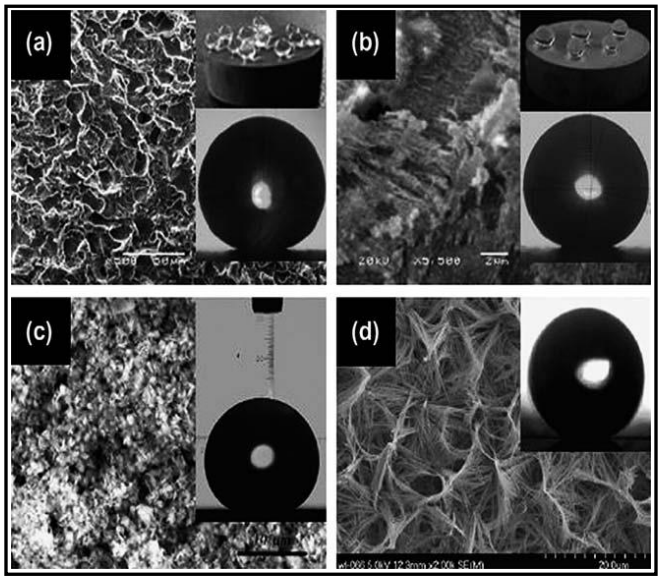

Figure 2.6: SEM images of biomimetic superhydrophobic surfaces fabricated by wet chemical reaction. (a) and (b) SEM images of the etched steel and copper alloy treated with fluoroalkylsilane, respectively, both showing good superhydrophobicity (inset); (c) SEM image of copper immersed in 0.5 wt% oxalic acid for 5-7 days and treated with PDMSVT, showing superhydrophobicity (inset); (d) SEM image of a copper plate immersed in an aqueous solution of 2.0 M NaOH and 0.1 M $K_2S_2O_8$ for 60 min, showing good superhydrophobic properties after dodecanoic acid modification (inset). (Reproduced with permission from References 40, 42 and 43).

The hydrothermal technique is a recently developed method that uses a ‘‘bottom up’’ route in efficiently fabricating functional materials with different patterns and morphologies [45-48]. Nanolamellate structures on titanium were produced by an in-situ hydrothermal synthesis method (Figure 2.7 a) [49]. The obtained superhydrophilic surface is converted to a superhydrophobic surface by chemical modification using PDMSVT (inset of Figure 2.7 a). Zou *et al.* established a new technique in which they used an inorganic precursor route to produce superhydrophobic complex metal oxide monoliths by selective leaching of a self-generated MgO sacrificial template from the sintered two phase composites (Figure 2.7 b) [50]. A superhydrophobic surface with an array of spiral Co_3O_4 nanorods was produced by a hydrothermal method in which $Co(N\text{-}O_3)_2.6H_2O$ is used as a resource under basic conditions (Figure 2.7 c) [51]. In recent years, an array of zinc nanorods exhibiting superhydrophobicity was fabricated due to its potential applications in short-wavelength lasing, gas sensors, catalysts and piezoelectric materials [52-54]. For example, Hou *et al.* synthesized superhydrophobic ZnO nanorod film on a zinc substrate by oxidizing zinc metal and subsequently modifying the surface using n-octadecyl thiol (Figure 2.7 d) [54].

Both these techniques are time saving and scalable. The flexibility and simplicity of these methods help in producing morphologies of reasonable shape and size.

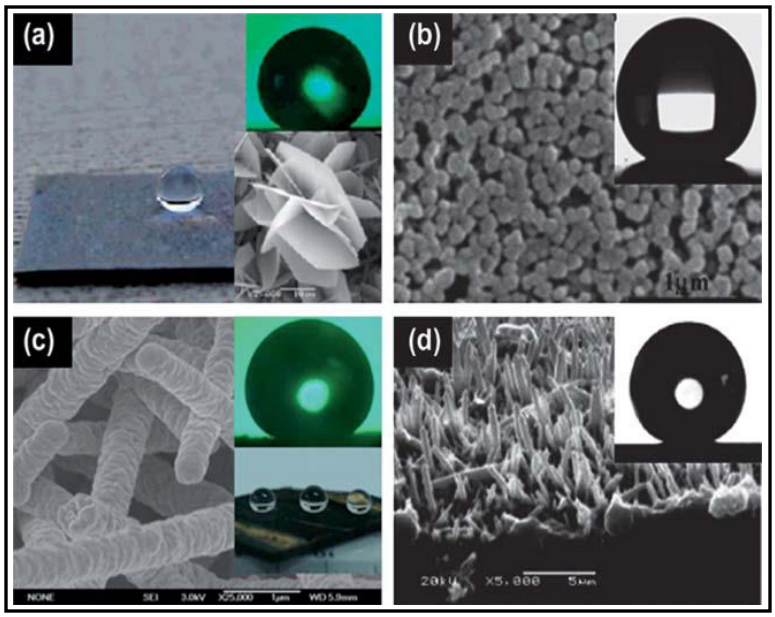

Figure 2.7: The biomimetic superhydrophobic surfaces constructed by hydrothermal reactions. (a) The shape of a water droplet on the surface with nanolamellate structures of $CaTiO_3$ (inset) by using an in situ hydrothermal synthesis on titanium, showing a water CA of about 160º (inset); (b) a typical SEM image of $MgAl_2O_4$ monolith obtained through a novel single-source inorganic precursor route, and after chemical modification with n-octadecanoic acid, the surface shows superhydrophobicity (inset); (c) SEM image of the spiral Co_3O_4 nanorod arrays on a glass slide, and after chemical modification, the surface shows good superhydrophobicity with a water CA of about 162º (inset); (d) SEM image of the prepared ZnO, overview of the cross section on zinc substrate, and after chemical modification, the surface shows superhydrophobic with a water CA of about 153º (inset). (Reproduced with permission from References 49, 50, 51 and 54).

4.2.2.2. Electrochemical deposition: Electrochemical deposition is widely used to develop biomimetic superhydrophobic surfaces since it is a versatile technique to prepare microscale and nanoscale structures [55-60]. Larmour *et al*. [61] employed a galvanic deposition technique on metals to deposit metallic salts solution, which resulted in the formation of superhydrophobic surface with WCA of about 173º (Figure 2.8 a). The surface produced can effortlessly float on a water surface similar to pond skaters (Figure 2.8 b). Wang *et al.* [62] employed

electrochemical deposition method, inducing long chain fatty acids to produce micro and nanoscale hierarchical structured copper mesh that exhibited superhydrophobicity and superoleophilicity (Figure 2.8 c). Superhydrophobic 3D porous copper films were fabricated by using hydrogen bubbles as the dynamic template for metal electrodeposition [63]. Since the films were electrodeposited and grew within the interstitial spaces between the hydrogen bubbles, the pore diameter and wall thickness of the porous copper films were successfully tailored by adjusting the concentration of the electrolyte, as shown in Figure 2.8 d. The magnified SEM image [inset of Figure 2.8 d] clearly shows the porous structure with numerous dendrites in different directions forming a strong film.

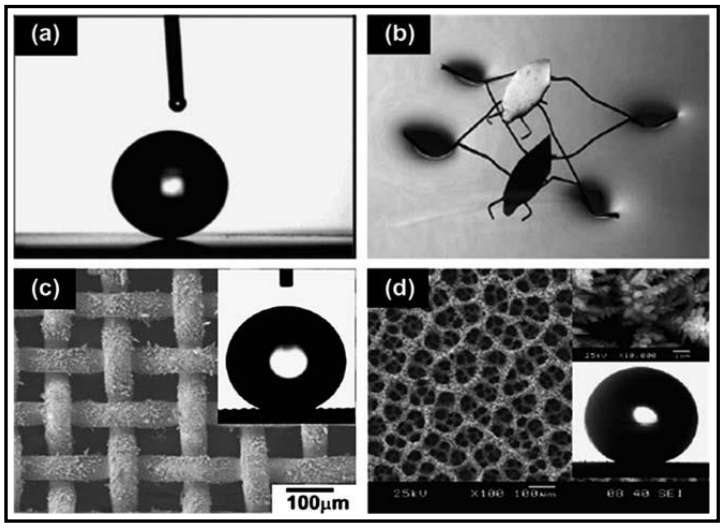

Figure 2.8: Biomimetic superhydrophobic surfaces fabricated by electrochemical deposition. (a) A water drop (8 mm^3) on a silver/heptadecafluoro- 1-decanethiol (HDFT) superhydrophobic surface deposited on a copper substrate; (b) a metallic model ‘‘pond skater’’ (body length 28 mm) of copper legs treated with silver and HDFT; (c) SEM image of the deposited films on one copper mesh knitted by about 55 mm wires as substrates, and the surface shows superhydrophobicity after chemical modification with n-dodecanoic acid; (d) SEM image of porous copper films created by electrochemical deposition at a 0.8 A cm^{-2} cathodic current density in 0.5 M H_2SO_4 and 0.1 M $CuSO_4$ for 45 s. (Reproduced with permission from References 61, 62 and 63).

4.2.2.3. Electrospinning technique: Electrospinning is a dominant technique for fabricating fine nanofibers. This technique is widely used by several research groups to provide sufficient surface roughness for inducing superhydrophobicity. Electrospinning a hydrophobic material will directly result in superhydrophobicity. Ma *et al*. [64] employed electrospinning and chemical vapour deposition techniques to produce superhydrophobic surfaces. In this process, poly (caprolactone) (PCL) was first electrospun and then it was coated with a thin layer of hydrophobic polymerized perfluoroalkyl ethyl methacrylate (PPFEMA) by chemical vapor deposition (CVD) (Figure 2.9). The WCA obtained by this process was about 175º.

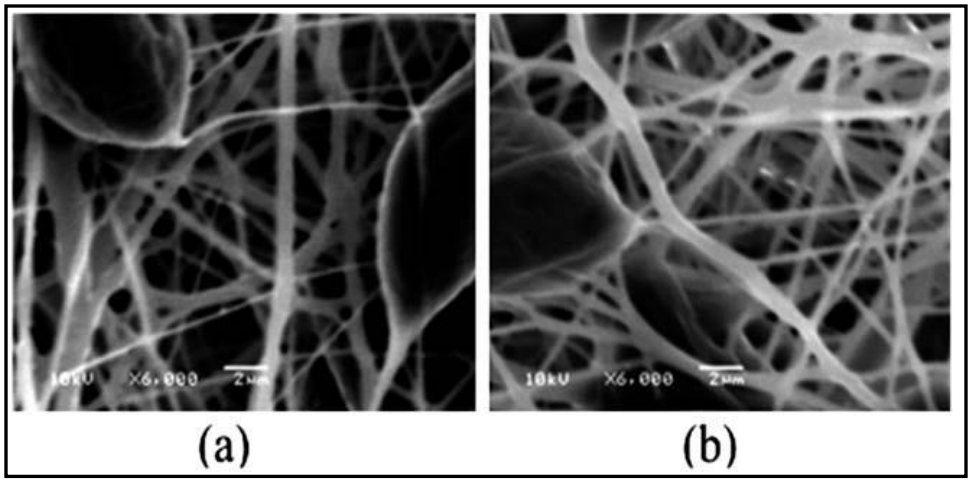

Figure 2.9: SEM image of electrospun nanofibers (a) before (b) after iCVD coating. (Reproduced with permission from Reference 64).

4.2.2.4. Etching and chemical vapor deposition (CVD): CVD and plasma etching processes have been extensively used with polymers to fabricate functional surfaces with different morphologies [65,66]. Engineered surfaces exhibiting hydrophobic properties were synthesized by plasma based techniques to obtain different surface topographies (Figure 2.10 a) [67].

Vourdas *et al.* [68] employed nano rinse and a mass production amenable plasma process to fabricate superhydrophobic poly (methyl methacrylate) (PMMA) surfaces under low pressure conditions in high density plasma reactor (Figure 2.10 b). Garrod *et al*. [69] (Figure 2.10 c) analyzed the stenocara beetle's back and replicated the surface by employing a micro condensation process using plasma chemical patterns. The micro textures were designed and constructed over Si surfaces and they exhibited superhydrophobic behavior with WCA of about 174º (Figure 2.10 d) [70].

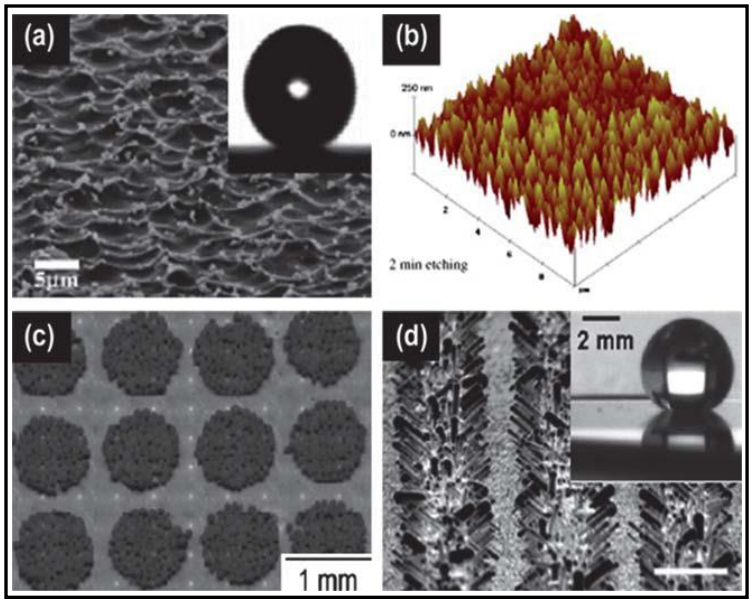

Figure 2.10: Biomimetic superhydrophobic surfaces constructed by plasma etching. (a) SEM image of the rough surface after 3 min of SF_6 etching, showing superhydrophobicity; (b) AFM image of an O_2 plasma treated PMMA sample; (c) an optical image showing the pulsed plasma deposited poly(glycidyl methacrylate) array reacted with 50 mm amino polystyrene microspheres; (d) SEM image of Si nanowires grown on the Si islands with Au cluster on the tips of the nanowires treated by plasma etching, the scale bar is 5 mm. (Reproduced with permission from References 67, 68, 69 and 70).

Teshima *et al.* [71] produced a transparent superhydrophobic surface by a novel method consisting of two dry processing techniques. In this method, nano-texture was first formed on a poly(ethylene terephthalate) (PET) substrate via selective oxygen plasma etching followed by plasma enhanced chemical vapor deposition using tetramethylsilane as the precursor (Figure 2.11). The surface fabricated by this process showed a WCA greater than 150º.

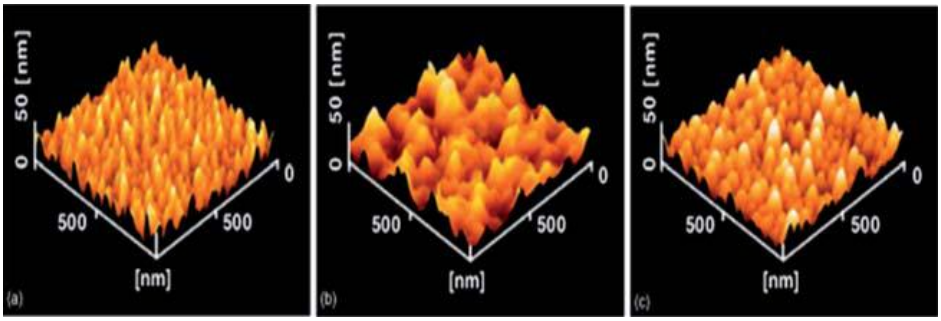

Figure 2.11: AFM images of the PET surfaces (a) treated with oxygen plasma, (b) coated with FAS layer (low-temperature CVD) after the oxygen plasma treatment and (c) coated with TMS layer (PECVD) after the oxygen plasma treatment. (Reproduced with permission from Reference 71).

CVD is a competent technique to produce micro and nano surface topographies on a macroscopic substrate [72-74]. Yan *et al*. [72] produced pyramid like micro structures through capillary driven self-assembly during the evaporation of water from aligned CNTs wrapped by poly (sodium 4-styrenesulfonate). The surface exhibited good superhydrophobicity.

Ci *et al*. [73] constructed an array of vertically aligned large diameter double walled carbon nanotubes by a water-assisted CVD process. The prepared surface exhibited a WCA of about 170º.

***4.2.2.5. Sol–gel method and polymerization reaction*:** The sol-gel method can be employed in the fabrication of superhydrophobic surfaces on all kinds of solid substrates [75-81] Huang *et al*. [80] fabricated biomimetic superhydrophobic surfaces on alloys of copper using hexamethylenetetramine and ethylene glycol, a strong bidentate chelating agent to Cu^{2+} and Fe^{2+} ions with a high stability constant, as the capping reagent. Li *et al*. [81] produced ordered pore indium oxide array films by a sol dipping method using polystyrene colloidal monolayers. It was found that the superhydrophobic properties exhibited by the film can be controlled by increasing the pore size on the film. Shirtcliffe *et al.* [82] used different proportions of (organo-triethoxysilane) methyltriethoxysilane (MTEOS) to produce sol-gel foams. These foams, when exposed to different temperatures, exhibited binary switching between superhydrophilicity and superhydrophobicity. Hikita *et al.* [83] prepared sol-gel films by hydrolysis and condensation of alkoxysilane compounds. Colloidal silica and fluoroalkylsilane were used to control the surface energy and roughness of the film. By optimizing the amount of colloidal silica and fluoroalkylsilane in the film, superhydrophobicity was created in it (Figure 2.12). Shang *et al*. [84] described an easy method to fabricate a transparent superhydrophobic film by the modification of silica based gel films with a fluorinated silane.

4.2.2.6. Other techniques: Besides the techniques cited above, researchers around the world are working on several other methods like texturing [85] and electrospraying [86] which were employed to fabricate superhydrophobic surfaces in recent times. In year 2009, Wang *et al*. [85] fabricated superhydrophobic

surfaces by surface texturing the porous silicon films with capillary stress. Burkarter *et al*. [86] used an electrospray technique to deposit polytetrafluoroethylene (PTFE) films on fluorine doped tin oxide coated glass slides. Liu *et al*. [87] demonstrated an inexpensive technique for the fabrication of superhydrophobic surfaces with a crater like structure on Ti_6Al_4V alloy substrate by means of sandblasting with SiO_2 microparticles, which is a pure physical process, and the surface compositions remain unchanged. It is believed that this method should be easily applied to other metals and their alloys.

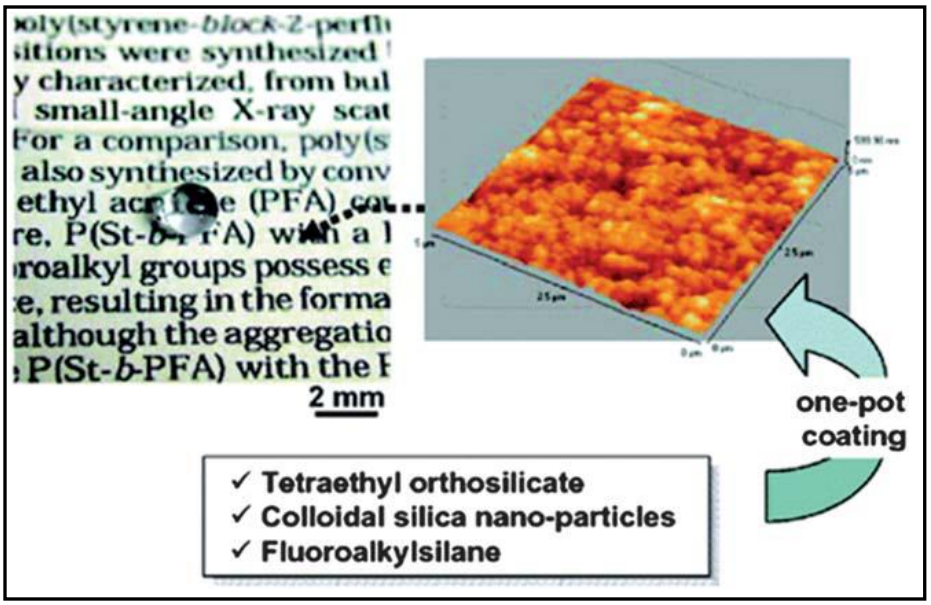

Figure 2.12: Superhydrophobic surface produced by a sol-gel method. The image in the left shows the transparency of the coating. The image on the right is the AFM image of a sol-gel film containing 30 wt.% colloidal silica. (Reproduced with permission from Reference 83).

5. Functions of hydrophobic surfaces

Though lots of research works are centred on fabrication techniques of superhydrophobic surfaces, in recent years, the researchers started focusing on various functions and applications of these surfaces (Figure 2.13). The literature review will explain only the primary functions of the superhydrophobic surfaces such as anti-icing, electrowetting and elucidate different research works carried on in these areas.

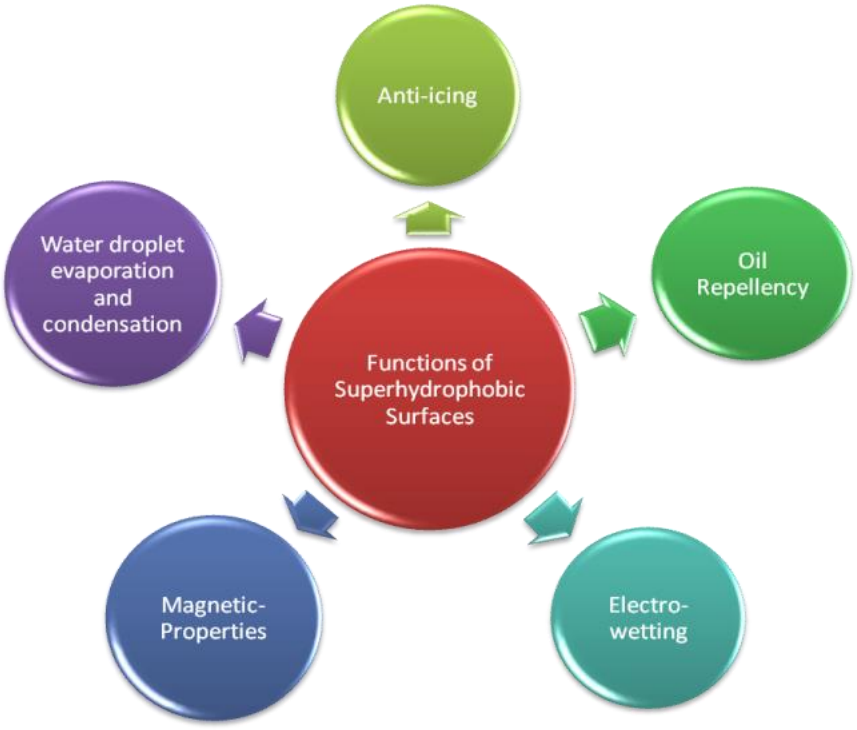

Figure 2.13: Functions of Superhydrophobic surfaces. (Reproduced with permission from Reference 162)

5.1. Anti-icing

In cold regions, layers of ice get deposited on solid materials, particularly on the overhead transmission lines which results in the mechanical failure of the system. Recent research works orbits around the fabrication of superhydrophobic surfaces to reduce the accumulation of snow and to even eliminate the formation of ice on solid surfaces [88-93].

Kulinich *et al.* [90-92] investigated the adhesion strength of artificially created glaze ice (similar to accreted in nature) on rough fluoropolymer based superhydrophobic coatings with similar self-assembled monolayers. Glaze ice is prepared by spraying supercooled water microdroplets on the target substrates at sub-zero temperature. Ice adhesion is evaluated by spinning the samples at constantly increasing speed until ice de-lamination occurred. Na *et al.* [93] gave a fundamental understanding of various factors affecting frost nucleation, particularly the surface energy of the base surface. The experimental results showed that air at the cold surface should be supersaturated to ensure frost nucleation. But the super-saturation degree is mainly dependent on the surface energy, which will in turn affect the initial frost nucleation. They concluded that cold substrates of lower surface energy require higher super-saturation degree for nucleation than higher energy surfaces, and surface roughness will also reduce the required super-saturation degree. As the extreme of low energy surface, superhydrophobic films are also considered as promising materials for alleviating frost growth on cold substrates. Cao *et al.* [94] used nanoparticle polymer composites to fabricate anti-icing superhydrophobic coatings which can prevent

the formation of ice upon impact of super-cooled water. The experimental results showed that the anti-icing capability of these composites depends on the superhydrophobicity and also on the size of the particles exposed on the surface.

Icing of water on superhydrophobic surfaces is a complicated phenomenon and there are lots of factors like temperature, contact area, surface roughness and surface thermodynamics, all of which play a vital role in the occurrence of this phenomenon. Further research is needed to get a clear understanding on the effect of these factors on icing.

5.2. Electrowetting and other functions

Electrowetting on superhydrophobic surfaces is an interesting phenomenon which attracted much attention in recent years [95-105]. In the year 2004, for the first time Krupenkin *et al.* [100] demonstrated a technique for dynamic electric control over the wetting behaviour of the liquid droplets on a superhydrophobic surface by etching an array of microscopic cylindrical nanoposts into the surface of silicon wafer. He found that the wetting properties of the surface can be tuned from superhydrophobic behaviour to nearly complete wetting as a function of applied voltage and liquid surface tension (Figure 2.14 a). Herbertson *et al.* [101] investigated the electrowetting on a patterned layer of SU-8 photo-resist with amorphous Teflon coating, finding that contact angle decreased from 152^0 to 114^0 after a cycle from 0 to 130 V and back to 0 V (Figure 2.14 b).

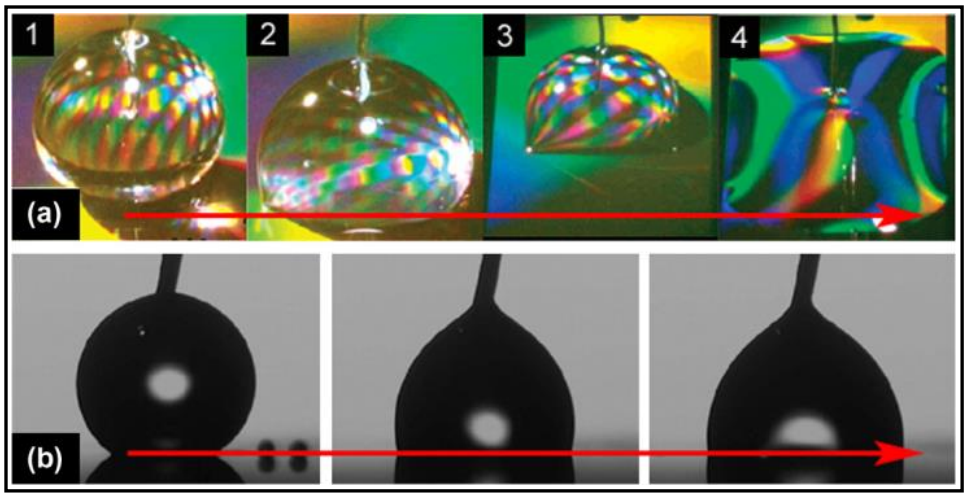

Figure 2.14: The Optical images of the electrowetting of liquid droplets on superhydrophobic surfaces with no reversible effect. (a) Four images demonstrating electrically induced transitions between different wetting states of a liquid droplet on the nanostructured substrate; (b) images of a water droplet on a SU-8 patterned surface with a Teflon-AF under various applied voltage. (Reproduced with permission from References 100 and 101).

Besides the works referred above, lots of research works have been carried out in this area which may lead way to the designing of electrowetting systems at very low voltages with potential applications in the field of lab-on-chip and also in developing functional microfluidic devices.

Evaporation and condensation of water droplet on solid substrate was first explained in the year 1977. Picknett *et al*. proposed two kinds of models to explain the phenomenon of evaporation of water droplets on the solid surface [106]. The first model is constant contact angle with diminishing contact area and the second is constant area with diminishing contact angle. Birdi *et al.* [107] found that there are two possibilities for a volatile liquid drop on low surface energy substrates: (1) the rate of evaporation is linear and follows the constant

contact area mode for the initial CA < 90^0. (2) The rate of evaporation is non-linear and follows the constant CA mode for CA > 90^0. Inspired by this work, several research works have been carried out in investigating the evaporation and condensation phenomenon of water droplets on superhydrophobic surfaces [108-112].

Sticky and magnetic properties of the water droplets [113-115], interaction between water droplet and solid surfaces [116,117] and the Leidenfrost droplets [118-120] are the other functions which are the areas of attention for the researchers in recent times.

6. Hydrophilic photocatalytic coatings

Unlike hydrophobic/superhydrophobic surfaces that rely solely on the flow of water to clean the surface, hydrophilic coatings chemically break down dirt and other impurities when exposed to sunlight. This process is called *''Photocatalysis''*. The technique is basically inspired from the photosynthesis process of the green leaves, which uses sunlight to drive the chemistry. Although a few products that work on the principle of hydrophilicity are commercialized, this field is far from attaining maturity. Several research works are under way in developing superhydrophilic self-cleaning coatings.

6.1. Materials and mechanism to produce hydrophilic coatings

6.1.1. Titanium dioxide (TiO_2)

In the year 2001, 'Pilkington Glass' commercialized the first self-cleaning coating for glass windows that was made of a thin transparent layer of TiO_2. The

TiO_2 cleans the window in sunlight through two distinct properties: (1) photocatalysis (2) hydrophilicity. During photocatalysis, organic dirt and other impurities present on the coatings are chemically broken down by absorption of sunlight. Hydrophilicity causes water to form sheets by reducing the contact angle and washes away the dirt. TiO_2 is highly efficient at photocatalyzing dirt in sunlight. It is non-toxic, cheap, and easy to deposit in the form of a thin film, chemically inert in the absence of light and can easily reach the state of superhydrophilicity. All these properties made TiO_2 a highly suitable material to produce hydrophilic surfaces. In normal conditions, TiO_2 absorbs light with energy equal to or greater than its band-gap energy, producing excited charge carriers: positively charged holes (h^+) and negatively charged electrons (e^-) (Figure 2.15). Though most of these charges undergo recombination, few of them migrate to the surface. On the surface, holes oxidise the organic molecules while electrons combine with atmospheric oxygen to give superoxide radicals, which in turn attack nearby organic molecules. This results in the cleaning of surfaces by conversion of organic molecules into carbon dioxide and water at ambient temperature. This process is called *Cold combustion*. An example is the total decomposition of stearic acid [$CH_3(CH_2)_{16}CO_2H$] in the presence of atmospheric oxygen to CO_2 and H_2O on TiO_2 surfaces (Figure 2.16) [121]. A large number of organic pollutants can be broken down by this technique, which includes aromatics, polymers, dyes and surfactants. Superhydrophilicity in TiO_2 is also a light-induced property in which the holes produced by the photo-excitation process oxidize the lattice oxygen at the surface of the material. This results in

oxygen vacancies that can be filled by adsorbed water, resulting in surface hydroxide groups that make the wetted surface more suitable than the dry surface, lowering the static contact angle [121] to almost 0º after irradiation. The self-cleaning properties of TiO_2 are basically governed by the absorption of ultra-band gap light and electron-hole pair generation. The band gap of bulk anatase TiO_2 is 3.2 eV, corresponding to light of wavelength of 390 nm (near UV range).

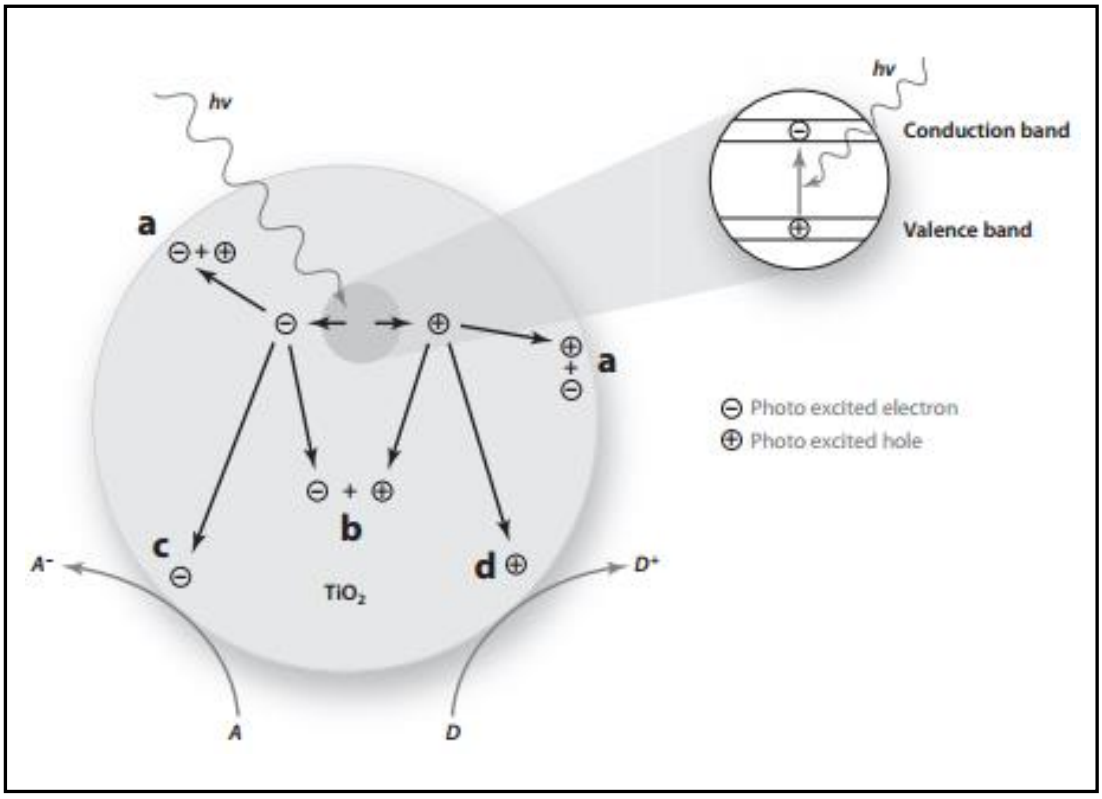

Figure 2.15: Upon irradiation of TiO_2 by ultra-band gap light, the semiconductor undergoes photo-excitation. The electron and the hole that result can follow one of several pathways: (a) electron-hole recombination on the surface; (b) electron-hole recombination in the bulk reaction of the semiconductor; (c) electron acceptor A is reduced by photogenerated electrons; and (d) electron donor D is oxidized by photogenerated holes. (Reproduced with permission from Reference 121).

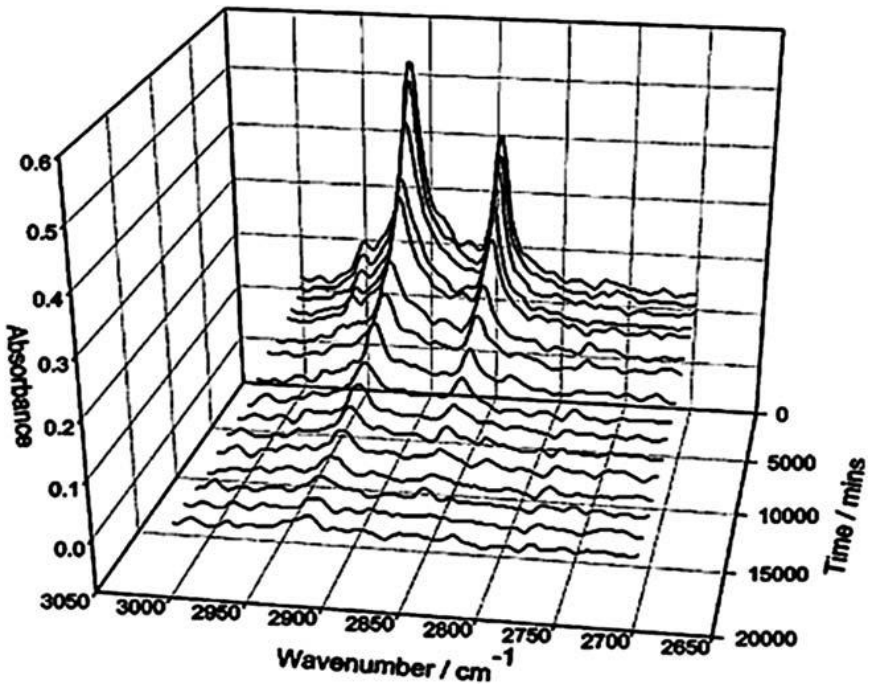

Figure 2.16: Photocatalytic decomposition of stearic acid is monitored by infrared spectroscopy. The two C–H stretching bands decrease in area with irradiation, indicating that the surface is self-cleaning. The photocatalysis takes place on a nanocrystalline TiO_2 film under $\lambda = 365$ nm irradiation. (Reproduced with permission from Reference 121).

6.1.2. Improving TiO_2

TiO_2 has become the most significant material for photocatalytic hydrophilic coatings. The photocatalytic activity of TiO_2 decreases by a considerable amount when it is deposited as a smooth, nanocrystalline film. But most of the requirements in the optical and glazing industries involve the use of a robust, nanocrystalline film. Therefore, a lot of research effort is going into improving the self-cleaning properties of these nanocrystalline films. Recent research work has shown that the photocatalytic activity of thick films is higher than thin TiO_2 films. TiO_2 coatings of 3 mm thickness produced by spin coating and annealing TiO_2 paste was tested for photocatalysis against a 25 nm coating.

The thicker coatings absorb near-UV light more strongly and the photocatalytic activity was very high, exhibiting quantum yields of around 0.15% while it was only 0.04% for the thin film. This indicated that the thicker films absorb more light and thus generate more excited charge carriers, which have a life time long enough to reach the surface to induce chemical reaction in the surface. But there is a limit to increasing the thickness of the film. When all available UV light is absorbed, or the distance to the surface is very high so that the charge carriers have very little chance of reaching it before they recombine, a still thicker film will not increase the photocatalytic activity. The properties like optical clarity and durability are very poor for thicker films and these issues have to be addressed in future research.

6.1.3. Improving TiO_2 by doping

Doping of TiO_2 is an effective technique to improve the photocatalytic activity and it can also be easily incorporated into CVD or sol-gel processes [122]. Based on the methods that are employed to deposit coatings, dopants can exist as a single phase, mixed oxide or a separate phase. Recent work in this direction mainly focuses on the transition metal dopants. These dopants, when present as a metal oxide, can be divided into two, based on their oxidation state with respect to the metal in the metal oxide: (1) lower oxidation state ones and (2) higher oxidation state ones [122,123]. Metals with higher oxidation states, like Mo^{5+}, Nb^{5+} and W^{6+}, increase the photocatalytic activity whereas metals with lower oxidation states (< +4) like Fe^{3+}, Co^{2+} and Ni^{2+} slow it down. Park *et al*. [123] used differential scanning calorimetry (DSC) to study the low oxidation

state dopants. He found that lower oxidation state dopants caused crystallization to occur at around 20 ºC higher than the higher oxidation state dopants when they are in the form of mixed oxides. A study made using X-ray photoelectron spectroscopy (XPS) explained that the higher oxidation state metal-doped films had a higher concentration of hydroxyl groups adsorbed onto the surface than the un-doped and lower oxidation state metal-doped TiO_2. Since hydroxyl groups play a vital role in the process of photocatalysis, this could explain the increase in the photocatalytic activity in the presence of higher oxidation state dopants. Phase separated dopants have also been experimented to improve the self-cleaning property in which a pure phase of TiO_2 contains a pure phase of a second material. Recent studies have centered on the use of nanoparticles (use of metallic gold or platinum nanoparticles that can assist photocatalysis in TiO_2) as a method of incorporating a phase separated dopant [124,125].

6.1.4. Other materials

Though TiO_2 has been the main focus of study in self-cleaning applications, other materials like WO_3, ZrO_2, ZnO, CdS and polyoxometallates have been investigated in recent years. However, none of the materials could surpass TiO_2, which uses only light to activate the process.

6.2. Mechanisms employed to produce hydrophilic coatings

Various mechanisms are employed to produce hydrophilic surfaces using TiO_2 and other inorganic metal oxides. In the year 1978, Harrop *et al*. [126] reported the first hydrophilic protective coatings on a glass substrate. In this

method, he used vinyl tricholosilane films on float glass that converts an olefinic bond into other carbon functional groups resulting in hydrophilic properties. Though this work was not very effective, it paved the way for the evolution of research work in superhydrophilic coatings. Yu *et al*. [127] employed a sol-gel technique using alkoxide solutions containing polyethylene glycol (PEG) to fabricate superhydrophilic TiO_2 coatings. Ding *et al*. employed a sol-gel technique to fabricate TiO_2-based nanocomposite hydrophilic coatings by mixing TiO_2 nanoparticles with a sol-gel derived silica sol and methoxysilane group-bearing styrene-co-acrylate (SA) oligomer, and curing with aminopropyltriethoxysilane at ambient temperature. The resulting surface exhibited excellent self-cleaning properties.

Zhang *et al*. [128] reported self-cleaning particle coatings by using an LbL assembly technique. A sub-monolayer of SiO_2 particles was covered with TiO_2 nanoparticles with the help of oppositely charged polyelectrolytes to generate a low-refractive-index film exhibiting superhydrophilicity. The same research group [129] investigated further the possibility of creating the dual functions of self-cleaning and antireflection in double-layered TiO_2-SiO_2 films that consisted of a dense top layer of TiO_2 and a porous bottom layer of SiO_2. The films were prepared by LbL assembly of SiO_2 nanoparticles and titanate nanosheets with polycations. Yaghoubi *et al*. [130] produced a self-cleaning TiO_2 coating on a polycarbonate substrate by employing a chemical surface treatment method to create hydrophilic groups on the polycarbonate substrate. Prado *et al*. [131] employed dip-coating technique to produce multi-functional coatings consisting

of two-layer stacks with a mesoporous SiO_2 layer and a dense/mesoporous TiO_2 layer. This coating exhibited both anti-reflective and self-cleaning properties. Xu *et al*. [132] employed an LbL dip coating method using a TiO_2 sol and a methanol solution of NH_4F as precursors to fabricate transparent, visible light activated C–N–F co-doped TiO_2 films exhibiting superhydrophilicity. The WCA of these films were 2.3-3.1º (Figure 2.17). Bhatia *et al*. [133] employed a nanoscale surface texturing technique to induce superhydrophilicity on a glass substrate. In this process a thin layer of nickel is deposited on the glass substrates, followed by annealing to create Ni (nickel) nanoparticles. These Ni nanoparticles were used as an etch mask to pattern the glass substrates and removed after etching by nitric acid rinse. The resulting glass surface exhibited excellent self-cleaning properties.

Fujishima's group [134-139] and a few other groups [140,141] did novel works in the area of superhydrophilicity and photocatalysis. Recently, Akira *et al*. [127] developed hydrophobic/superhydrophilic patterns by a new fabrication technique consisting of five steps: (1) photocatalytic reduction of Ag^+ to Ag (nucleation), (2) electroless Cu deposition, (3) oxidation of Cu to CuO, (4) deposition of a self-assembled monolayer (SAM), and (5) photocatalytic decomposition of selected areas of the SAM. A hydrophobic/superhydrophilic pattern with 500 mm^2 hydrophilic areas was obtained in this process. This group also fabricated a SiO_2/TiO_2 bi-layer film with self-cleaning and antireflection properties by employing sol-gel and dip coating techniques. Pan *et al*. [142] produced TiO_2 nanofibers with diameters of 200-550 nm by high temperature calcinations of the as electrospun tetrabutyl titanate $[Ti(OC_4H_9)_4]$/polystyrene

(PS) composite fibers prepared by sol-gel processing and electrospinning techniques. The fiber films exhibited extremely stable superamphiphilicity and self-cleaning properties.

Though much research works have been carried out; this literature review within its scope has highlighted only a few novel and important works conducted in the area of hydrophilic surface fabrication.

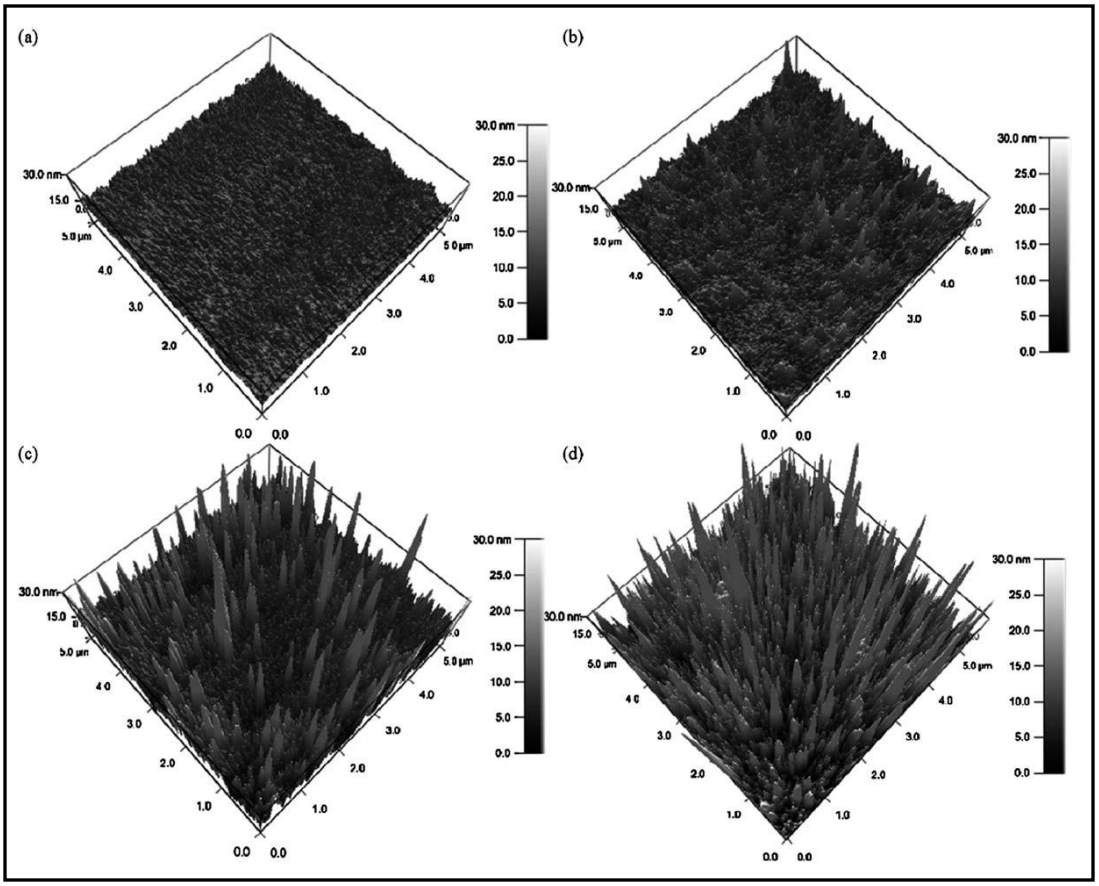

Figure 2.17: AFM 3D images of the surface of (a) C–TiO_2 film; (b) C–N–F–TiO_2-0.5 film; (c) C–N–F–TiO_2-1 film; (d) C–N–F–TiO_2-2 film. (Reproduced with permission from Reference 132).

7. Recent advancements in self-cleaning coatings

Though, superhydrophobic and photocatalytic superhydrophilic coatings can perform effective self-cleaning functions using the flow of water, current industrial needs are slightly beyond dust and particulate pollutants cleaning. Today, in addition to the regular dust and particulate pollutants, the surfaces are exposed to several other pollutants like oil, crease, industrial wastes, smoke, automobile exhaust, corrosive chemicals etc. Hence, the recent research works are more focused towards developing robust and transparent coatings that have the ability to repel not only water but also other organics. Such coatings are referred as Superamphiphobic/Superomniphobic coatings [143-147]. The key criteria to achieve the phenomenon of superamphiphobicity/superomniphobicity are not yet clearly defined; however, lower surface energy and surface roughness are the necessary factors for oil/water repellency [148].

Tuteja *et al.* [149,150] designed and fabricated surface topographies involving surface overhangs and re-entrant geometries to develop superamphiphobic/omniphobic surfaces (Figure 2.18). Based on the approach of designing surface topographies, researchers have developed numerous superamphiphobic/omniphobic surfaces [151-155]. Nevertheless, designing such surfaces involves complicated surface topographies and hence scaling up to larger areas is a big challenge and cost intensive.

In 2012, Deng *et al.* demonstrated a new approach to develop self-cleaning superamphiphobic surfaces without complicated surface designs and surface overhangs [156]. They formulated a simple, scalable and novel, chemical

approach to fabricate transparent superamphiphobic surfaces using candle soot. The contact angle achieved using water and hexadecane were reported to be 165º and 156º, respectively. Based on chemical approaches, many superamphiphobic/omniphobic self-cleaning surfaces have been fabricated in recent past [157-161].

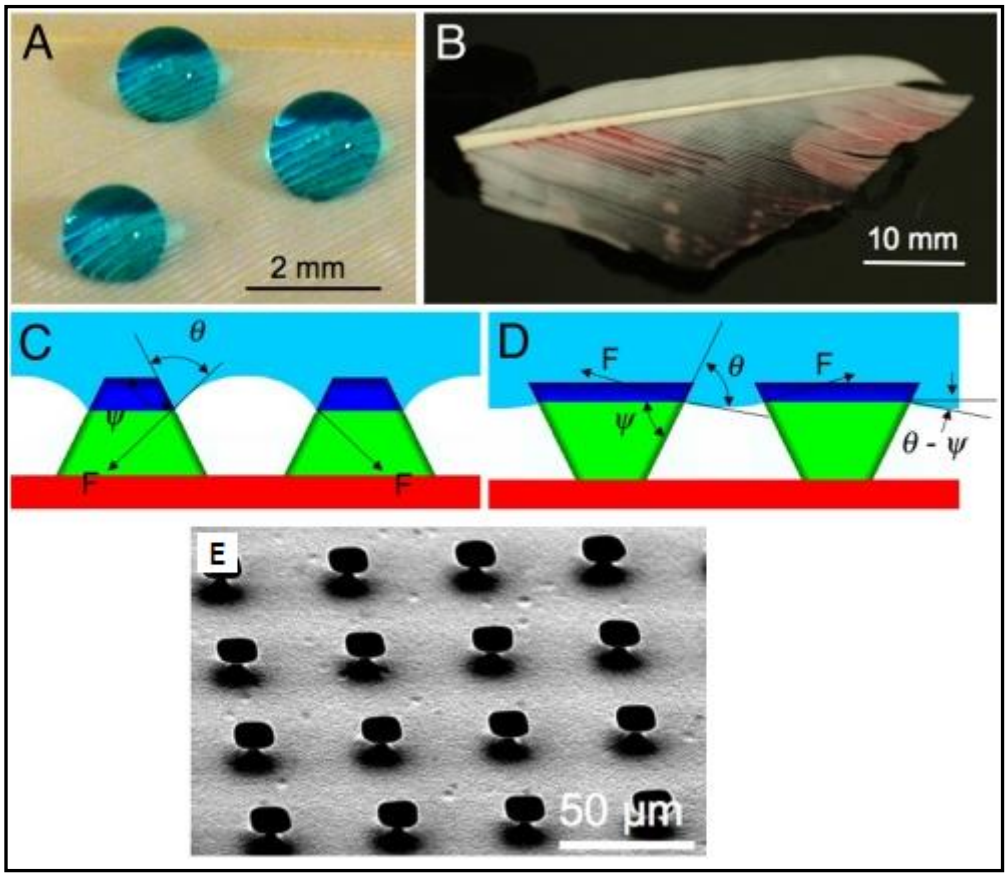

Figure 2.18: Critical role of re-entrant texture. (A and B) Droplets of water (colored with methylene blue) and rapeseed oil (colored with oil red O) on a duck feather. (C and D) Schematic diagrams illustrating possible liquid-vapor interfaces on two different surfaces having the same solid surface energy and the same equilibrium contact angle (θ), but different geometric angles (ψ). (E) An SEM micrograph of a microhoodoo surface (with W = 10 μm, D = 20 μm and H = 7 μm). The samples are viewed from an oblique angle of 30º. (Reproduced with permission from Reference 150).

8. Characterization techniques

Several characterization techniques are employed to analyze the surface morphology and to compute the water contact angle of hydrophilic, hydrophobic, amphiphobic/omniphobic surfaces. Contact angle measurements play a pivotal role in the characterization of self-cleaning coatings. Dodiuk *et al*. used this technique (contact angle goniometer) to compute the contact angle and sliding angle of hydrophobic surface made of polycarbonate (PC). Atomic force microscopy (AFM) is a technique widely used in surface roughness measurements of the self-cleaning coatings. Teshima *et al*. used this technique to analyze the roughness of the superhydrophobic surface produced by etching using PET (Polyethylene terephthalate). Environmental ellipsometric porosimetry (EEP), grazing incidence X-ray analyzes at low and wide angles (GI-SAXS and GI-WAXS), electronic and near-field microcopies, field-emission scanning electric microscopy (FE-SEM), transmission electron microscopy (TEM), Fourier-transform infrared spectroscopy (FTIR), UV-visible transmittance and X-ray photoelectron spectroscopy (XPS) are a few other techniques that are widely used in characterizing self-cleaning surfaces.

9. Applications of self-cleaning coatings

Self-cleaning coatings are expected to find potential applications in diverse fields. Potential application sectors include the textile industry (self-cleaning clothing), automobile industry (self-cleaning windshield glass, car bodies and mirrors), optical industry (cameras, sensors, lenses and telescopes), marine

industry (anti-corrosion) and aerospace industry (non-sticky surfaces). Self-cleaning coatings can also be used in windows (window coatings), solar modules (self-cleaning coatings for solar modules) and in paints (exterior paints with self-cleaning properties). Because of the potential applications of self-cleaning coatings, many companies have already been attracted to this technology and they have commercialized a few products. The Pilkington group of companies commercialized the first self-cleaning coated float glass product called Pilkington Activ (http://www.pilkington.com/). Self-cleaning paints have been commercialized by a German based company named Lotusan (www.lotusan.de) and they are now commonly available in Europe. Cardinal Glass Industries (Neat Glass) (www.cardinalcorp.com), Saint-Gobain (SGG Aqua Clean) (www.saint-gobain.com) and PPG Industries (www.ppg.com) are a few other companies working on this technology.

10. Conclusion

All the research efforts are poised to emulate the supreme strategies perfected by nature over billions of years. The self-cleaning surface on naturally occurring leaves and wings of certain insects is multipurpose in achieving self-cleaning, anti-reflective, camouflage and various other functionalities which have got researchers across the globe to take stock and attempt to mimic. Though the self-cleaning surfaces designed by them are yet to match their naturally occurring counterparts, the fabrication techniques have indeed evolved into more environmentally compatible and cost-effective. As discussed in the literature

review, several fabrication techniques are adopted to produce durable and transparent self-cleaning coatings on glass surface.

The thesis within its scope will focus on ***Electrospinning/Electrospraying*** techniques to develop liquid repellent self-cleaning surfaces (Hydrophobic/Superhydrophobic, Amphiphobic/Superamphiphobic coatings) on glass substrate with high robustness and optical transparency. Since their inception in the year 1934, the electrospinning/electrospraying techniques have been widely employed to fabricate metal oxide and polymer nanofibers, nanoparticles and other anisotropic nanostructures. Compared to the hydrothermal and other complex chemical processes, these methods provide cost-effective way of producing nanostructures in the large scale by a simple set-up comprising of three major parts: a high-voltage power supply, a spinneret containing a precursor solution and a collector. The experimental set-up for both electrospinning and electrospraying process are very similar. Both these techniques employ electric charge to produce nanosturctures. The former uses electric charge to draw fine micro/nanofibers from the sol-gel solution; while the later employs electricity to disperse sol-gel solution to produce micro/nanoparticles (spheres). The viscosity of the sol-gel solution plays a key role in determining the formulation of nanofibers or nanoparticles; high viscous sol-gel solutions results in nanofibers (electrospinning) while low viscosity results in nanoparticles (electrospraying) formation. In addition to the viscosity of the solution, flow-rate and applied voltage are the other parameters that determine the formation of nanofibers or nanoparticles.

Thus Electrospinning/Electrospraying techniques have been chosen to fabricate liquid repellent self-cleaning surfaces using metal oxide and polymer based nanostructures. The thesis will focus not only on the fabrication of robust and transparent liquid repellent self-cleaning surfaces by employing electrospinning/electrospraying techniques but also on studying and analyzing the surface morphologies and surface modifications that can be performed on the fabricated nanostructures to enhance the self-cleaning performance parameters with good optical properties.

The outcomes of this research will improve the existing knowledge base by revealing innovative approaches through electrospinning/electrospraying process to fabricate robust and transparent liquid repellent self-cleaning surfaces without implementing complex surface topographies. Furthermore, achieving a stable, homogenous coating of lubricating materials (Example: PFPE) on a smooth/flat surface remains as a challenge due to the poor adhesion of the lubricating material with the surface (glass/silicon). The thesis will address this challenge by formulating a new chemical approach to fabricate a smooth, stable, homogenous coating of PFPE on a flat substrate. Lastly, this research will also establish electrospinning/electrospraying as a potential technique to produce robust, transparent and durable self-cleaning surfaces on glass with remarkable liquid repellent properties.

Chapter 3

Superhydrophobic coating

3. Superhydrophobic coating from electrospun fluorinated POSS-PVDF-HFP nanocomposite mixture

1. Introduction

The phenomenon of superhydrophobicity can be achieved by the combination of low surface energy material with surface roughness in micro and nano-scale regimes [162-166]. As discussed in Chapter 2, the techniques to produce hydrophobic and superhydrophobic surfaces can be broadly classified into two categories: a) modifying a rough surface with a material of low surface energy, and b) making a rough surface using a low surface energy material; the latter of which is the focus of this work. Fluorinated materials generally exhibit low surface energy and roughening them will collectively result in superhydrophobic surfaces [167-170]. A class of recently developed materials that has received a great deal of attention for potential water repellent coatings is polyhedral oligomeric silsesquioxanes (POSS) [171]. POSS compounds are thermally stable because of the presence of silica cages. The organic groups attached at the periphery facilitate functionality which makes POSS an excellent building block for materials in electronic, biological and aerospace applications [172,173]. POSS molecules can be covalently attached to polymers and the resulting nanocomposites exhibited enhanced processability, glass transition

temperature, chemical and mechanical resistance [174]. Recent studies have proved that coatings using fluorinated POSS-polymer blends exhibit very low surface energy with enhanced superhydrophobic property [175,176].

Here electrospinning technique is employed to deposit fluoroPOSS-PVDF-HFP composites uniformly on glass substrates (the method works for other substrates as well, but glass was chosen as a model substrate in the present case). This technique has been used extensively by many researchers to produce nanofibers for applications in dye and quantum dot-sensitized solar cells as active and scattering layers, tissue engineering, chemical sensors and also to produce self-cleaning coatings [177-181].

In the present work, a transparent, uniform, superhydrophobic coating is produced on the glass substrate using a low surface energy polymer (PVDF-HFP) with fluoroPOSS by electrospinning technique. Two different kinds of fluoroPOSS tethered with perfluoroalkylthioether corner groups (FP8 and FPSi8) were experimented and their optical properties and superhydrophobic properties such as surface wettability and surface energy were thoroughly analyzed.

2. Experimental section

2.1. Materials

Poly(vinylidene fluoride-co-hexafluoro propylene) (PVDF-HFP, Mw = 455,000) was purchased from Aldrich, Germany. *N*,*N*-dimethylacetamide (DMAc, 99.8%, GC Grade) and tetrahydrofuran (THF, 99.8%) were purchased from Sigma Aldrich, USA. FP8 and FPSi8 were synthesized in lab.

2.2. Synthesis of FPSi8 and FP8 fluoroPOSS

A catalytic amount of 2,2'-azobisisobutyronitrile (AIBN, 1 mol%) was added to octakis(vinyl)octasilsesquioxane (for FP8) or octakis(vinyldimethylsilyloxy)octasilsesquioxane (for FPSi8) in the presence of 1H,1H,2H,2H-heptadecafluorodecylthiol at room temperature [182].

The mixture was purged with argon for 45 min. The argon purged mixture was then heated up to 80 ºC and stirred at this temperature for 2 days (more catalytic amount of AIBN was added into the reaction system in the 2nd day to make sure the reaction is complete). Once the reaction was completed, the reaction mixture was poured into acetonitrile. The resulting white solid was collected by filtration and it was cleaned with acetonitrile for a few times. The cleaned samples were pure enough to perform analysis after drying in a vacuum oven at 40 ºC. The molecular structures of the two types of POSS are shown in Figure 3.1.

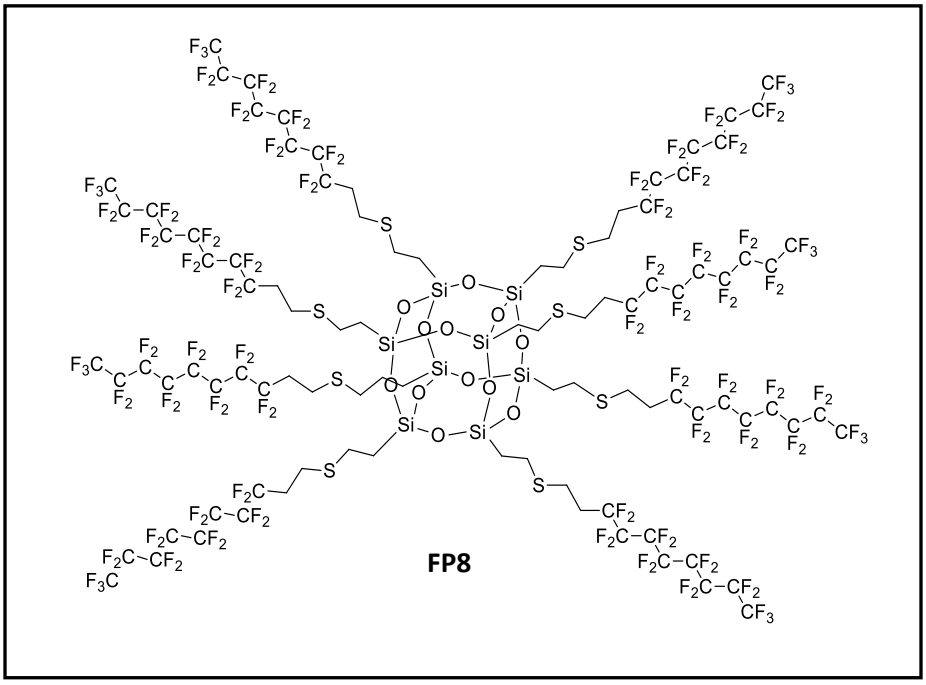

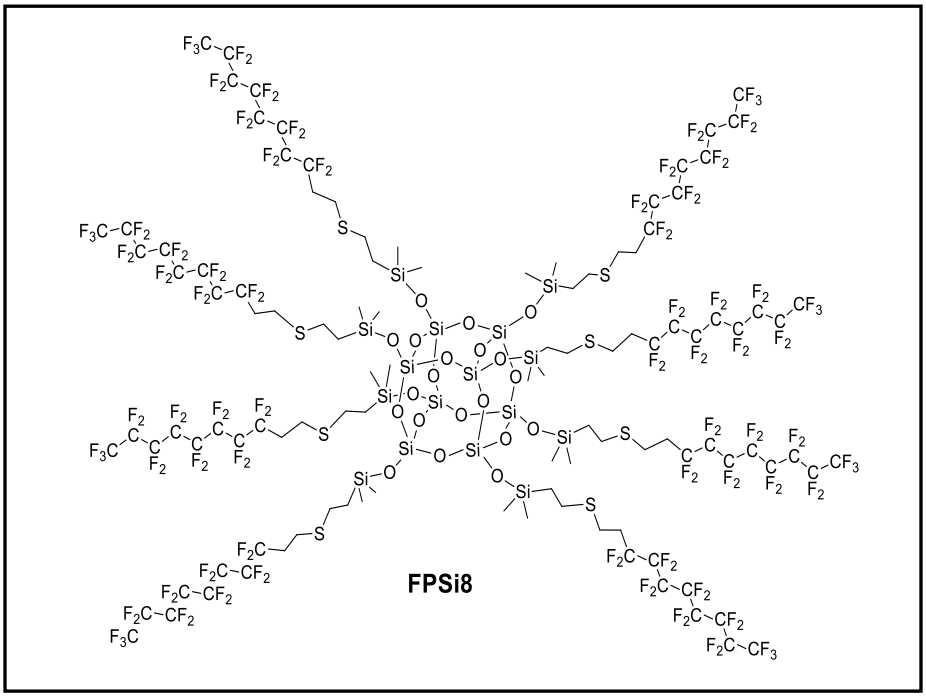

Figure 3.1: Molecular structures of the synthesized fluoroPOSS (FP8 and FPSi8).

2.3. Solutions and substrate preparation

The solutions for electrospinning of fluoroPOSS-PVDF-HFP nanocomposite mixture were prepared as follows. A solution was prepared by adding 0.8 g of PVDF-HFP in 10 mL of a solvent mixture (5 mL of *N*,*N*-dimethyl acetamide and 5 mL of tetrahydrofuran). Using this, four solutions with different wt.% of FP8 fluoroPOSS and four solutions using FPSi8 fluoroPOSS were prepared by adding 8 mg (1 wt.%), 40 mg (5 wt.%), 80 mg (10 wt.%) and 120 mg (15 wt.%), of the respective fluoroPOSS materials (FP8 and FPSi8). The prepared solutions were stirred at room temperature for about 12 h to ensure that the fluoroPOSS and PVDF-HFP to be fully soluble in solvent and thus acquire sufficient viscosity for subsequent electrospinning.

Microscopic slide glass plates (24.4 mm × 76.2 mm × 1.2 mm) were thoroughly cleaned by ultra-sonication in de-ionized water, acetone, ethanol and 2-propanol, respectively, for about 10 min each. In order to ensure that the glass plates are free from surface contaminants, they were treated with Piranha solution for 2 h (3:7 by volume of 30% H_2O_2 and H_2SO_4) followed by rinsing in de-ionized water. The cleaned glass plates were dried in an oven at 80 ºC.

2.4. Electrospinning

The fluoroPOSS-PVDF-HFP precursor solutions were then loaded into the electrospinning machine (NANON, MECC - Japan). The cleaned glass slides were then mounted on an aluminum foil-wrapped static collector. The voltage applied was set to 30 kV and the distance between the needle (27G ½) tip and the static collector was set to 10 cm. The humidity level inside the electrospinning chamber was maintained between 50-60%. Different wt.% precursor solutions were electrospun on the glass substrates for 15 min with a flow-rate of about 0.2 mL/h. A schematic of the electrospinning process is shown in Scheme 3.1. The as-spun fluoroPOSS-PVDF-HFP composite nanofibers coated glass samples were then heated at 130 ºC for 4 h. The heat treatment process evaporates solvent residues resulting in a transparent, uniform fluoroPOSS-PVDF-HFP nanocomposite coating on the glass substrates.

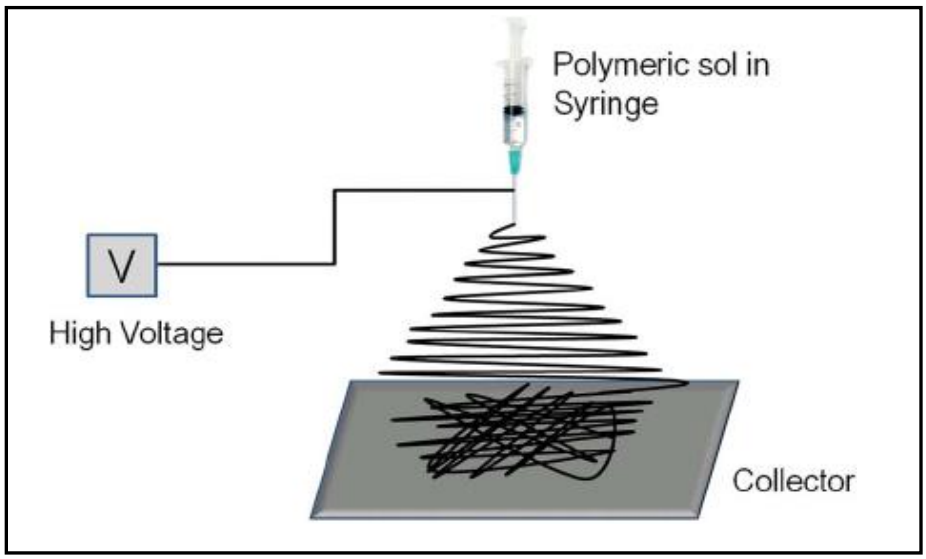

Scheme 3.1: Schematic diagram of electrospinning set-up.

3. Instrumentation and characterization

The surface morphology of the coated samples was analyzed using scanning electron microscope (JEOL JSM – 6701F operated at 5 kV). SEM samples were prepared by sputtering a platinum conducting layer onto the POSS-PVDF-HFP-coated surface of the glass. The energy dispersive X-ray spectroscopy (EDS) measurements were also done using the same machine. The thickness of the film was measured by a surface profiler (Alpha-Step IQ Surface Profiler) and the optical properties were examined by UV-Vis spectroscopy (Shimadzu UV-3600 UV–VIS–NIR spectrophotometer) with a spectral resolution of 1 nm.

Water contact angle and sliding angle measurements were carried out using a contact angle measurement setup (VCA optima contact angle equipment from AST Products) in static/dynamic sessile drop mode at room temperature. The values reported are the averages of at least five measurements made on different areas of every single sample coated with the respective fluoroPOSS materials.

Surface energy of the coating was calculated by measuring the contact angle between the sample surfaces, de-ionized water and ethylene glycol (as a second probe liquid) using Owen-Wendt method and Fowkes equation [183,184].

4. Results and discussion

Except for the optical property, other properties such as the fiber diameter and superhydrophobicity of the coatings fabricated using FP8 fluoroPOSS-PVDF-HFP mixture and FPSi8 fluoroPOSS-PVDF-HFP mixture are very similar. So the results of the latter are discussed below.

4.1. Nanofiber diameter – concentration dependence

It has been shown in the literature that the concentration of the electrospinning solution has a significant effect on the diameter of the synthesized nanofibers [185]. Solution surface tension and viscosity also play important roles in determining the range of concentrations from which continuous fibers can be obtained in electrospinning. At lower concentration, the fibers have an irregular, undulating morphology with large variations in diameter along a single fiber. The fibers produced will be very thin. As the concentration increases, the nanofibers will have a more regular, cylindrical morphology and on average have a larger and more uniform diameter [186].

Figure 3.2 shows the SEM images of the electrospun FPSi8 fluoroPOSS-PVDF-HFP coated glass surface revealing continuous, uniform and non-beaded nanofibers. Figure 3.2 (a) and (b) show the low and high magnification images of pure PVDF-HFP nanofibers. Figure 3.2 (c), (d), (e) and (f) show the low and high magnification images of the fibers with 5 and 15 wt.% of FPSi8 fluoroPOSS-PVDF-HFP. [Figure 3.2 (g), (h) and (i)] shows the energy dispersive X-ray

spectra (EDS) of the pure PVDF-HFP, 5 wt.% and 15 wt.% of FPSi8 fluoroPOSS-PVDF coating, respectively.

As the concentration of the fluoroPOSS in the fluoroPOSS-PVDF-HFP composite mixture increases, the viscosity of the electrospinning solution increases thereby increasing the average diameter of the synthesized nanofibers [187,188]. The average diameter of PVDF nanofibers was 133 nm [see Figure 3.2 (a) and (b)] and it gradually increased and reached 222 nm for the 15 wt.% of FPSi8 fluoroPOSS-PVDF-HFP nanofibers [see Figure 3.2 (e) and (f)]. It is also observed that the amount of fluorine content [see Table 3.1] increases gradually with increase in the concentration of FPSi8 fluoroPOSS. As a result, the surface energy decreases and the water contact angle increases and attains a maximum of 157.3º for 15 wt.% of FPSi8 fluoroPOSS (see Table 3.2 and Figure 3.3 and 3.4).

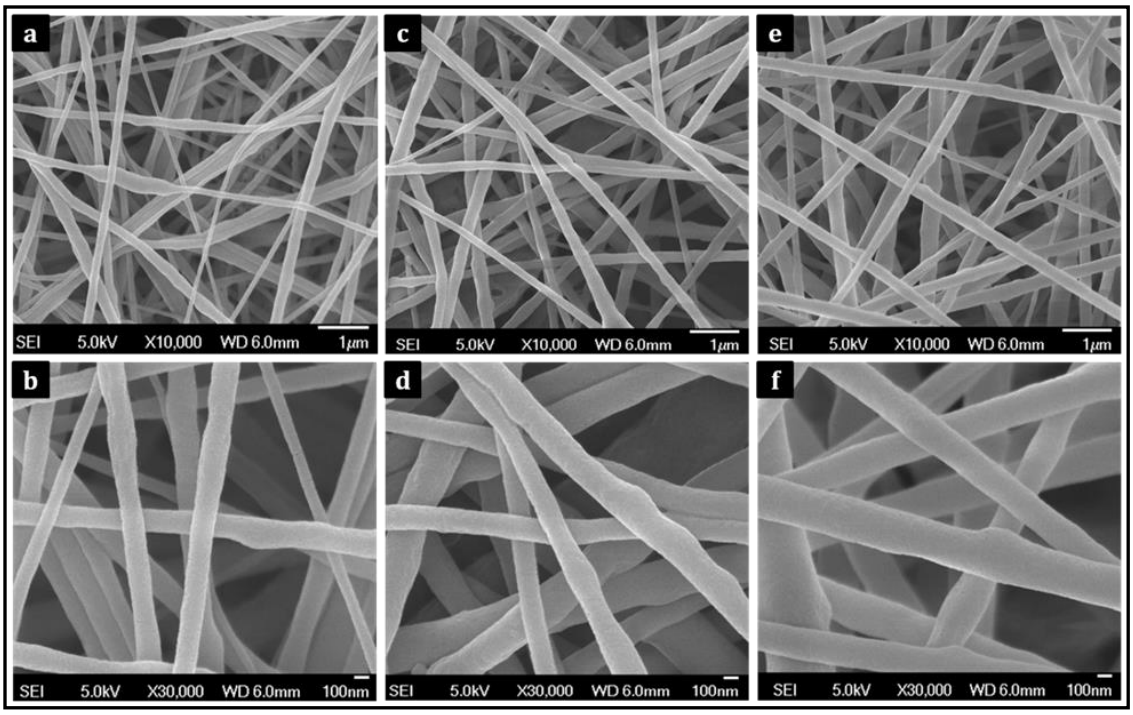

Figure 3.2: (a) and (b) SEM images of PVDF-HFP nanofibers; (c) and (d) SEM images of 5 wt.% of FPSi8 fluoroPOSS-PVDF-HFP nanofibers; (e) and (f) SEM images of 15 wt.% of FPSi8 fluoroPOSS-PVDF-HFP nanofibers.

Table 3.1: Wt% of fluoro-POSS in PVDF and the respective percentage of fluorine atoms.

S. No	Wt % FPSi8 fluoroPOSS in fluoroPOSS-PVDF mixture	Fluorine atom (%)
1	0 (pure PVDF solution)	38.58
2	5	40.93
3	15	44.99

The sliding angle (SA) and the advancing (θ_a)/receding angle (θ_r) were measured using a tilting base surface contact angle measurement and the contact angle hysteresis (CAH) was calculated by taking the difference of advancing and receding angles. Thus the 15 wt.% FPSi8 fluoroPOSS exhibited a WCA as high as 157.3º with SA < 5º and CAH was calculated to be 3º.

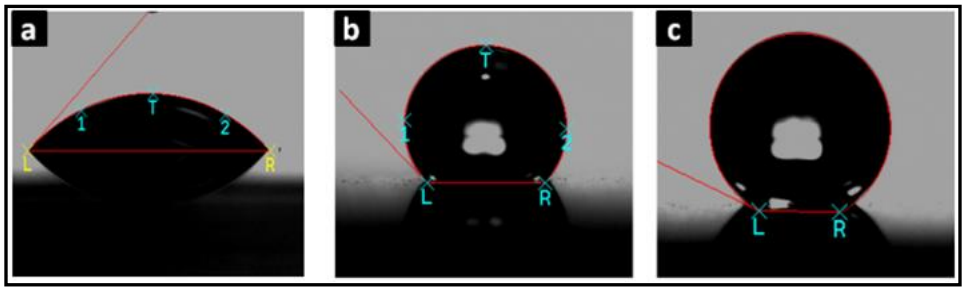

Figure 3.3: Interaction of water droplet (2 µL) with plain, PVDF-HFP and FPSi8 fluoroPOSS-PVDF-HFP coated glass samples. (a) Plain glass (WCA: 48.6º), (b) PVDF coated (WCA: 134.6º) and (c) 15 wt.% of FPSi8 fluoroPOSS-PVDF coated (WCA: 157.3º).

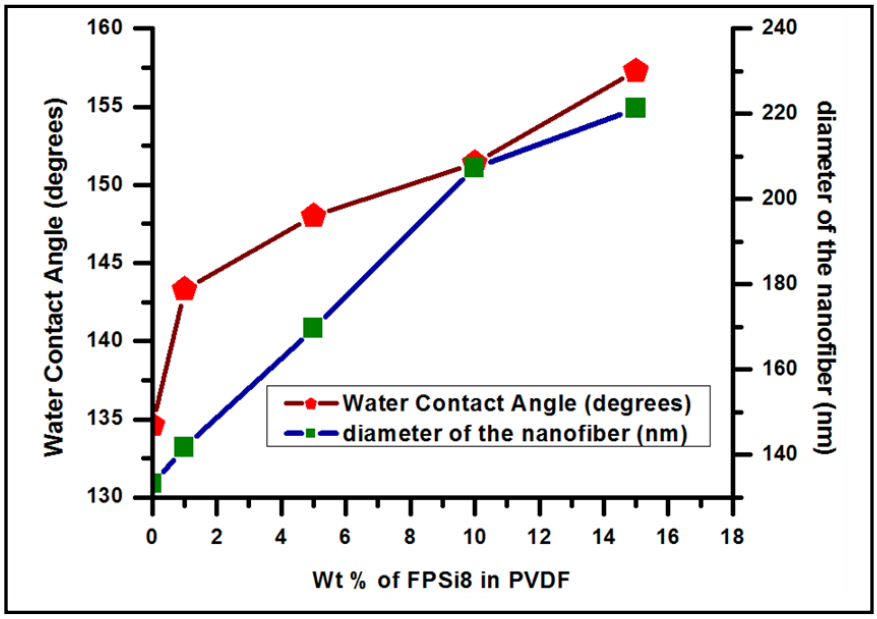

Figure 3.4: Effect of fiber diameter and wt.% of FPSi8 fluoroPOSS on static water contact angle.

Table 3.2: Static water contact angle and respective fiber diameter of different wt.% of FPSi8 fluoroPOSS.

S.No	Wt.% of FPSi8 fluoroPOSS in fluoroPOSS PVDF mixture	Average diameter of nanofibers (nm)	Static Water Contact Angle (degrees)	Sliding angle (SA) (degrees)	Advancing (θ_a) / receding (θ_r) contact angles (degrees)	Contact Angle hysteresis (CAH) (θ_a - θ_r)
1	Plain Glass	NA	48.6 ± 0.8	NA	NA	NA
2	0	133	134.6 ± 1.2	23 ± 0.8	135/123	12
3	1	142	143.3 ± 1.0	14 ± 1.2	147/138	9
4	5	167	148.0 ± 0.9	11 ± 0.7	151/144	7
5	10	207	151.4 ± 1.4	8 ± 1.1	155/151	4
6	15	222	157.3 ± 1.1	< 5 ± 0.9	159/156	3

The electrospun nanofibers could also be removed from the aluminium foil in the form of a freestanding sheet if electrospinning is done for a reasonable amount of time. Figure 3.5 shows a freestanding film of the fluoroPOSS-PVDF containing 15 wt.% of the FPSi8 which was electrospun for 2 h and subsequently removed from the aluminium foil. The superhydrophobicity of the material is demonstrated using dyes of different colors.

Figure 3.5: Trypan and Alizarin red dye solutions (in water) on FPSi8 fluoroPOSS-PVDF electrospun membrane.

4.2. Surface energy of the coating

When a liquid droplet is placed on a flat surface, the spreading of the liquid over the surface is controlled by mechanical and thermodynamic forces [189]. It spreads on the surface until these two forces balance each other. The surface energy exhibited by the coated samples is calculated using Owen-Wendt and Fowkes equations [183,184].

$$\frac{[\sigma_L\,(\cos\theta+1)]}{2} = \sqrt{\sigma_{PS}}\,\sqrt{\sigma_{PL}} + \sqrt{\sigma_{DS}}\,\sqrt{\sigma_{DL}} \quad \text{---- (1)}$$

In the above equations, σ_{PS} and σ_{DS} represents the polar and dispersive components of the coated samples. The sum of these two components gives the total surface energy (σ_S) of the coated sample. σ_{PL} and σ_{DL} represents the polar and dispersive components of the probe liquids (water and ethylene glycol, respectively) and σ_L represents the total surface tension of the probe liquid used for the measurements.'θ' represents the measured static contact angle made by the

probe liquids on the coated glass samples. Measured static contact angle (θ), the standard surface tension values of polar (σ_{PL}) and dispersive component (σ_{DL}) of water and ethylene glycol were substituted in equation 1 which results in the formation of two equations with two unknowns (σ_{PS} and σ_{DS}). By solving the two equations, the values of polar (σ_{PS}) and dispersive component (σ_{DS}) were obtained and the sum of the obtained values gives the surface energy exerted by the coated surface (σ_S). Static contact angle obtained with water and ethylene glycol and the respective surface energies of samples coated with different wt.% of FPSi8 fluoroPOSS are given in Table 3.3. It was observed that the surface energy of the coating decreases with increase in the concentration of FPSi8 fluoroPOSS in the fluoroPOSS-PVDF mixture (Figure 3.6).

Table 3.3: Static water contact angle and surface energy of different wt.% of FPSi8 fluoroPOSS in fluoroPOSS-PVDF coatings.

S.No	Wt.% of FPSi8 fluoroPOSS in fluoroPOSS PVDF mixture	Static Contact Angle of ethylene glycol (degrees)	Static Contact Angle of water (degrees)	Surface Energy mN/m		
				Polar component σ_{PS}	Dispersive component σ_{DS}	Total Surface Energy σ_S
1	0	93.2 ± 1.3	134.6 ± 1.2	6.9	40	46.9
2	1	101.5 ± 1.1	143.3 ± 1.0	8.4	32.9	41.3
3	5	113.3 ± 0.8	148.0 ± 0.9	4.4	19.3	23.7
4	10	120.8 ± 1.0	151.4 ± 1.4	2.9	12.6	15.5
5	15	128.6 ± 0.7	157.3 ± 1.1	2.2	8.3	10.5

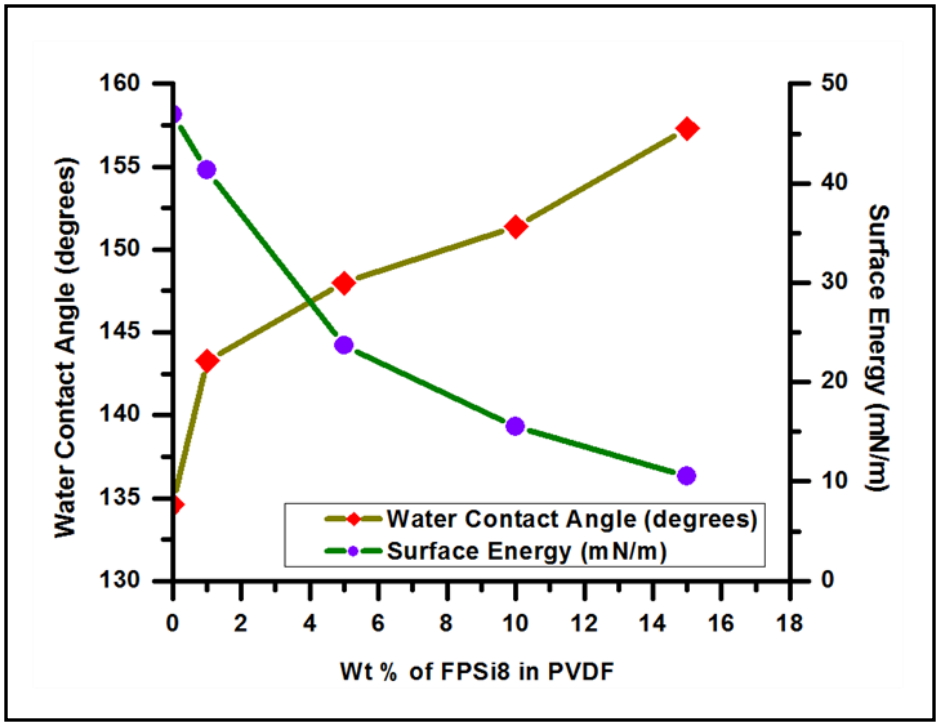

Figure 3.6: Effect of surface energy and wt.% of FPSi8 fluoroPOSS in fluoroPOSS-PVDF mixture on static water contact angle.

4.3. Optical properties

The UV-Vis spectra (in transmittance mode) of FP8 and FPSi8 fluoroPOSS coated samples were studied. Results indicate that the transmittance of the coating was slightly less than that of the plain glass (Transmittance of plain glass: 91.4%). However, the coating was still transparent (see inset of Figure 3.7). It was also observed that FPSi8 fluoroPOSS (15 wt.%) showed a slightly higher transmittance (around 88%) than FP8 fluoroPOSS (around 86%) for coatings of similar thickness (thickness of the coating is around 1 µm ± 15 nm) (Figure 3.7). This difference may be due to the relatively poorer solubility of FP8 fluoroPOSS in PVDF-HFP than that of FPSi8 fluoroPOSS in PVDF-HFP which it may lead to

its aggregation or crystallization during the electrospinning, thus causing the slight decrease in transmittance.

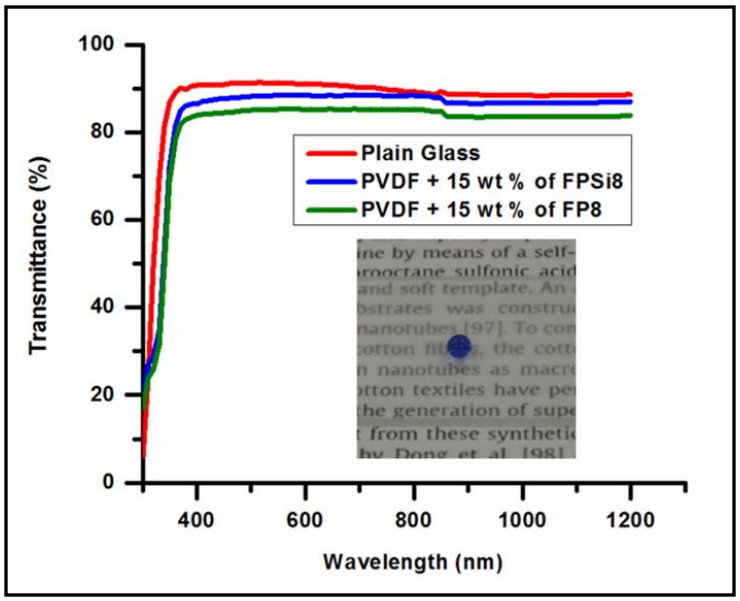

Figure 3.7: Comparison of transmittance of plain, FPSi8 and FP8 fluoroPOSS containing coated glass samples. Inset shows the photograph exhibiting the interaction of Trypan blue dye (water solution) with FPSi8 fluoroPOSS coated sample.

4.4. Peel-off and durability tests

A 90° peel-off test was conducted on the FPSi8 fluoroPOSS coated sample using an adhesion tape (3M scotch tape). The tape was peeled-off from the coated surface (test distance: 40 mm) by applying a fixed force of 1 N. After the peel-off test, it was observed that the coating remained stable without forming any cracks/scratches on the surface. The samples before and after peel-off test were imaged under SEM to check for the presence of cracks, if any. The images confirm that there were no changes even in micrometer scale regimes (Figure 3.8). The coated samples were kept in an environment which was maintained at

Standard Ambient Temperature and Pressure condition (temperature: 25 ± 2 ºC; pressure: 0.986 atm; humidity: 40-60%) [214]. Water contact angle measurements were carried out on bi-weekly basis (Table 3.4). The results indicated that the coating is environmentally stable and retained the superhydrophobic property.

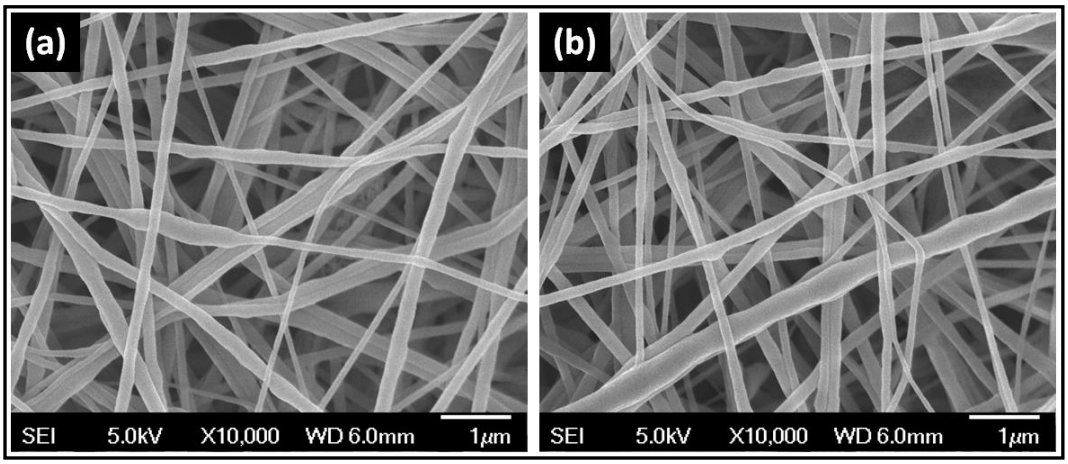

Figure 3.8: SEM images (a) before peel-off test; (b) after peel-off test; The SEM images confirm that the coating remained stable without forming any cracks/scratches on the surface.

Table 3.4: SCA measurements of the superhydrophobic coated samples when kept in SATP (Standard Ambient Temperature and Pressure) conditions.

S. No	Time duration (in weeks)	Surface contact angle made by water droplet (degrees)
1	After 2 weeks	157.1
2	After 4 weeks	157
3	After 6 weeks	157.2
4	After 8 weeks	156.8

5. Conclusion

Transparent, superhydrophobic fluoroPOSS-PVDF-HFP nanocomposite coatings were fabricated on glass substrates using two different kinds of fluoroPOSS materials (i.e. FP8 and FPSi8) by electrospinning. The synthesized nano structures were characterized using SEM, EDS and spectrophotometry. The fabricated coatings exhibited continuous, uniform and non-beaded nanofibers. The optical properties and superhydrophobic properties such as surface wettability and surface energy were studied. The results show that the water contact angle increased with increase in concentration of fluoroPOSS in PVDF-HFP. As the concentration of fluoroPOSS increases, the viscosity of the solution increases and as a result the fiber diameter increases thereby enhancing the superhydrophobic property. 15 wt.% of FPSi8 fluoroPOSS in PVDF coating exhibited a very high static contact angle (157.3º) with low surface energy (around 10 mN/m). This type of POSS-based nanocomposite materials would be utilized as transparent superhydrophobic coating for self-cleaning application.

However, current industrial needs are beyond dust and particulate pollutants cleaning. Today, in addition to the regular dust and particulate pollutants, the surfaces are exposed to several other pollutants like oil, crease, industrial wastes, smoke, automobile exhaust, corrosive chemicals etc.

Hence, in order to have an efficient self-cleaning system with enhanced properties, the coating should have the ability to repel organic liquids in addition to water.

Chapter 4 will discuss about the fabrication of transparent self-cleaning amphiphobic surface (surface that has the ability to repel water and organics) using lubricating polymer (Perfluoropolyether, PFPE).

Note: The research work presented in Chapter 3 has been published in Journal of Materials Chemistry (V. A. Ganesh, A. S. Nair, H. K. Raut, T. T. Yuan Tan, C. He, S. Ramakrishna and J. Xu, *J. Mater. Chem.*, 2012, 22, 18479-18485) and reproduced with permission of The Royal Society of Chemistry.

(Link: http://pubs.rsc.org/en/content/articlelanding/2012/jm/c2jm33088a)

Chapter 4

Amphiphobic coating

4. Electrospraying of lubricating material to fabricate robust and transparent amphiphobic surfaces

1. Introduction

Superhydrophobic surfaces provide effective self-cleaning ability for dust and particulate pollutants. However, the current industrial and architectural sectors demand for surfaces that have the ability to repel organic liquids in addition to water [190-208]. The advancement in the field of designing oleophobic/superoleophobic surfaces (oil repellent surfaces) is relatively slow. This is because the surface tension of non-polar liquids is very low, hence engineering surfaces that can de-wet these liquids involves complicated micro/nano structures designs, overhangs, and re-entrant surface curvatures [143-150]. Nonetheless, recently developed lubricants infused textured surfaces have gained lots of attention because these surfaces use a thin layer of lubricating material that offers a smooth, transparent, and homogeneous interface which provides an exceptional slippery surface to a broad range of liquids [1,160].

In this work we have developed a transparent amphiphobic surfaces using Perfluoropolyether (PFPE, a lubricating liquid). PFPE is a nontoxic, biologically inert, fire resistant and highly transparent lubricating liquid with a very low surface tension and volatility. It is immiscible with both aqueous and hydrocarbon

phases. Hence it can form a stable interface with several polar and non-polar liquids.

Herein, we have employed electrospraying technique to produce a thin layer of Perfluoropolyether on a smooth glass surface to achieve amphiphobicity (ability to repel water and organic solvents). In this method, the liquid dispensing nozzle (needle) is maintained at very high electrical potential and hence, the liquid at the outlet of the needle is subjected to an electrical shear stress. As a result, the droplet sprayed onto the substrate can be extremely small and the size of the droplet can be controlled by adjusting the flow rate and the voltage applied to the needle [209-210]. This is a cost-effective technique and can deposit nanoparticles on large scale by a simple set-up consisting of sol-gel solution, a collector and high voltage power supply.

To achieve a homogeneous coating of pure PFPE on a flat surface is extremely difficult, due to the poor adhesion of PFPE with the surface (glass/silicon) [160]. In present work, we have addressed this issue by adding a small amount of (tridecafluoro-1,1,2,2-tetrahydrooctyl)-1-trichlorosilane (FTS) with PFPE. The FTS interacts with PFPE and also with the substrate, resulting in the formation of a homogeneous, transparent, thin blended surface (PFPE + FTS) over the substrate. The transmittance of the coating was around 91% and the surface contact angles achieved using conc. NaOH (sodium hydroxide, γ = 85 mN/m), water (γ = 72.1 mN/m), conc. H_2SO_4 (sulphuric acid, γ = 55.1 mN/m), and acetone (γ = 23.1 mN/m) were measured to be 119º, 116º, 99.5º and 40.8º, respectively.

2. Experimental section

2.1. Materials

Perfluoropolyether (PFPE) (Fomblin, Sigma-Aldrich, Mw = 2500 g/mol), (tridecafluoro-1,1,2,2-tetrahydrooctyl)-1-trichlorosilane (FTS, Alfa Aesar, 97%), iso-propanol, ethanol, methanol, acetone, chloroform, acetic-acid, toluene, *N*,*N*-dimethylformamide (DMF), ethylene glycol, glycerol, di-iodomethane, hexadecane, dodecane, conc. sulphuric acid (95-97%), conc. sodium hydroxide (1 M solution), hydrogen peroxide (31% H_2O_2 with 69% water) (all from Aldrich), and de-ionized water were used without any further purification.

2.2. Solution and substrate preparation

The sol-gel solution for electrospraying was prepared as follows: an optimized proportion of about 25 µL (0.0675 mM) of FTS was added to 2 mL (1.52 mM) of PFPE (the surface contact angle and the transmittance measurements were also made on the thin films fabricated using higher molar ratios of FTS with PFPE. As the values are similar, it is concluded that 25 µL of FTS in 2 mL of PFPE is the optimum proportion for thin film formation. Please refer Table 4.1).

Table 4.1: SCA and Transmittance measurements of amphiphobic coated samples fabricated using different amount of FTS in PFPE.

S. No	Amount of FTS (µL)	Amount of PFPE (mL)	Surface contact angle made by water droplet (degrees)	Surface contact angle made by acetone droplet (degrees)	Transmittance (%)
1	0	2	NA	NA	NA
2	25	2	116	40.8	91%
3	50	2	116.3	41	90.8%
4	75	2	115.7	40.4	91%
5	100	2	115.8	40.3	90.7%

Slide glass plates (24 mm × 24 mm × 1.2 mm) were thoroughly cleaned by ultra-sonication in de-ionized water, ethanol, acetone, and iso-propanol, respectively, for about 15 min each. To ensure that the glass slides are free from surface contaminants, they were cleaned with Piranha solution for 2 h (3:7 by volume of 30% H_2O_2 and H_2SO_4) followed by rinsing in de-ionized water. The cleaned glass plates were dried in an oven at 80 °C.

2.3. Electrospraying

The sol-gel solution was loaded into the electrospinning/spraying machine (NANON, MECC- Japan). The washed and dried microscopic glass slides were then mounted on a flat collector wrapped with aluminium (Al) foil. The applied voltage was set to 30 kV and the distance between the needle (27G 1/2) tip and the static collector was set to 10 cm. The humidity level in the electrospraying chamber was maintained between 50 and 60%. The FTS-PFPE solution was electrosprayed on the glass substrates for 20 min with the flow rate of about 1 mL h^{-1} to deposit a uniform layer of FTS-PFPE particles on the glass substrate. The

coated surfaces were subsequently annealed at 80 ºC for 8 h. After curing, the coated glass substrates were washed thoroughly with ethanol and acetone to remove the excess unreacted solution. The samples were then dried at 80 ºC for few minutes before characterization.

3. Instrumentation and characterization

The samples for scanning electron microscopy (SEM) were platinum sputtered and the images were captured using a field emission SEM instrument (FESEM, JEOL FESEM JSM-6700F) operated at 5 kV. The thickness of the film was measured by a surface profiler (Alpha-Step IQ Surface Profiler). The contact angle measurements (static, advancing, receding and slipping angles) were carried out using a contact angle measurement setup (VCA optima contact angle equipment from AST Products) in static/dynamic sessile drop mode at room temperature. The surface contact angle values reported were the averages of at least ten measurements made on different areas of the coated sample. The transmittance was measured using a Shimadzu SolidSpec 3700 UV-vis-NIR Spectrometer. Atomic Force Microscopic (AFM) images of the coated samples were taken using an Atomic Microscope Nanowizard 3 machine (JPK, Germany). X-ray photoelectron spectroscopy (XPS) was done using AXIS-HSi spectrometer (Kratos Analytical). Al K_α X-ray radiation ($h\nu$ = 1486.6 eV) was employed with an incident angle of 30º and collected at a take-off angle of 50º with respect to the surface normal. The analysis area and analysis depth were nearly 400 nm and 10 nm, respectively. Survey spectrum and high-resolution spectra of elements were acquired for elemental composition analysis and identification of chemical state

of the elements. Low energy electron flooding was adopted for charge compensation and carbon correction was made using the standard software from the manufacturer.

4. Results and discussion

4.1. Fabrication of amphiphobic surface

PFPE is a nontoxic, biologically inert, fire resistant and highly transparent lubricating liquid with very low surface tension and volatility. It is immiscible with aqueous and hydrocarbon phases (see Scheme 4.1 for the structure of PFPE employed). Hence it can form a stable interface with several polar and non-polar liquids. This material was, therefore, chosen for fabricating transparent amphiphobic surface by the electrospraying process. However, as explained by Ma *et al.*, it is difficult to achieve a stable homogeneous thin film of PFPE on a flat surface [160].

To overcome this issue, a small amount of FTS (see Scheme 4.1 for its structure) is added with PFPE. When FTS is added to PFPE, the solution mixing happens due to the Van der-Waal's force of attraction between (-CF_2-) present in the backbone chain of FTS and (-CF_2-) of PFPE, which leads to the proper mixing/coiling with the backbone chain. The solution was then electrosprayed (see Scheme 4.2 for a schematic of the electrospraying process employed) on a glass substrate followed by curing at 80 ºC for 8 h resulting in the formation of a smooth (surface roughness: < 5 nm), homogeneous, transparent and thin

(thickness: 180 ± 20 nm approx.) blended surface (PFPE + FTS) over the glass substrate.

The interaction mechanism between PFPE and FTS on the substrate is explained as follows. The highly reactive end groups of FTS bonds covalently with the substrate due to the formation of Si-O-Si bond. As a result of this, PFPE will also be able to form a layer along with FTS due to the Van der Waals's force of attraction that exists between FTS and PFPE (as explained before). During thermal annealing process, the air pockets and the residues will be removed; resulting in the formation of compact and dense layer of FTS + PFPE blended film. The excess/unbounded solution is removed from the substrate by ultra-sonication process.

A comparison of the FT-IR spectra of PFPE, FTS and their mixture (PFPE + FTS) reveal insights on the possible interaction of PFPE and FTS with the substrate (Figure 4.1). The IR spectrum of the mixture showed shifts and broadening of peaks at 1265, 1198, 1149 cm^{-1}, respectively, which are due to the interaction of PFPE with the highly reactive FTS reagent. The peak at 1149 cm^{-1} could be due to Si-O-Si bond formation between the PFPE + FTS mixture and the substrate. High resolution XPS scan (C1s) shows the presence of (-O-CF_2-) and (-O-CF_2-O) peaks which further confirms the presence of PFPE along with FTS on the substrate inducing the amphiphobic property (Figure 4.2). XPS wide scan spectrum of the thin film (PFPE + FTS blended surface) further confirms the elemental composition (Figure 4.3).

Perfluoropolyether (PFPE)

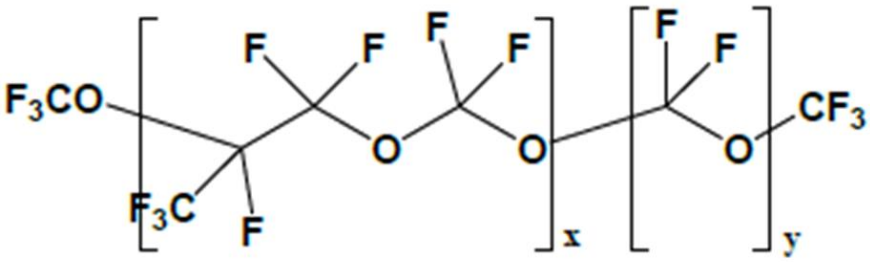

(tridecafluoro-1,1,2,2-tetrahydrooctyl)-1-trichlorosilane (FTS)

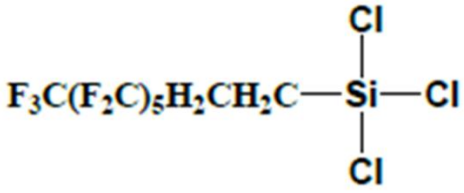

Scheme 4.1: Chemical structure of PFPE and FTS.

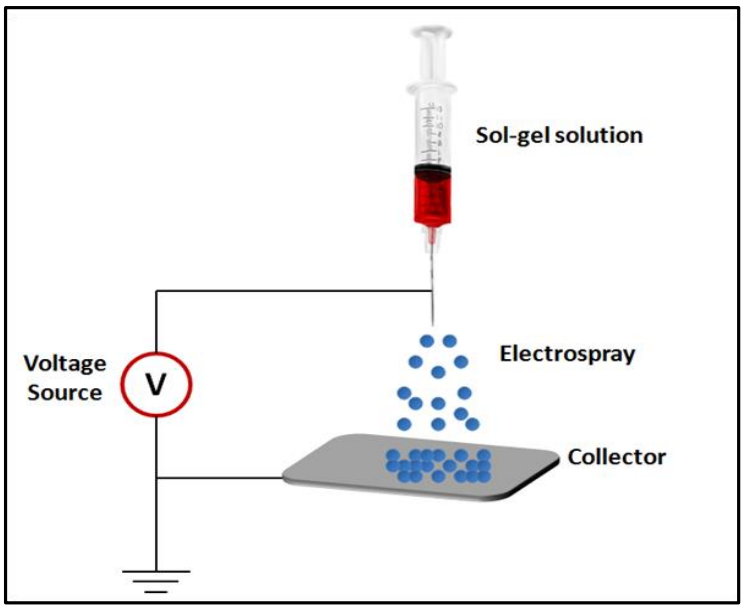

Scheme 4.2: Schematic representation of Electrospraying set-up employed.

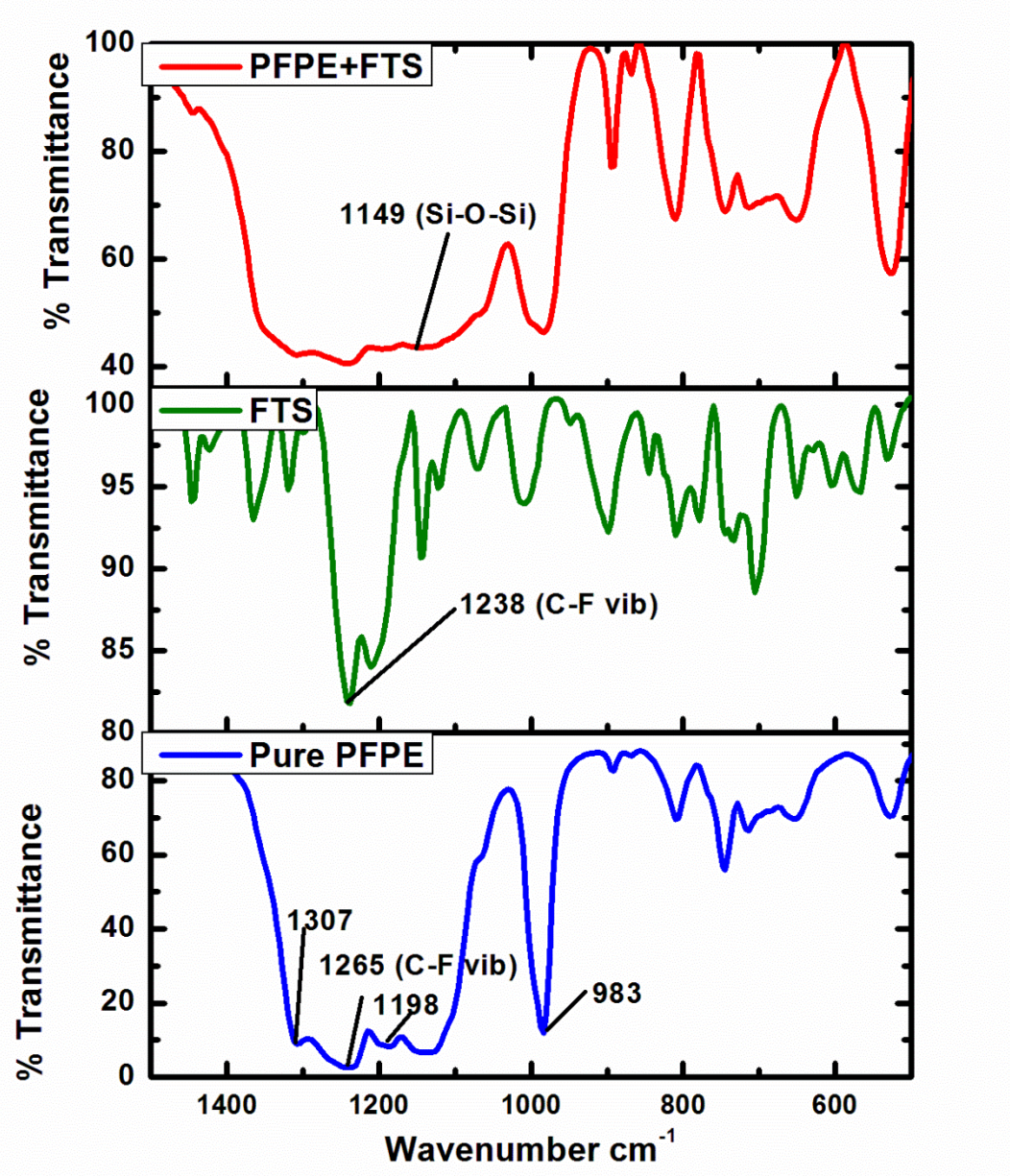

Figure 4.1: A comparison of the FT-IR spectra of the PFPE, FTS and their blended surface (PFPE + FTS).

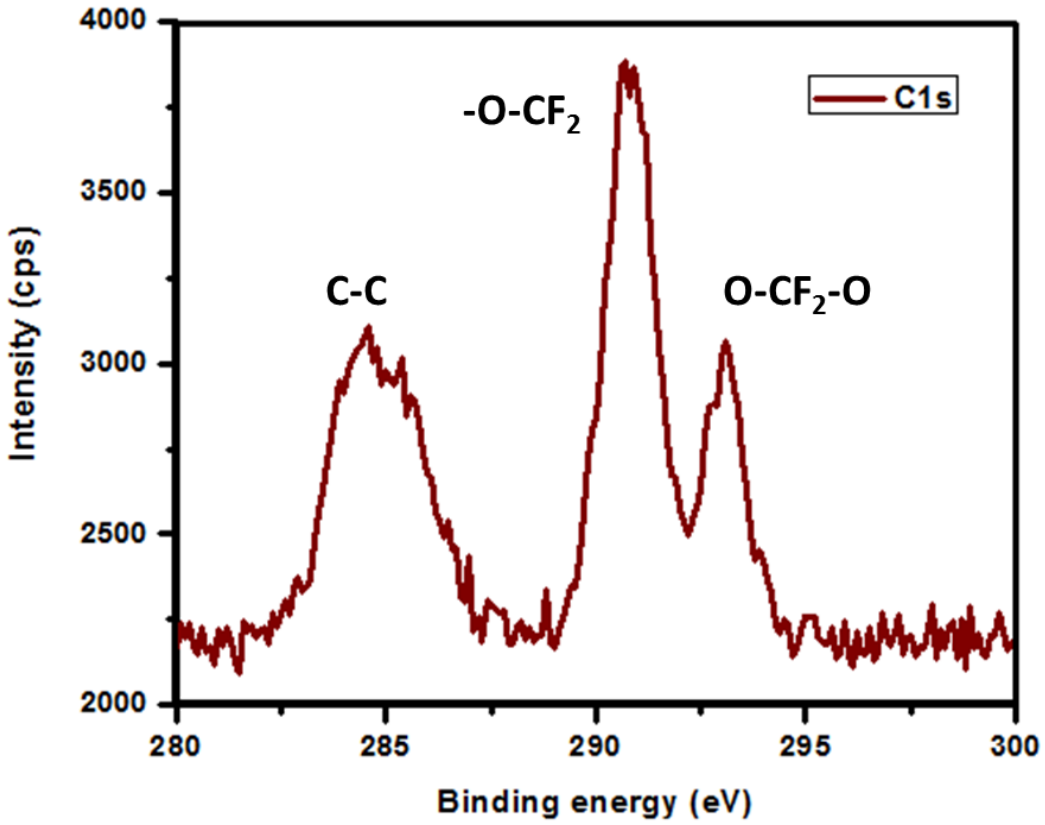

Figure 4.2: High resolution XPS pattern of Carbon (1s) showing the (-O-CF_2) and (-O-CF_2-O) peaks of electrosprayed PFPE + FTS blended surface.

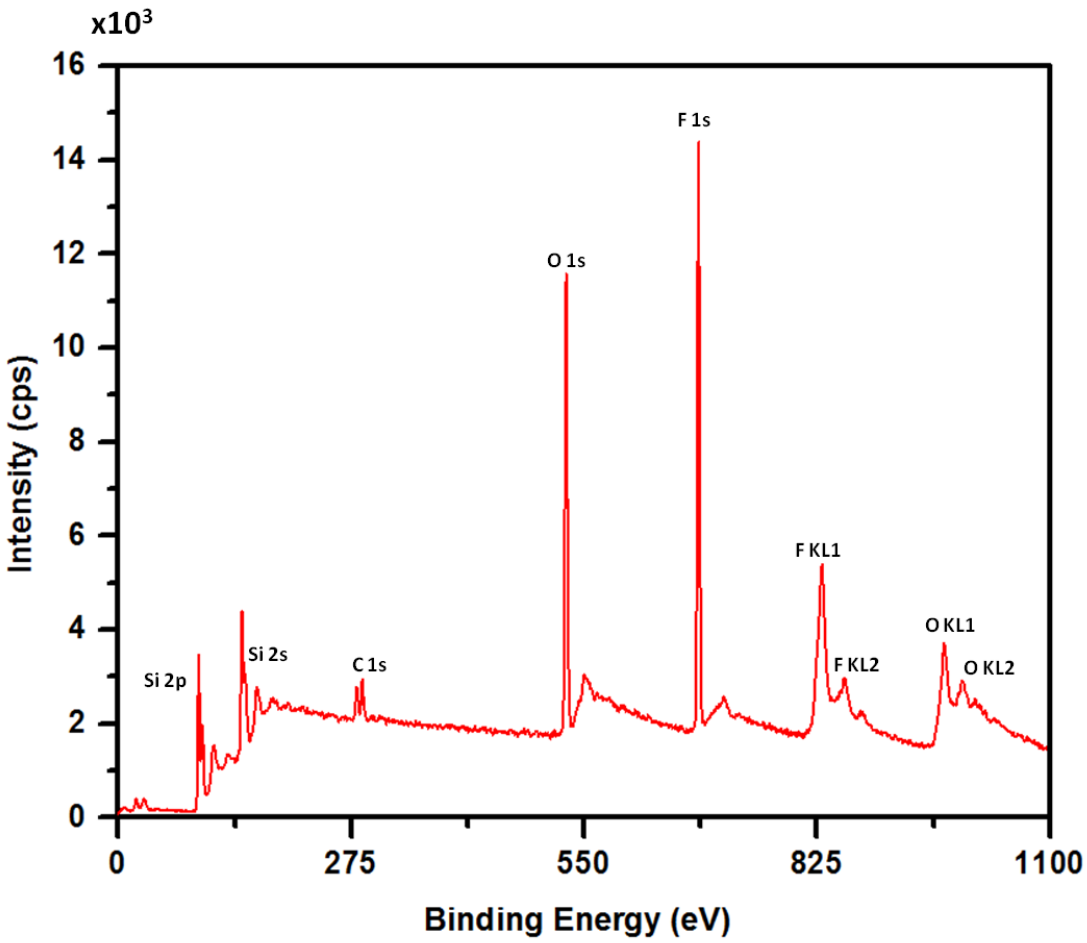

Figure 4.3: Wide scan XPS pattern showing the elemental compositions of electrosprayed PFPE + FTS blended surface.

Figure 4.4 (a), (b) and (c) show the optical microscope, SEM and AFM images, respectively, of the coated sample (coated with the FTS and PFPE mixture) exhibiting a homogenous and uniform film over the glass substrate. Figure 4.5 shows the optical microscope images of the electrosprayed samples with and without the addition of FTS in PFPE. It is observed that the pure PFPE coating gets de-wetted from the glass surface and it goes away when washed with acetone/ethanol (Figure 4.5). On the other hand, the presence of FTS has induced

the stacking of PFPE layers, resulting in the formation of a continuous and uniform thin film (Figure 4.4). As evident from the proposed interaction mechanism, in a blended surface, the low surface energy group tends to move to the surface which facilitates a decrement in the overall free energy of the system [211-213]. The thin film exhibited amphiphobic property.

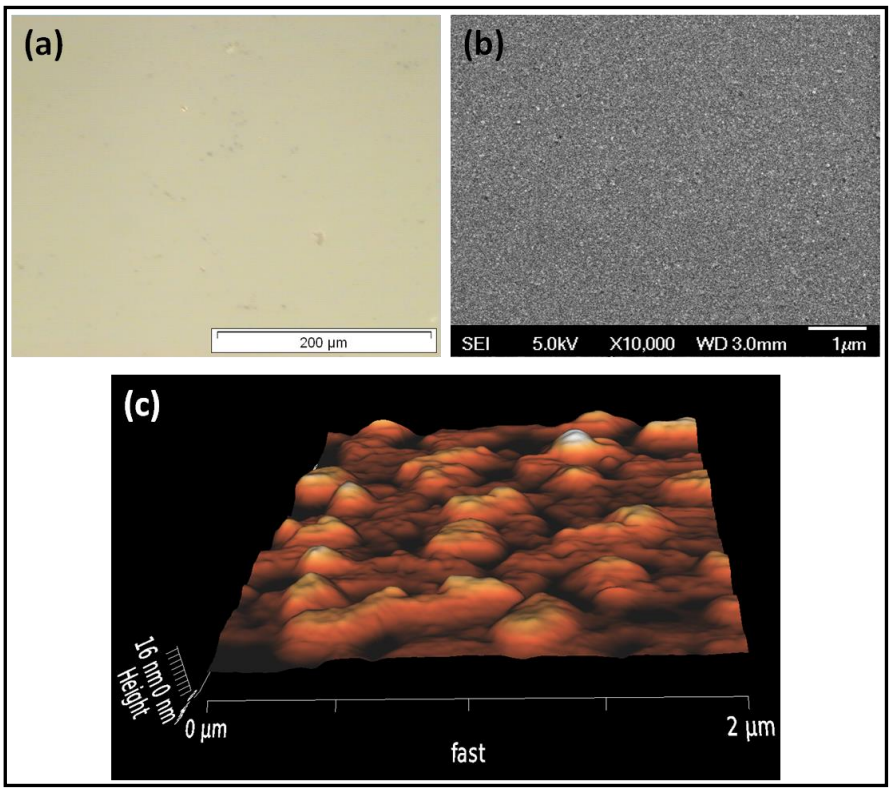

Figure 4.4: Images of electrosprayed PFPE + FTS blended surface. (a) Optical microscopic; (b) SEM; (c) AFM images.

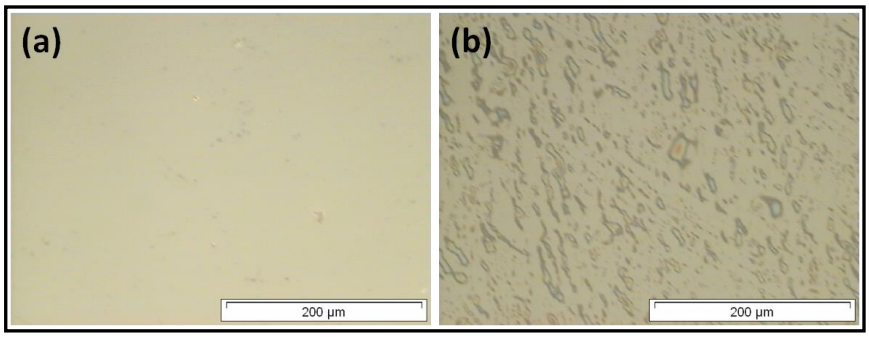

Figure 4.5: Optical microscopic images of (a) electrosprayed PFPE + FTS blended surface; (b) electrosprayed pure PFPE surface.

The contact angle and the sliding angle (SA) made by the water droplet (2 µL) on the coated sample was measured to be 116º ± 2.5 and 6º ± 0.6, respectively. Besides water repellency, the coated surface also exhibited excellent repellency for non-polar liquids and even for some solvents like acetone, chloroform, toluene and ethanol. The surface contact angles (SCA) and sliding angles and the advancing (θ_a)/receding angles (θ_r) were measured for several liquids with different surface tension values by using a "tilting base contact angle measurement set-up" and the contact angle hysteresis (CAH) was calculated by taking the difference of advancing and receding angles (Table 4.2; Figure 4.6). The CAH achieved for water, acetone, conc. H_2SO_4 and conc. NaOH was measured to be 5, 8, 7 and 5º, respectively. The drops (2 µL) of acetone and ethanol can slip at very low tilting angles (10º). However, the slipping rate strongly depends on the value of the tilting angles. We believe that the exceptional de-wetting behaviour of the coated surface is primarily due to the immiscible property of PFPE with various liquids and the high chain mobility of PFPE [1,160].

Table 4.2: Surface contact angle and sliding angle measurements of liquids with different surface tension on an amphiphobic coated glass substrate.

Liquid	**Surface Tension (mN/m)**	**Surface contact angle (degrees)**	**Sliding angle (Slipping angle) (degrees)**
Isopropanol	20.9	36.5	10
Ethanol	21.8	37.3	10
Methanol	22.5	39.1	10
Acetone	23.1	40.8	10
Dodecane	25.3	41.9	9
Chloroform	27.1	43.2	9
Acetic Acid	27.3	55.8	10
Hexadecane	27.4	62.4	10
Toluene	28.5	61.7	9
N,*N*-dimethyl formamide	37.1	68.6	8
Ethylene Glycol	48.2	77.2	8
Di-iodomethane	50.8	89.5	8
Conc. sulfuric acid	55.1	99.5	8
Glycerol	64	107.5	7
Water	72.8	116	6
Conc. hydrogen peroxide	79.7	117.5	5
Conc. sodium hydroxide	85	119	5

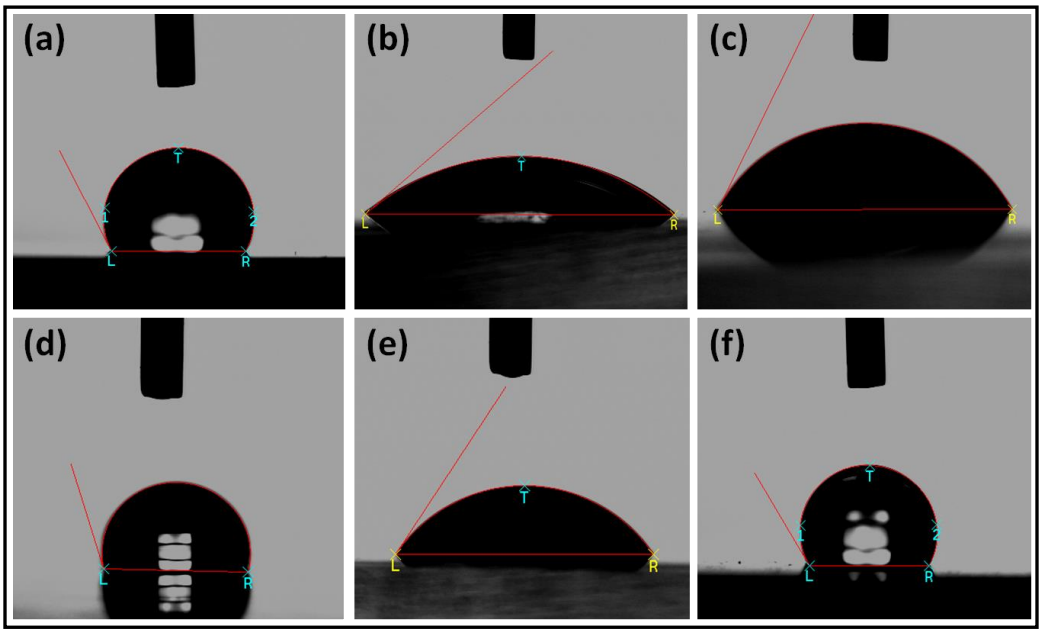

Figure 4.6: Interaction of liquid droplets with different surface tension. (a) Water (WCA: 116º); (b) Acetone (SCA: 40.8º); (c) *N*,*N*-dimethylformamide (SCA: 68.6º); (d) conc. sulfuric acid (SCA: 99.5º); (e) conc. acetic acid (SCA: 55.8º); (f) conc. sodium hydroxide (SCA: 119º).

4.2. Surface energy calculation

The surface energy exhibited by the amphiphobic surface was calculated using Owens-Wendt and Fowkes equations [183,184].

$$\frac{[\sigma_L\,(\cos\theta+1)]}{2} = \sqrt{\sigma_{PS}}\,\sqrt{\sigma_{PL}} + \sqrt{\sigma_{DS}}\,\sqrt{\sigma_{DL}} \quad \text{--- (1)}$$

In the above equation, σ_{PS} and σ_{DS} represent the polar and dispersive components of the coated samples. The sum of these two components gives the total surface energy (σ_S) of the coated sample. σ_{PL} and σ_{DL} represent the polar and dispersive components of the probe liquids (water and di-iodomethane, respectively, in the present case). σ_L represents the total surface tension of the

probe liquid used for the measurements. 'θ' represents the measured static contact angle made by the probe liquids on the coated glass samples. Measured static contact angle (θ) and the standard surface tension values of polar (σ_{PL}) and dispersive components (σ_{DL}) of water and di-iodomethane were substituted in equation (1) which resulted in the formation of two equations with two unknowns (σ_{PS} and σ_{DS}). By solving the two equations, the values of polar (σ_{PS}) and dispersive components (σ_{DS}) were obtained and the sum of the obtained values gives the surface energy of the amphiphobic surface (σ_S). The static contact angle values made by water and di-iodomethane droplets on the amphiphobic surface were 116º and 89.5º, respectively. Hence the surface energy of the amphiphobic surface was calculated to be (σ_S) 12.5 ± 0.5 mN/m.

4.3. Optical properties

A comparison of the UV-Vis spectra (in transmittance mode) of plain glass and amphiphobic coated glass sample is shown in Figure 4.7. Results indicated that the transmittance of plain glass and the amphiphobic glass were very similar (around 91%) for the entire wavelength range (300-1200 nm). This further implies that the coating did not affect the optical properties of the glass (mainly the light transmittance), which makes this coating suitable for applications in window and solar modules. The sol-gel solution is also coated on the silicon substrate and the amphiphobic property is studied (Table 4.3, Inset in Figure 4.7). It is observed that the coating remained stable and exhibited amphiphobic property irrespective of the type and nature of the substrate over

which it is coated. This shows that the coating is suitable for industrial and commercial applications as well.

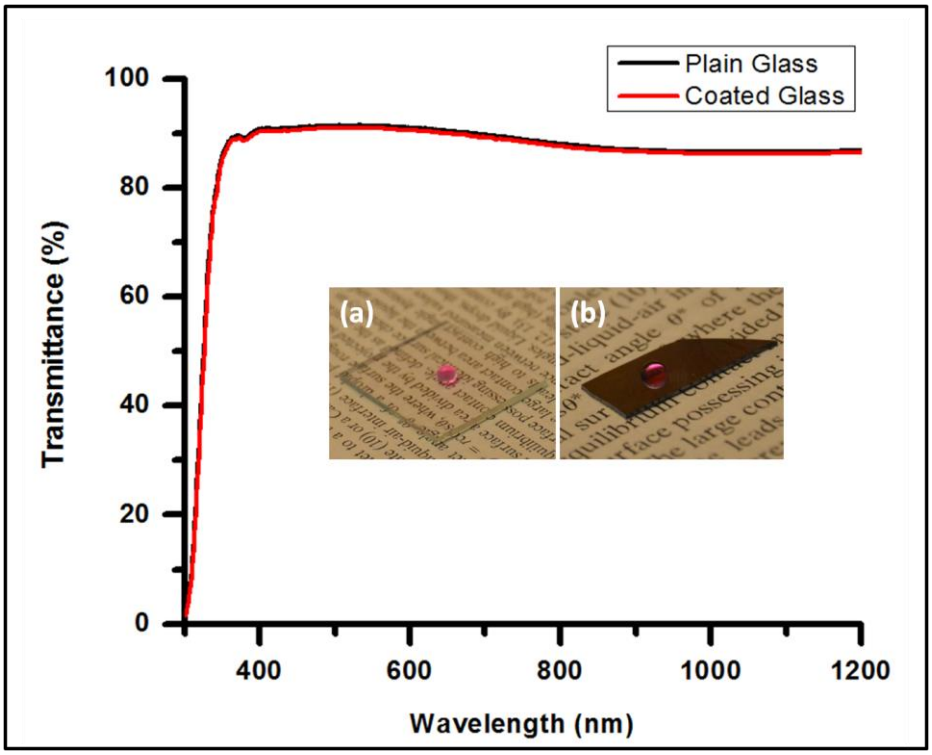

Figure 4.7: Comparison of the transmittance of the plain and amphiphobic coated glass samples. Inset shows the photograph of glycerol droplets (pink - dyed with rhodamine B) on the amphiphobic surfaces fabricated on different substrates; (a) Coated Glass (b) Coated Silicon.

Table 4.3: Surface contact angle measurements of liquids with different surface tension on amphiphobic coatings made over different substrates.

S. No	Substrate	Surface Contact Angle made by water droplet (degrees)	Surface Contact Angle made by acetone droplet (degrees)
1	Glass	116	40.8
2	Silicon	115	40.6

4.4. Peel-off and durability tests

A 90° peel-off test was conducted on the coated sample using an adhesion tape (3M scotch tape). The tape was peeled-off from the coated surface (test distance: 40 mm) by applying a fixed force of 2.5 ± 0.1 N. After the peel-off test, it was observed that the coating remained stable without forming any cracks/scratches on the surface. The samples before and after peel-off test were imaged under optical microscope and SEM, respectively, to check for the presence of cracks, if any. The images confirm that there were no changes even in micrometer scale regimes (Figure 4.8). The coated samples were kept in an environment which was maintained at Standard Ambient Temperature and Pressure condition (temperature: 25 ± 2 ºC; pressure: 0.986 atm; humidity: 40-60%) [214]. Surface contact angle measurements for water and acetone were carried out on bi-weekly basis (Table 4.4). The results indicated that the coating is environmentally stable and retained the amphiphobic property.

Table 4.4: SCA measurements of the amphiphobic coated samples when kept in SATP (Standard Ambient Temperature and Pressure) conditions.

S. No	Time duration (in weeks)	Surface contact angle made by water droplet (degrees)	Surface contact angle made by acetone droplet (degrees)
1	After 2 weeks	116	41
2	After 4 weeks	115.6	40.7
3	After 6 weeks	115.5	40
4	After 8 weeks	115.2	40.3

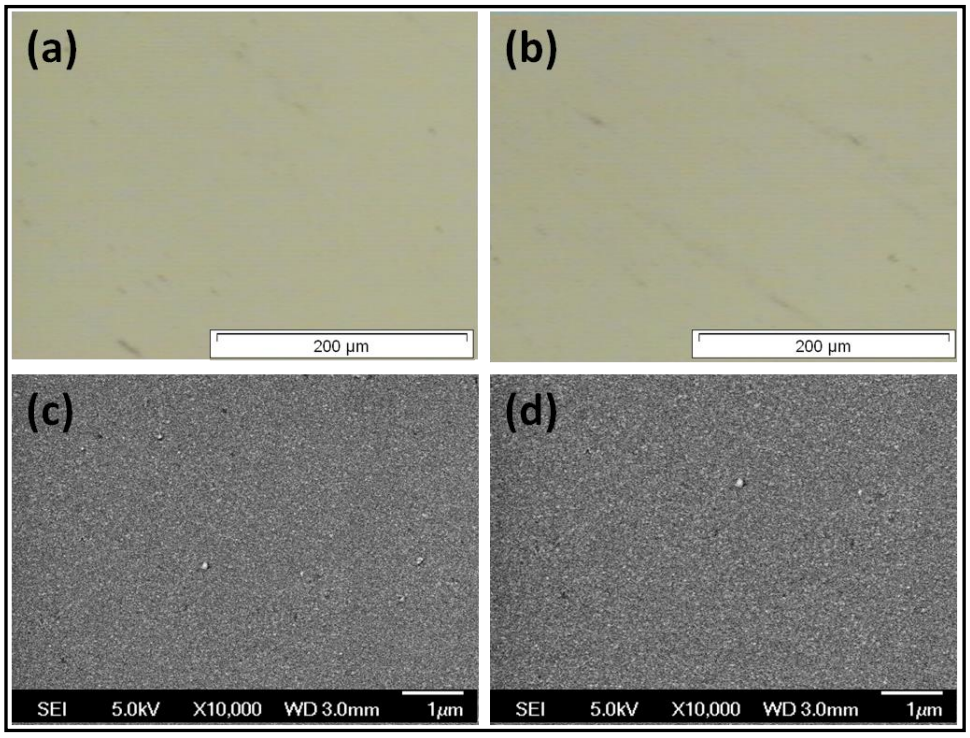

Figure 4.8: Optical microscopic images (a) before peel-off test; (b) after peel-off test; SEM images (c) before peel-off test; (d) after peel-off test; The SEM and optical microscopic images further confirm that the coating remained stable without forming any cracks/scratches on the surface.

5. Conclusion

In summary, a thin, transparent and homogeneous coating of perfluoropolyether (PFPE, a lubricating material) was produced on a glass surface by electrospraying technique. It was difficult to produce a homogeneous coating of PFPE alone on a flat surface due to the poor adhesion of PFPE with the surface (glass/silicon). This issue was addressed by adding a small amount of (tridecafluoro-1,1,2,2-tetrahydrooctyl)-1-trichlorosilane (FTS) with PFPE. The FTS facilitated stacking of PFPE layers, resulting in the formation of homogeneous, transparent, and highly slippery surface. The PFPE+FTS blended

surface was characterized by spectroscopy and microscopy. The coated surfaces (PFPE and FTS blended surface) exhibited amphiphobic property with surface contact angle values with conc. NaOH, water, conc. H_2SO_4, and acetone being 119º, 116º, 99.5º and 40.8º, respectively. The coatings were transparent and exhibited strong adhesion with the glass substrate, thus revealing the potential for applications in windows and solar modules.

Surface contact angle values achieved for organics using PFPE + FTS (amphiphobic) coating is < 120º. Nonetheless, for an improved and enhanced self-cleaning effect, the SCA values made by organics should be > 150º.

Chapter 5 and 6 will discuss about the fabrication of electrospun superamphiphobic surfaces using metal oxide nanostructures. The coatings developed using metal oxide nanostructures will be hard and have better mechanical properties when compared to the polymer coatings.

Note: The research work presented in Chapter 4 has been submitted to *Advanced Materials Interfaces* for publication.

Chapter 5

Superamphiphobic coating

5. Superamphiphobic coating from electrospun TiO_2 nanostructures

1. Introduction

In order to have an effective and enhanced self-cleaning effect, the surface contact angle achieved for water and organics should be > 150º. Furthermore, as the self-cleaning coatings are continuously exposed to open atmosphere, which is very hostile, we believe that the coatings must possess excellent mechanical strength in addition to exceptional liquid repellent properties. Hence, metal oxides were chosen for further studies to fabricate mechanically robust superamphiphobic surfaces.

Here we describe a simple and scalable way to fabricate a superior self-cleaning coating that exhibits exceptional superamphiphobic property. Electrospinning technique is employed to fabricate a coating consisting of porous rice-shaped TiO_2 nanostructures, which upon fluorinated silane treatment turns into superamphiphobic surface. The surface contact angle achieved using water ($\gamma = 72.1$ mN/m) and hexadecane ($\gamma = 27.5$ mN/m) were 166º ± 0.9 and 138.5º ± 1, respectively. The contact angle hysteresis for a droplet of water and hexadecane were measured to be 2º and 12º, respectively.

2. Experimental section

2.1. Materials

Polyvinyl acetate (Sigma Aldrich, Mw = 500,000), *N,N*-dimethylacetamide (DMAc, 99.8%, GC Grade, Aldrich, Germany), (tridecafluoro-1,1,2,2-tetrahydrooctyl)-1-trichlorosilane (Alfa Aesar, 97%), acetic acid (99.7%, LAB-SCAN Analytical Sciences, Thailand), absolute ethanol (Fisher Scientific, 99.5%), de-ionized water, ethylene glycol, glycerol, and di-iodomethane were used without any further purification.

2.2. Solution and substrate preparation

The sol-gel solution for the deposition of TiO_2 nanostructures on glass substrate was prepared as follows. About 1.2 g of polyvinyl acetate was added to 10 mL of *N,N*-dimethylacetamide (DMAc). This was followed by the addition of a TiO_2 sol prepared by mixing 2 mL of acetic acid and 1 mL of titanium (IV) iso-propoxide. The prepared solution was stirred at room temperature for about 12 h to acquire sufficient viscosity for electrospinning.

Microscopic slide glass plates (24.4 mm × 76.2 mm × 1.2 mm) were thoroughly cleaned by ultra-sonication in de-ionized water, ethanol, acetone, and isopropanol, respectively, for about 15 min each. To ensure that the glass slides are free from surface contaminants, they were cleaned with Piranha solution (3:7 by volume of 30% H_2O_2 and H_2SO_4) followed by rinsing in de-ionized water. The cleaned glass plates were dried in an oven at 80 ºC.

2.3. Electrospinning

The solution containing the TiO_2 precursor was loaded into the electrospinning machine (NANON, MECC-Japan). The washed and dried microscopic glass slides were then mounted on a flat collector wrapped with aluminium foil. The applied voltage was set to 30 kV and the distance between the needle (27G ½) tip and the static collector was set to 10 cm. The humidity level in the electrospinning chamber was maintained between 50 and 60%. The PVAc-TiO_2 precursor solution was electrospun on the glass substrate for 15 min with a flow rate of about 1 mL h^{-1} to deposit a uniform layer of PVAc-TiO_2 composite nanofibers on the glass substrate. The PVAc-TiO_2 composite nanofibers upon heat treatment process (500 ºC for 1 h) results in finely distributed porous rice-shaped TiO_2 nanostructures.

2.4. Chemical vapour deposition of fluorinated silane

After heat treatment (annealing) process, the porous rice-shaped TiO_2 coated glass samples were superhydrophilic in nature. In order to reduce the surface energy and to induce the superamphiphobic property into the superhydrophilic structures, the coated samples were put inside a desiccator along with a glass bottle containing 50 µL of fluorinated silane for 3 h under vacuum (Scheme 5.1). The samples were then subjected to characterization.

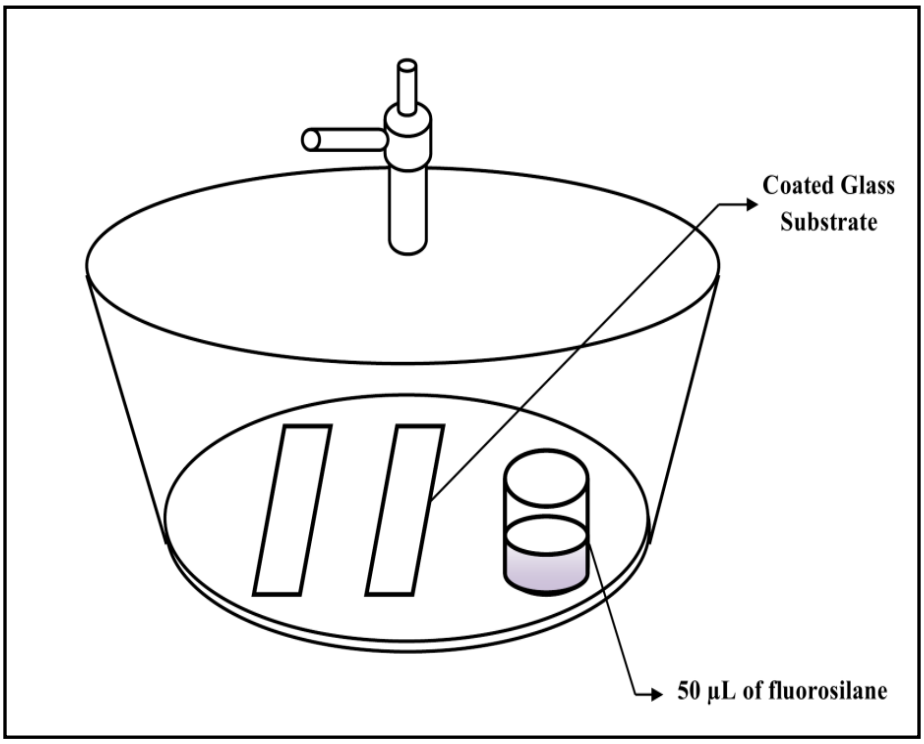

Scheme 5.1: Schematic showing the arrangement inside the desiccator.

3. Instrumentation and characterization

The samples for scanning electron microscopy (SEM) were gold sputtered and the images were captured using a field emission SEM instrument (FESEM, JEOL FESEM JSM-6700F) operated at 5 kV. The energy dispersive X-ray spectroscopy (EDS) data were also obtained from the same machine. The thickness of the film was measured by a surface profiler (Alpha-Step IQ Surface Profiler). The contact angle measurements (static, advancing, receding and roll-off angles) were carried out using a contact angle measurement setup (VCA optima contact angle equipment from AST Products) in static/dynamic sessile drop mode at room temperature. The surface contact angle values reported were the averages of at least five measurements made on different areas of the coated sample. Thermogravimetric analysis (TGA, TA Instruments Q100) was performed to study the degradation behavior of the sol-gel and formation of oxide. X-ray Diffraction (XRD) pattern was obtained using General Area Detector Diffraction System (Bruker D8,GADDS-XRD). TEM images of the sintered rice-shaped nanostructures were taken by a high resolution transmission electron microscope (HR-TEM, JEOL 3010 operated at 300 kV). The sample for the HR-TEM was prepared by dispersing the sintered TiO_2 powder (TiO_2 nanofibers were deposited on the aluminium foil and after sintering, the pure TiO_2 material was scratched off from the aluminium foil) in methanol under sonication and then a drop of this suspension is allowed to dry on a carbon coated copper grid.

4. Results and discussion

4.1. Fabrication of superamphiphobic surface

The rice-shaped TiO_2 obtained from electrospun PVAc-TiO_2 (PVAc - Polyvinly acetate) composite nanofibers was used to fabricate superamphiphobic coating (Scheme 5.2).

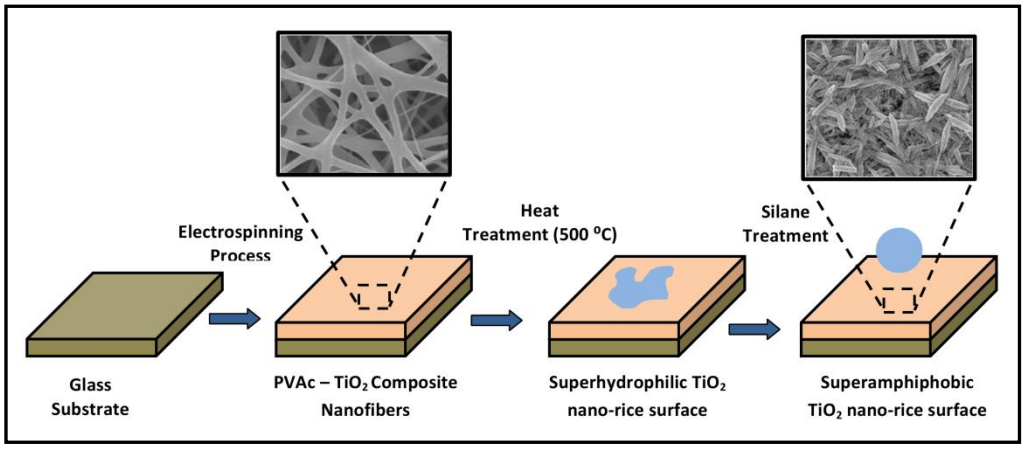

Scheme 5.2: Fabrication of Superamphiphobic Coating: Process flow chart (this schematic is not drawn to scale).

A thick layer (2 µm) of electrospun PVAc-TiO_2 composite nanofibers (average fiber diameter: 125 ± 15 nm) were deposited on the cleaned glass substrate. The coated glass samples were then sintered at 500 ºC for 1 h (in air medium) with a ramping rate of 5 ºC per min. During the heat treatment process, the continuous fiber morphology breaks down resulting in the formation of rice-shaped TiO_2 nanostructures. The uniquely shaped nanostructures were the result of micro-scale phase separation between the PVAc and the TiO_2 occurring during the sintering process (note that if PVP, polyvinyl pyrrolidone, is used instead of

PVAc, the result will always be continuous TiO_2 nanofibers and not the rice-shaped TiO_2) [177,178]. Electrospinning is essential to get the rice-shaped structures as the same evolved from the smooth electrospun fibers were interconnected and well defined in size, shape and porosity [215-218]. The degradation of the polymer (PVAc) from the PVAc-TiO_2 composite imparts high porosity (and hence surface roughness) to the TiO_2 nanostructures (BET surface area of ~ 60 m^2/g) [178].

Figure 5.1 (a) and (b) shows the low and high magnification SEM images of the electrospun TiO_2 coated sample, exhibiting a uniform distribution of porous rice-shaped nanostructures. Figure 5.1 (c) shows the TEM image of a single nano-rice structure. From the image, it could be observed that a single TiO_2 nanostructure is made of numerous spherical particles with an average diameter of 12-15 nm. The TGA analysis (Figure 5.2) and the EDS spectrum (inset in Figure 5.1 (c)) confirmed that after the heat treatment process, the sample was free from polymer or other organics [219].

The lattice resolved TEM image (*d* spacing = 0.35 nm, Figure 5.1(d)) and XRD measurement (Figure 5.1(e)) further confirmed that the coating contained particles of anatase TiO_2.

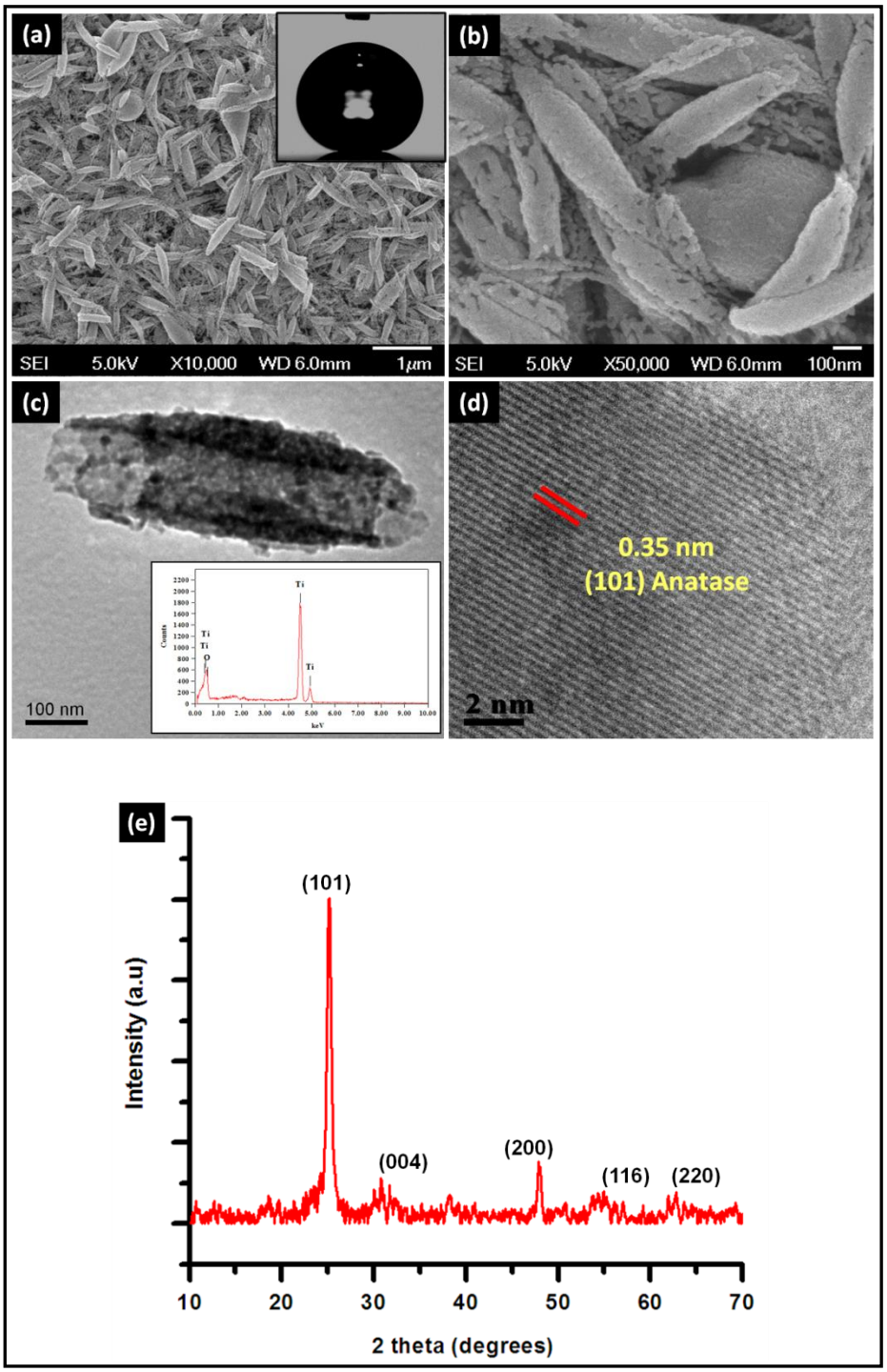

Figure 5.1: (a), (b) SEM images (low and high magnification) of the TiO_2 coated samples (inset: interaction of water droplet (1 μL) with the coated surface. WCA: 166°); (c) TEM image of a single nano-rice structure (inset: EDS spectrum of the TiO_2 coated sample); (d) the lattice-resolved image; (e) XRD of the TiO_2 coated sample sintered at 500 °C.

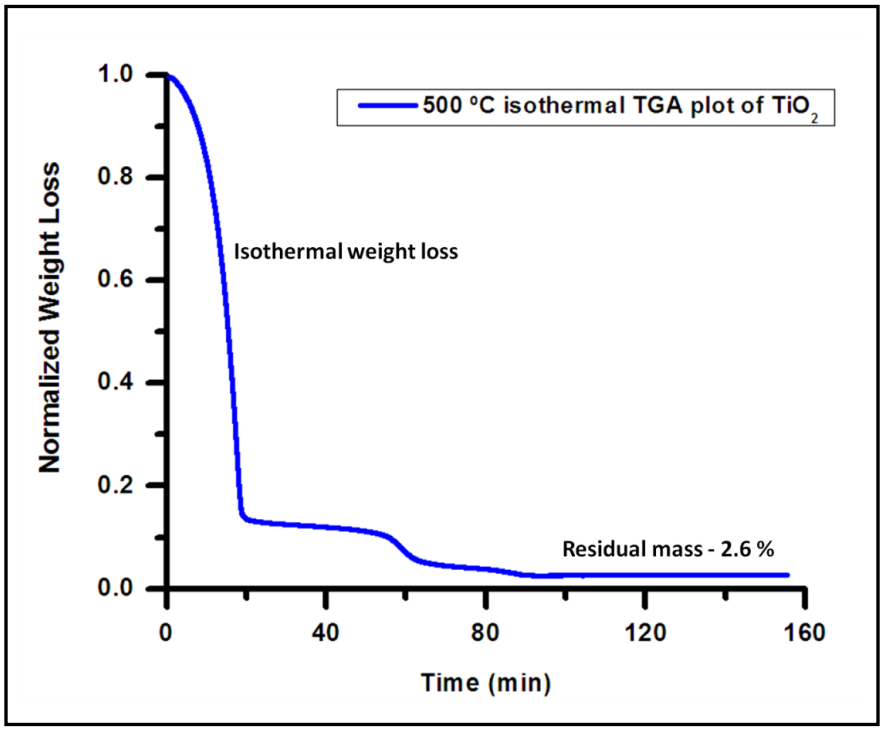

Figure 5.2: TGA analysis of TiO_2 sol-gel solution showing the mass losses during the isothermal heating at 500 ºC.

The rice-shaped TiO_2 coated samples (thickness of the coating: 375 ± 10 nm) exhibited superhydrophilic property (water contact angle, WCA approx. equal to 0) [220]. In order to reduce the surface energy of the superhydrophilic TiO_2 nanostructures, the samples were coated with fluorinated silane for 3 h using chemical vapor deposition (CVD) process (Scheme 5.1). The high porosity and hence the large surface area of the nanostructures ensured sufficient intake of flourosilane upon silane treatment. After silanization, the coating exhibited superamphiphobic property with contact angle as high as 166º and 158.3º, respectively, were achieved for 1 µL droplet of water and glycerol (Figure 5.3).

It must also be noted that the rice like structures were actually made of very small spherical particles of 12-15 nm sizes (see TEM image) and the innumerable number of such small fluorinated particles prevent water/oil from wetting the surfaces resulting in superamphiphobicity. Due to the extremely low adhesion and surface energy, it was very tough to deposit water droplet on the coating. The water droplet (2 µL) immediately started rolling-off when it comes in contact with the coated surface.

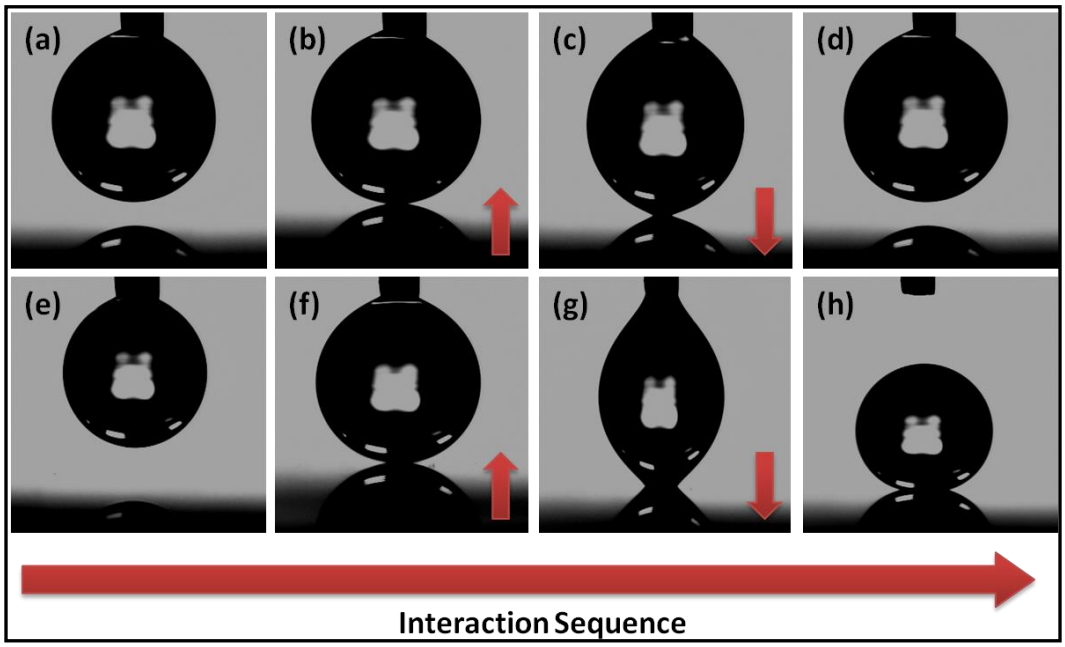

Figure 5.3: (a) - (d) shows the interaction of water droplet (1µL) with superamphiphobic surface; (e) - (h) shows the interaction of glycerol droplet (1µL) with the superamphiphobic surface (SCA: 158.3º).

The surface contact angle (SCA), roll-off angle and the advancing (θ_a)/receding angle (θ_r) were measured for several liquids with different surface tension (such as water, glycerol, di-iodomethane, ethylene glycol, vegetable oil, dodecane and hexadecane) by using a 'tilting base surface contact angle measurement set-up' and the contact angle hysteresis (CAH) was calculated by taking the difference of advancing and receding angles (Table 5.1, Figure 5.4 and 5.5). The CAH achieved for water, ethylene glycol and hexadecane were 2º, 8º and 12º, respectively.

Table 5.1: Surface contact angle and roll-off angle measurements of liquids with different surface tension on a superamphiphobic glass substrate.

S. No	Liquid	Surface Tension (mN/m)	Surface Contact Angle (degrees)	Advancing (θ_a) / Receding (θ_r) contact angles (degrees)	Contact Angle Hysteresis (CAH) ($\theta_a - \theta_r$) (degrees)	Roll-off angle (RA) / Sliding angle (SA) (degrees)
1	Water	72.1	166 ± 0.9	169/167	2	1 ± 1 (RA)
2	Glycerol	64	158.3 ± 0.7	160/156	4	6 ± 1 (RA)
3	Di-iodomethane	50.9	155.7 ± 0.8	157/150	7	9 ± 1 (RA)
4	Ethylene glycol	47.3	152.6 ± 1.1	155/147	8	9 ± 1 (RA)
5	Vegetable oil	34.5	147.3 ± 1	153/142	11	13 ± 1 (SA)
6	Hexadecane	27.4	138.5 ± 1	147/135	12	15 ± 1 (SA)
7	Dodecane	25.3	127.6 ± 0.7	138/124	14	15 ± 2 (SA)

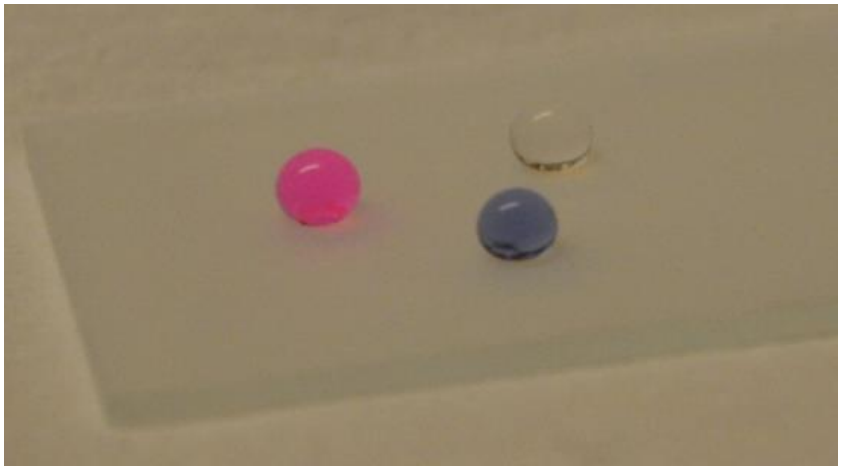

Figure 5.4: Photograph of water (blue - dyed with trypan blue dye), glycerol (pink - dyed with rhodamine B) and ethylene glycol (colorless) droplets on the superamphiphobic surface.

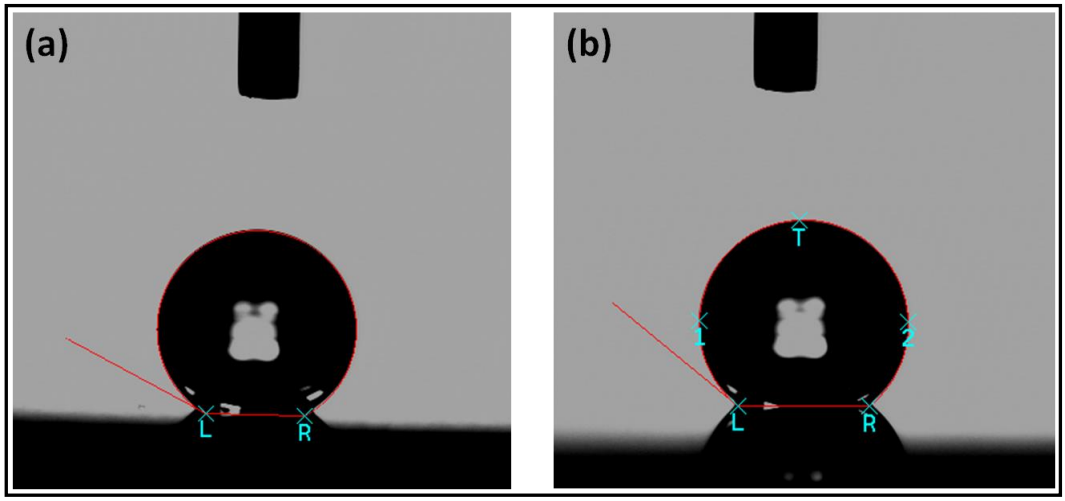

Figure 5.5: Interaction of (a) vegetable oil droplet (SCA = 147.3º) and (b) hexadecane droplet (SCA = 138.5º) with the coated surface.

4.2. Hardness and modulus measurements

To analyze the mechanical stability of the coated samples, indentation studies were carried out using a nanoindentation setup equipped with a Berkovick tip. The measurements were conducted at five different places of the coated sample and the average hardness & Young's modulus values of the coating were measured to be 0.12 ± 0.031 GPa and 3.26 ± 0.711 GPa, respectively (Table 5.2).

Table 5.2: Hardness and modulus values of the coated sample.

Test Number	Young's Modulus (GPa)	Hardness (GPa)
1	2.6394	0.1094
2	2.9419	0.0865
3	3.2094	0.0938
4	4.4802	0.1557
5	3.0471	0.1471

4.3. Peel-off and durability tests

A 90º peel-off test was conducted on the coated sample using an adhesion tape (3M scotch tape). The tape was peeled-off from the coated surface (Test distance: 50 mm) by applying a fixed force of 5 ± 0.1 N. After the peel-off test, it was observed that the coating remained stable without forming any cracks/scratches on the surface (Figure 5.6). The samples before and after peel-off test were imaged under SEM to check whether there was any change in the

morphology of the nanostructures. Images in Figure 5.6 confirm that there were no changes even in micrometer scale regimes.

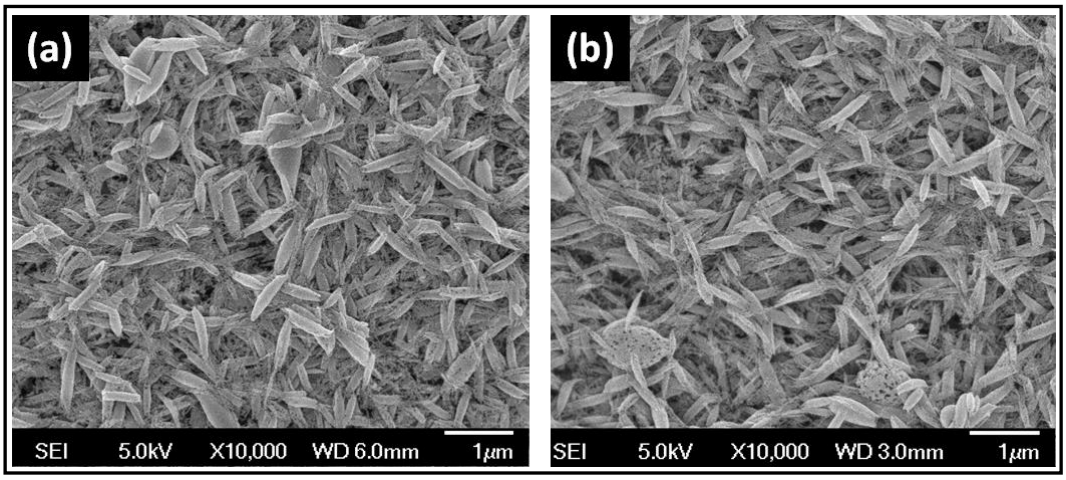

Figure 5.6: SEM images of (a) before peel-off test; (b) after peel-off test. The SEM images further confirm that the coating remained stable without forming any cracks/scratches on the surface.

The coated samples were placed in an environment which was maintained at Standard Ambient Temperature and Pressure condition (Temperature: 25 ± 2 ºC; Pressure: 0.986 atm., humidity: 40-60%) [214]. SCA measurements for water, ethylene glycol and hexadecane were carried out on bi-weekly basis (Table 5.3). The results indicated that the coating is environmentally very stable and retained the superamphiphobic property.

Table 5.3: SCA measurements of the superamphiphobic coated samples when kept in SATP (Standard Ambient Temperature and Pressure) conditions.

S. No	Time duration (in weeks)	Surface Contact Angle made by water droplet (SCA) (degrees)	Surface Contact Angle made by ethylene glycol droplet (SCA) (degrees)	Surface Contact Angle made by hexadecane droplet (SCA) (degrees)
1	After 2 week	165.9	151.6	138.7
2	After 4 weeks	166.6	152.4	138
3	After 6 weeks	166.1	152	138.1
4	After 8 weeks	166.4	152.7	138.2

5. Conclusion

To summarize, we have fabricated a robust superamphiphobic coatings on the glass substrate from electrospun TiO_2 rice-shaped nanostructures. The electrospun PVAc-TiO_2 composite nanofibers on sintering resulted in the formation of porous superhydrophilic rice shaped nanostructures which upon silanization turn into superamphiphobic surface. The synthesized coatings were characterized using SEM, EDS, XRD, TEM and TGA. The superamphiphobic property of the coatings was studied. The results indicated that the porous electrospun anatase TiO_2 films were able to exhibit superamphiphobic property with surface contact angle values achieved for water (γ = 72.1 mN/m) and hexadecane (γ = 27.5 mN/m) were 166º and 138.5º, respectively.

The fabricated TiO_2 coating exhibited exceptional superamphiphobic property. The transmittance achieved using this coating is around 74% (Figure 5.7). However, optical and architectural applications demands for coatings with much higher transmittance.

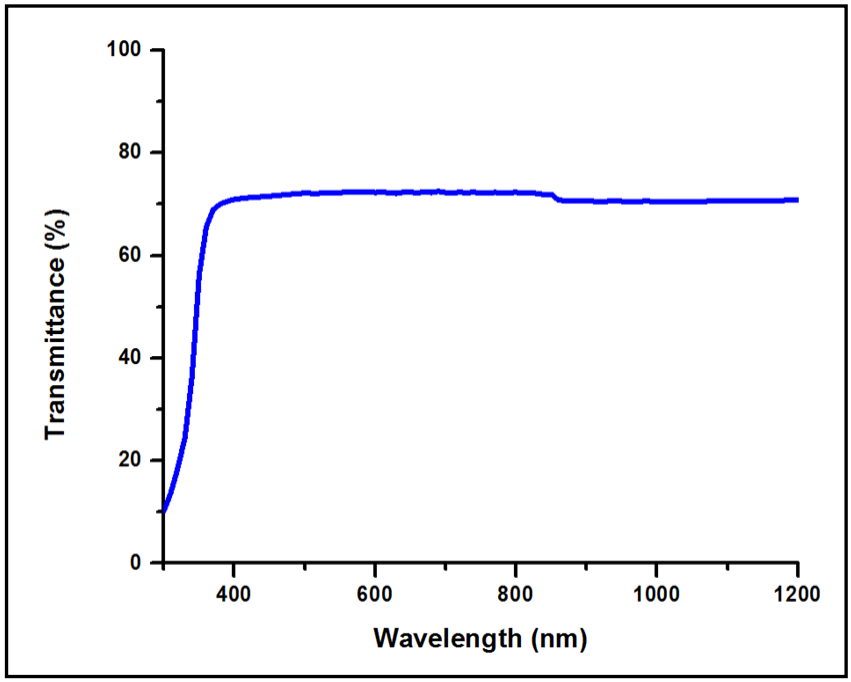

Figure 5.7: Transmittance of superamphiphobic coated glass samples.

Chapter 6 will discuss about the fabrication of transparent superamphiphobic surfaces using SiO_2 nanostructures. The coatings developed using SiO_2 nanostructures will be hard and have better mechanical and optical properties making it highly suitable for windows and other architectural applications.

Note: The research work presented in Chapter 5 has been published in ACS Applied Materials & Interfaces and reproduced with permission from [V. A. Ganesh, S. S. Dinachali, A. S. Nair and S. Ramakrishna, *ACS Appl. Mater. Interfaces*, 2013, 5, 1527-1532], Copyright [2013] American Chemical Society.

(Link: http://pubs.acs.org/doi/abs/10.1021/am302790d)

Chapter 6

Transparent superamphiphobic coating

6. Transparent superamphiphobic coating from electrospun SiO_2 nanostructures

1. Introduction

Though the TiO_2 coating exhibited exceptional superamphiphobic property, the refractive index of anatase TiO_2 is 2.48. Therefore, there is a considerable decrease in the transmittance of the fabricated superamphiphobic coating [221]. In order to have a superamphiphobic coating with better optical properties, the refractive index of the coating material should be less. Hence, we have chosen SiO_2 (refractive index: 1.55) to develop superamphiphobic coating with good optical and mechanical properties [222].

In this work, we have employed electrospinning to deposit SiO_2 nanofibers uniformly on glass substrate. The SiO_2 nanofibers act as a template to fabricate superamphiphobic coatings. The nanofiber template was produced by depositing electrospun SiO_2 nanofibers on the glass substrate and the coated substrates were then subjected to vapor deposition process to obtain the desired superamphiphobic property. The transmittance of the coating was around 85% and the surface contact angles achieved using water ($\text{surface tension}, \gamma =$

72.1 mN/m) and hexadecane ($\gamma = 27.5$ mN/m) were 161°± 0.8 and 146.5°± 0.7, respectively.

2. Experimental section

2.1. Materials

Triethoxysilane (TS) (Sigma Aldrich, 95%), polyvinyl pyrrolidone (Sigma Aldrich, Mw = 1,300,000), *N*,*N*-dimethylformamide (DMF, 99.8%, GC Grade, Aldrich, Germany), tetraethylorthosilicate (TEOS) (Sigma Aldrich, 98%), acetic acid (99.7%, LAB-SCAN Analytical Sciences, Thailand), ammonia solution (Merck, 25%), (tridecafluoro-1,1,2,2-tetrahydrooctyl)-1-trichlorosilane (Alfa Aesar, 97%), de-ionized water, hexadecane, ethylene glycol, glycerol and di-iodomethane were used without any further purification.

2.2. Solution and substrate preparation

The sol-gel solution for the deposition of SiO_2 on glass substrate was prepared as follows: 1.2 g of polyvinyl pyrrolidone was added to 10 mL of *N*,*N*-dimethylformamide. This was followed by the addition of a SiO_2 sol prepared by mixing 2 mL of acetic acid and 1 mL of tetraethylorthosilicate. The prepared solution was stirred at room temperature for about 10 h to acquire sufficient viscosity for electrospinning.

Microscopic slide glass plates (24.4 mm × 76.2 mm × 1.2 mm) were thoroughly cleaned by ultra-sonication in de-ionized water, acetone, ethanol and iso-propanol, respectively, for about 10 min each. To ensure that the glass plates

are free from surface contaminants, they were cleaned with piranha solution (3:7 by volume of 30% H_2O_2 and H_2SO_4) followed by rinsing in de-ionized water. The cleaned glass plates were dried in an oven at 100 ºC.

2.3. Electrospinning

The SiO_2 precursor solution was loaded into the electrospinning machine (NANON, MECC- Japan). The washed and dried microscopic glass slides were then mounted on an aluminum foil-wrapped static collector. The applied voltage was set to 30 kV and the distance between the needle (27G ½) tip and the static collector was set to 10 cm. The humidity level in the electrospinning chamber was maintained between 50 and 60%. The SiO_2 precursor solution was electrospun on the glass substrate for 30 min with a flow rate of about 1 mL h^{-1} to produce a uniform coating.

2.4. Deposition of triethoxysilane (TS)

The as-spun SiO_2 nanofiber coated glass slides were kept inside a desiccator with two bottles containing 2 mL of ammonia solution and TS respectively (Scheme 6.1). According to Stöber reaction, TS undergoes hydrolysis followed by condensation to form a nano porous silica membrane. Ammonia acts as a catalyst in this reaction [223]. To facilitate uniform deposition of silica over the nanofibers, the desiccator setup should not be disturbed for 24 h [224,225]. After deposition, the samples were heat treated to around 600 ºC for 2 h (in air medium) with a ramping rate of 10 ºC per min. During the heat treatment process, the polymer, solvent/acid residues diffuse through the porous silica membrane and subsequently evaporate resulting in the formation of a hybrid silica network containing SiO_2 nanofibers enclosed by an ultrathin layer of porous silica membrane [156]. The resulting hybrid coating on the glass was transparent, uniform and superhydrophilic in nature. In order to transform the superhydrophilic surface into superamphiphobic surface, the coated samples were put inside a desiccator along with a glass bottle containing 40 µL of fluorinated silane for 2 h. The samples were then subjected to characterization.

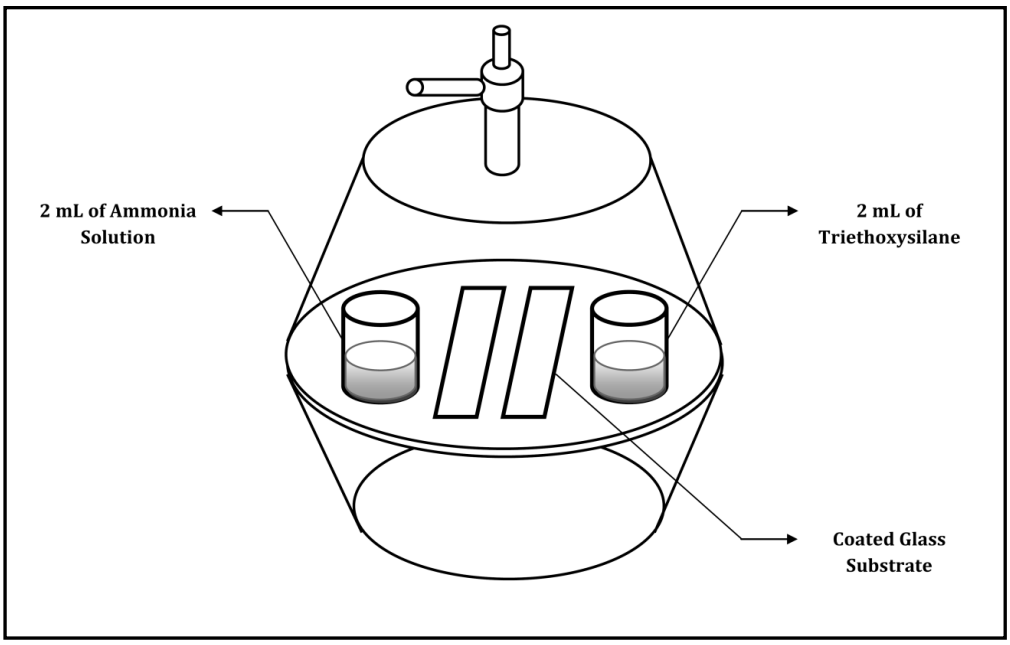

Scheme 6.1: Schematic diagram showing the arrangement inside the desiccator.

3. Instrumentation and characterization

The samples for scanning electron microscopy (SEM) were platinum sputtered and the images were recorded using a field emission SEM instrument (FESEM, JEOL FESEM JSM-6700F) operated at 5 kV. The same machine was used to obtain the energy dispersive X-ray spectroscopy (EDS).The thickness of the film was measured by a surface profiler (Alpha-Step IQ Surface Profiler) and the optical properties were examined by UV-Vis spectroscopy (Shimadzu UV-3600 UV-VisNIR spectrophotometer) with a spectral resolution of 1 nm. The contact angle measurements (static, advancing, receding and roll-off angles) were carried out using a contact angle measurement setup (VCA optima contact angle

equipment from AST Products) in static/dynamic sessile drop mode at room temperature. The surface contact angle values reported were the averages of at least five measurements made on different areas of the coated sample. Thermogravimetric analysis (TGA, TA Instruments Q100) was performed to follow the degradation behavior of the sol-gel and formation of oxide. Hardness and modulus values of the coating were measured by nanoindentation set-up (Agilent Nanoindenter, G200 equipped with a Berkovich tip). X-ray Diffraction (XRD) pattern was obtained using General Area Detector Diffraction System (Bruker D8, GADDS-XRD).

4. Results and discussion

4.1. Fabrication of transparent superamphiphobic surface

Herein, the one-dimensional morphology of electrospun nanofibers was used as a template to fabricate superamphiphobic coating (Scheme 6.2). A thick layer (2.3 μm) of electrospun SiO_2 nanofibers were deposited on the cleaned glass substrate. (Figure 6.1 (a) and (c)) show the low and high magnification SEM images of the as-spun SiO_2 nanofibers (average fiber diameter: 110 ± 10 nm).

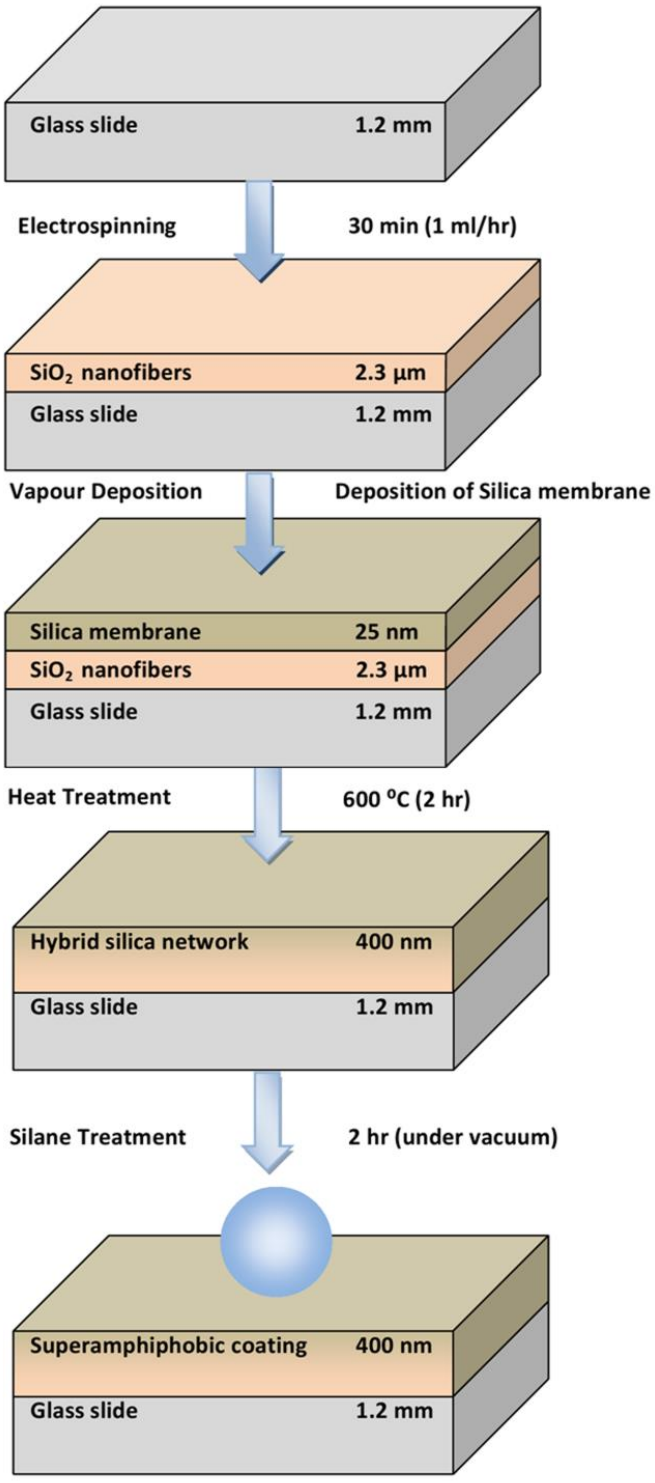

Scheme 6.2: Fabrication of Superamphiphobic Coating: Process flow chart (this schematic is not drawn to scale).

The coated glass substrates were then subjected to vapor deposition of TS (triethoxysilane) catalyzed by ammonia solution (Scheme 6.1). During this process, an ultrathin layer of porous silica membrane was formed over the substrate due to the hydrolysis and condensation of TS (Stöber reaction) [223,224]. The thickness of the deposited silica membrane was reported to be 25 nm [156,225]. In our case, the silica membrane gets deposited over the SiO_2 nanofibers.

The samples were then heat treated at 600 ºC for 2 h, during which the polymer from the nanofibers diffuses through the porous silica membrane and evaporates, resulting in the formation of a superhydrophilic hybrid silica network. (Figure 6.1 (b) and (d)) show the low and high magnification SEM images of the hybrid silica network consisting of SiO_2 nanofibers covered by an ultrathin layer of porous silica membrane. The SiO_2 nanofibers acted as a template over which the silica membrane was formed and the fiber morphology assisted the layer to keep its roughness and surface texture. The silica membrane reinforced the SiO_2 nanofibers and prevented the fibers from disintegrating into nano particles during the heat treatment process. (Figure 6.1 (e) and (f)) show the EDS spectra of the SiO_2 nanofibers before and after heat treatment process. The carbon peak in (Figure 6.1 (e)) indicated the presence of polymer in the SiO_2 nanofiber matrix. After heat treatment, the sample consisted of only hybrid silica network (SiO_2 nanofibers/silica membrane) without any organics (Figure 6.1 (f)).

The TGA measurement further confirmed that the sample was free from polymer (Figure 6.2) and the XRD measurement (Figure 6.3) confirmed that the coating contained amorphous SiO_2.

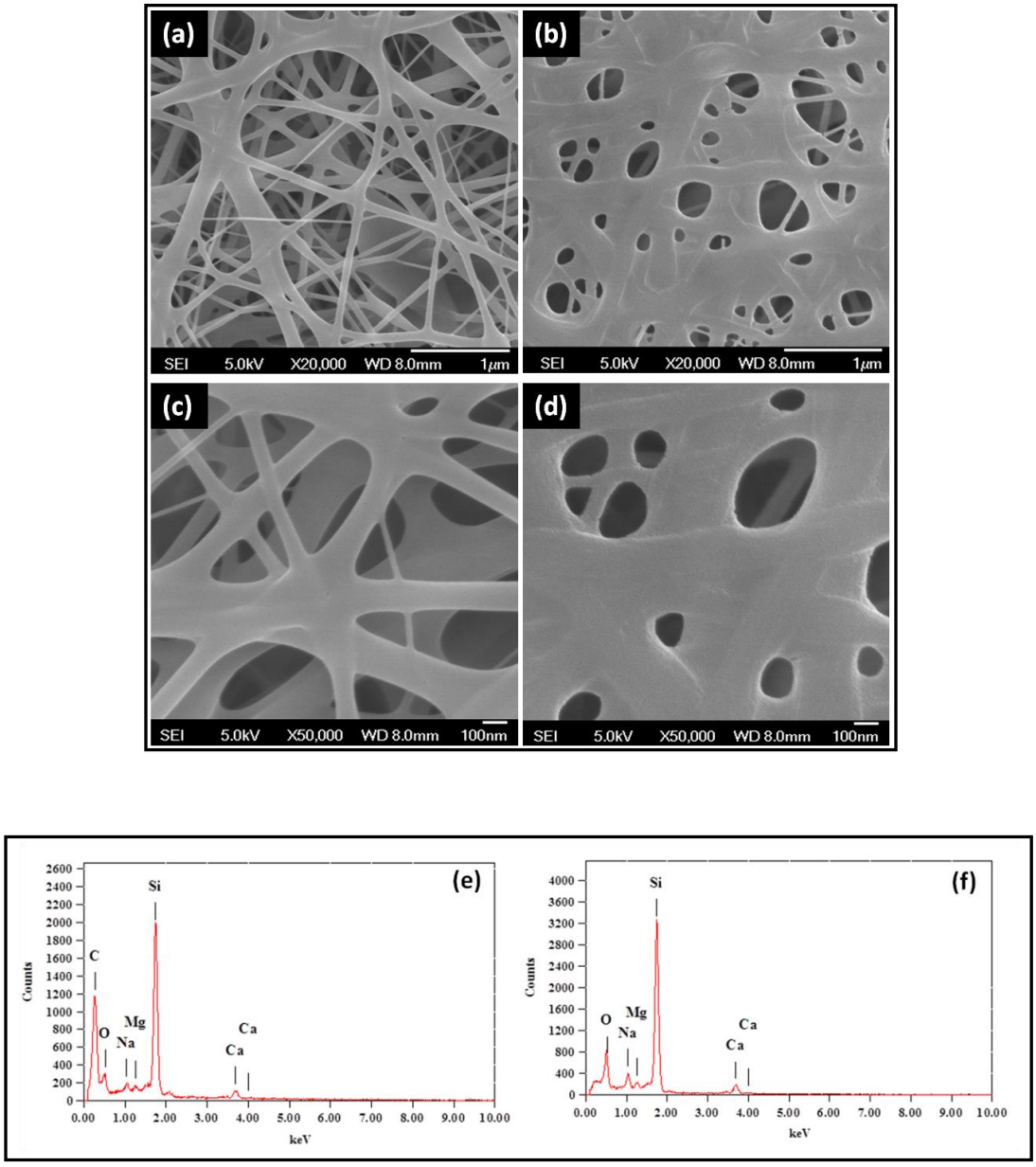

Figure 6.1: (a) and (c) SEM images (low and high magnification) of as-spun SiO_2 nanofibers; (b) and (d) SEM images (low and high magnification) of hybrid silica network (SiO_2 nanofibers/silica membrane); (e) EDS spectrum of as-spun SiO_2 nanofibers before heat treatment; (f) EDS spectrum of the coated sample (with hybrid silica network) after heat treatment (600 ºC).

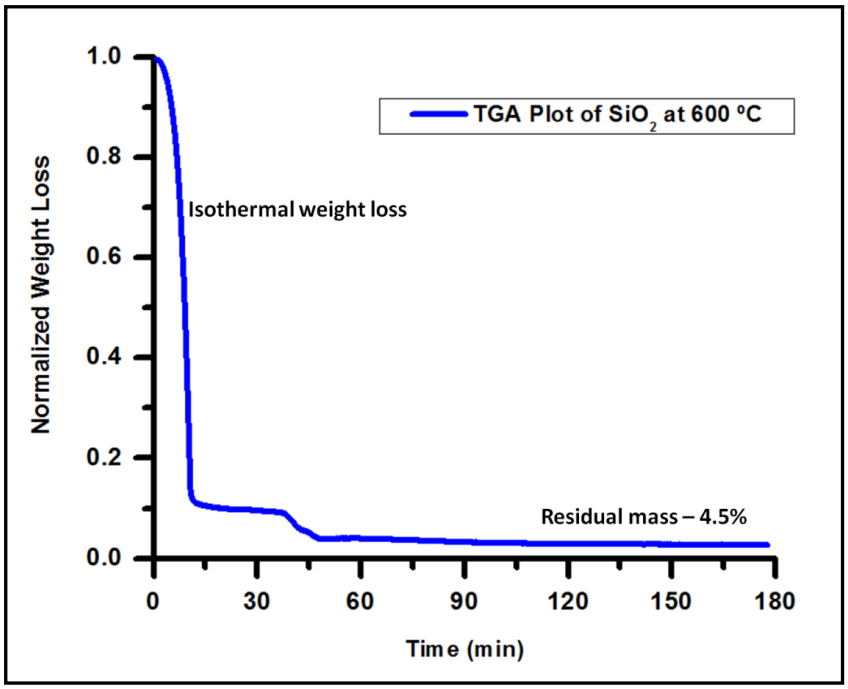

Figure 6.2: TGA analysis of SiO_2 sol-gel solution showing the mass losses during isothermal heating at 600 °C.

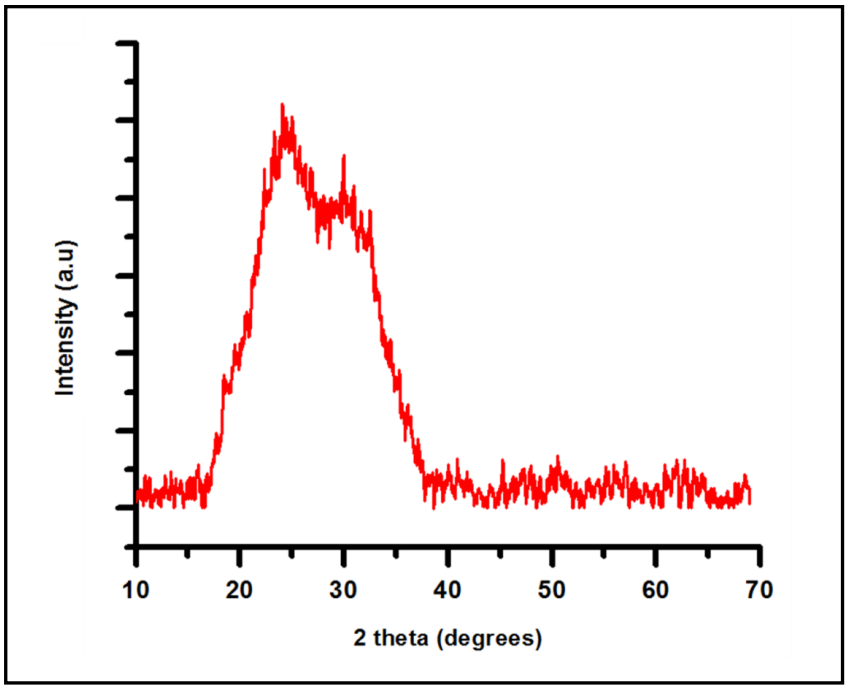

Figure 6.3: XRD pattern of the superamphiphobic coated sample.

In order to reduce the surface energy of the hybrid silica network, the samples were coated with fluorinated silane for 2 h using vapor deposition process (Figure 6.4). After silane treatment, the coating exhibited superamphiphobic property with a contact angle as high as 161º was achieved for 1µL water droplet (Figure 6.5). Due to the extremely low adhesion and surface energy, it was very difficult to deposit water droplet on the coating. The water droplet immediately started rolling off when it comes in contact with the coating. The surface contact angle, roll-off angle and the advancing (θ_a)/receding angle (θ_r) were measured for several organic liquids with different surface tension by employing a tilting base surface contact angle measurement set-up and the contact angle hysteresis (CAH) was calculated by taking the difference of advancing and receding angles (Table 6.1, Figure 6.6). The roll-off angle and CAH achieved for hexadecane ($\gamma = 27.5\ \mathrm{mN/m}$) were 9º and 6º respectively.

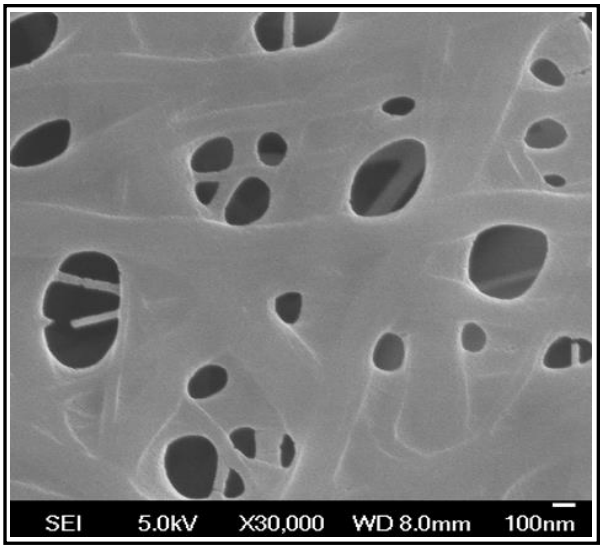

Figure 6.4: SEM image of the hybrid silica network after fluorinated silane treatment. (It is observed that the morphology of the hybrid silica network remains the same.)

Table 6.1: Static contact angle and roll-off angle measurements of liquids with different surface tension on a superamphiphobic glass substrate.

S. No	Liquid	Surface Tension (mN/m)	Surface Contact Angle (degrees)	Advancing (θ_a) / Receding (θ_r) contact angles	Contact Angle Hysteresis (CAH) ($\theta_a - \theta_r$)	Roll-off angle (degrees)
1	Water	72.1	161 ± 0.8	163/161	2	1 ± 1
2	Glycerol	64	158.3 ± 1	160/157	3	2 ± 1
3	Di-iodomethane	50.9	154.6 ± 0.9	156/152	4	4 ± 1
3	Ethylene glycol	47.3	152.4 ± 1.1	153/148	5	7 ± 1
4	Hexadecane	27.5	146.5 ± 0.7	149/143	6	9 ± 1

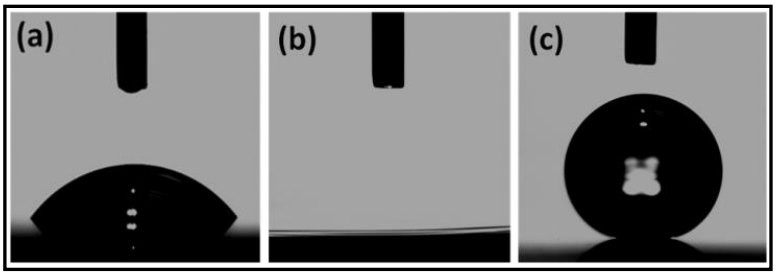

Figure 6.5: Interaction of water droplet with (a) plain glass (WCA: 51.6º), (b) superhydrophilic hybrid silica network surface (WCA: 0º) and (c) superamphiphobic surface (after silanization) (WCA: 161º).

Figure 6.6: Photograph of water (blue - dyed with trypan blue dye), hexadecane (red - dyed with alizarin red dye) and ethylene glycol (colourless) droplets on the superamphiphobic surface.

We have investigated the behavior of SiO_2 nanofibers without the deposition of silica membrane. After heat treatment process, the fibers broke into unevenly distributed SiO_2 nanoparticles (Figure 6.7). We have also studied the water contact angle achieved using the sample with SiO_2 nanoparticles after fluorinated silane treatment. The contact angle achieved was around 132.8º (Figure 6.8).

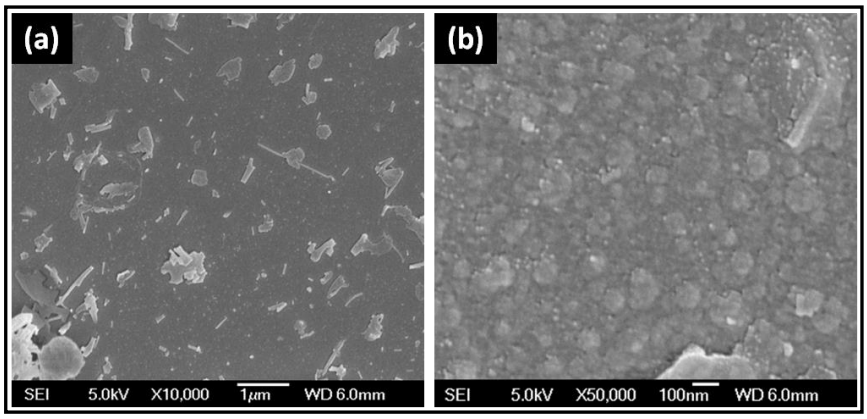

Figure 6.7: (a) and (b) SEM images (low and high magnification) of the SiO_2 coated sample without the silica membrane. SiO_2 nanofibers get disintegrated into nanoparticles after heat treatment (600 ºC for 2 hr).

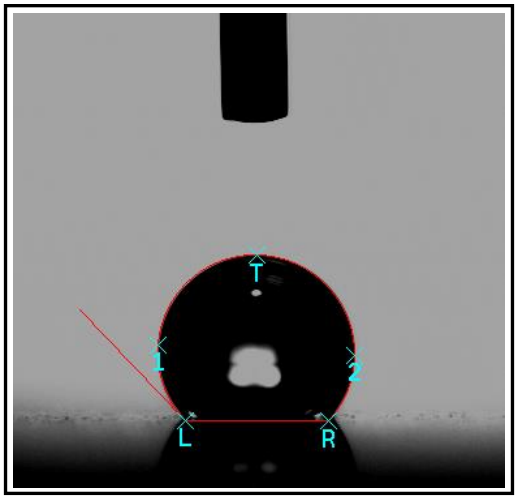

Figure 6.8: Water contact angle achieved on the SiO_2 coated sample without hybrid silica network (132.8º).

4.2. Self-cleaning property

To study the self-cleaning phenomenon, a mixture of ashes and sand particles were deposited on the coated sample. Water droplets were made to roll on the coated surface which resulted in the removal of all the surface pollutants. The water droplets took away all the surface contaminants encountered on its way (Figure 6.9).

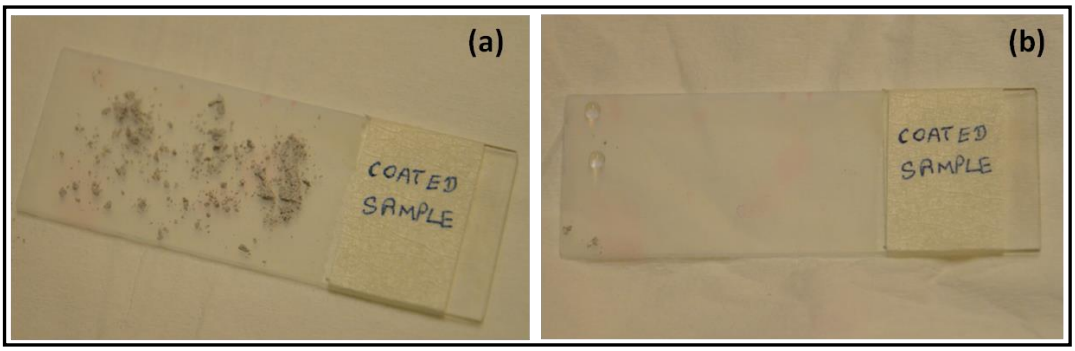

Figure 6.9: (a) Photograph of superamphiphobic coating polluted with surface contaminants (mixture of ashes and sand particles) and (b) Photograph showing the self-cleaning property of the superamphiphobic coating (water droplets rolls-off and cleans the surface).

4.3. Hardness measurement and optical property (Transmittance)

To study the hardness and modulus of the superamphiphobic coating, measurements were carried out at 5 different places on the coated samples using a nanoindenter equipped with a Berkovich tip. The results showed that the coating was relatively hard with average hardness of about 1.6 ± 0.23 GPa and Young's modulus around 24.7 ± 1.18 GPa.

The UV-Vis spectrum (in transmittance mode) of the superamphiphobic coated sample was studied (Figure 6.10). Results indicated that the transmittance of the superamphiphobic glass was less than that of the plain glass. However, the coating was hard and transparent enough to make it suitable for windows and other applications.

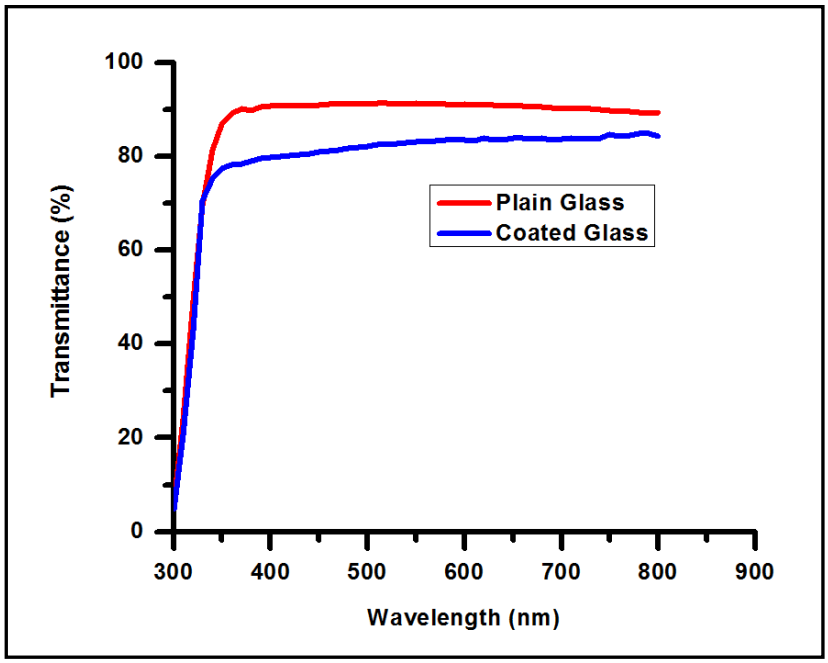

Figure 6.10: Comparison of transmittance of plain and superamphiphobic coated glass samples.

4.4. Peel-off and durability test

A 90º peel-off test was conducted on the superamphiphobic coated sample using an adhesion tape (3M scotch tape). The tape was peeled-off from the coated surface (Test distance: 50 mm) by applying a fixed force of 5 ± 0.1 N. After the peel-off test, it was observed that the coating remained stable without forming any

cracks/scratches on the surface. The samples before and after peel-off test were imaged under SEM to check whether there was any change in the morphology of the nanostructures. Images in Figure 6.11 confirm that there were no changes even in micrometer scale regimes.

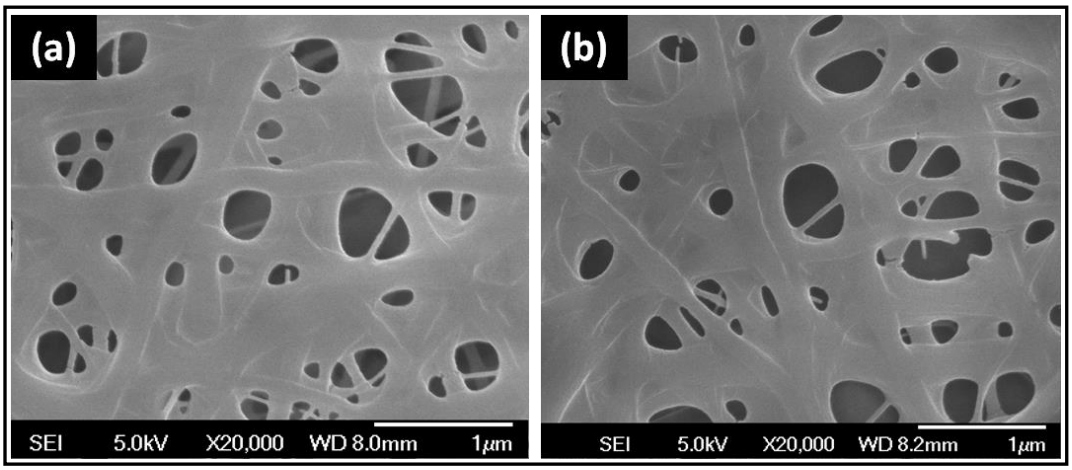

Figure 6.11: SEM images of (a) before peel-off test; (b) after peel-off test. The SEM images further confirm that the coating remained stable without forming any cracks/scratches on the surface.

The coated samples were placed in an environment which was maintained at Standard Ambient Temperature and Pressure condition (Temperature: 25 ± 2 ^{o}C; Pressure: 0.986 atm., humidity: 40-60%) [214]. SCA measurements for water, ethylene glycol and hexadecane were carried out on bi-weekly basis (Table 6.2). The results indicated that the coating is environmentally very stable and retained the superamphiphobic property.

Table 6.2: SCA measurements of the superamphiphobic coated samples when kept in SATP (Standard Ambient Temperature and Pressure) conditions.

S. No	Time duration (in weeks)	Surface Contact Angle made by water droplet (SCA) (degrees)	Surface Contact Angle made by ethylene glycol droplet (SCA) (degrees)	Surface Contact Angle made by hexadecane droplet (SCA) (degrees)
1	After 2 week	161	152.4	146.5
2	After 4 weeks	161.2	152	146.2
3	After 6 weeks	160.6	152.1	146
4	After 8 weeks	160.9	152.3	146.4

5. Conclusion

In summary, we have demonstrated the procedure to fabricate robust, transparent superamphiphobic coatings on glass substrate by using the unique nanofiber morphology as a template. The electrospun SiO_2 nanofibers acted as a template over which a thin layer of porous silica membrane was deposited by chemical vapor deposition technique. After heat treatment, the fabricated coating exhibited a hybrid silica network consisting of SiO_2 nanofibers enclosed by a layer of porous silica membrane. The synthesized superamphiphobic coatings were characterized using SEM, EDS, XRD and TGA. From the results, it is observed that the deposited silica membrane protected the SiO_2 nanofibers and prevented the fibers from disintegrating into nanoparticles during heat treatment

process. The fiber morphology assisted the hybrid silica network to keep its roughness and surface texture.

The hardness, transmittance and superamphiphobic properties were also studied. The transmittance of the coating was measured to be 85% and the surface contact angle achieved using water (γ = 72.1 mN/m) and hexadecane (γ = 27.5 mN/m) were 161º and 146.5º. The hardness and modulus of the coating were measured to be 1.6 GPa and 24.7 GPa respectively. We believe that this coating can effectively act as a self-cleaning coating when applied to windows and other applications.

Note: The research work presented in Chapter 6 has been published in RSC Advances (V. A. Ganesh, S. S. Dinachali, H. K. Raut, T. M. Walsh, A. S. Nair and S. Ramakrishna, *RSC Adv.*, 2013, 3, 3819-3824) and reproduced with permission of The Royal Society of Chemistry.

(Link: http://pubs.rsc.org/en/content/articlelanding/2013/ra/c3ra22968h)

Chapter 7

Conclusion and Future work

7. Conclusion and Future work

1. Conclusion

In conclusion, this research work within its scope has successfully demonstrated electrospinning/electrospraying approaches that can be employed to fabricate liquid repellent self-cleaning surfaces (Hydrophobic/Superhydrophobic, Amphiphobic/Superamphiphobic coatings) on glass substrate with high robustness and optical transparency. Furthermore, the thesis also analyzed and reported the surface morphology and surface modifications that can be performed to enhance the self-cleaning performance parameters with good optical and mechanical properties.

A complete comparison on various attributes of self-cleaning coatings such as liquid repellency, optical and mechanical properties of different surfaces fabricated and reported in this thesis are given below (Table 7.1).

Table 7.1: Comparison on the properties of different self-cleaning liquid repellent coatings fabricated and reported in this research work.

Self-cleaning attributes	**Liquid repellent Self-cleaning coatings**			
	POSS based coating (Chapter 3)	**PFPE based coating (Chapter 4)**	**TiO_2 based coating (Chapter 5)**	**SiO_2 based coating (Chapter 6)**
Liquid Repellency	Superhydrophobic (repels only water) (WCA > 150º)	Amphiphobic (repels both water and organics) (SCA < 120º)	Superamphiphobic (repels both water and organics) (SCA > 150º)	Superamphiphobic (repels both water and organics) (SCA > 150º)
Optical Property (Transmittance) %	88%	91%	74%	85%
Mechanical Property - 1 (Peel-off test) (N)	1 ± 0.1 N	2.5 ± 0.1 N	5 ± 0.1 N	5 ± 0.1 N
Mechanical Property - 2 (Nano-indentation test) (GPa)	NA	NA	Hardness: 0.12 GPa; Modulus: 3.26 GPa.	Hardness: 1.6 GPa; Modulus: 24.7 GPa.
Durability Test (SATP Test)	Passed	Passed	Passed	Passed

From the table, it can be observed that SiO_2 based coating exhibits excellent liquid repellency (SCA for water (γ = 72.1 mN/m) - 161º; SCA for hexadecane (γ = 27.5 mN/m) - 146.5º) with good optical (Transmittance: 85%) and mechanical properties (Hardness: 1.6 GPa; Modulus: 24.7 GPa) when compared to the other coatings fabricated by electrsopsinning/electrospraying process. Hence, it can be concluded that SiO_2 based liquid repellent self-cleaning coating will be more suitable for optical and architectural industrial sectors. However, for non-metallic substrates like plastics and polymers which cannot withstand high temperature sintering process, PFPE (Perfluoropolyether) based coatings will be suitable to achieve self-cleaning phenomenon.

Thus, Self-cleaning coatings with exceptional liquid repellent properties have been successfully fabricated by Electrospinning/Electrospraying process. The fabricated coatings exhibited good mechanical and optical properties making them suitable for industrial and commercial applications.

The results reported in the thesis have also been compared with the literature reported values and it was observed that thesis results falls well in the range of other significant works reported in the literature (Table 7.2). Hence, it can be concluded that electrospinning/electrospraying is a potential technique to fabricate robust, transparent and highly durable liquid repellent self-cleaning surfaces.

Table 7.2: Comparison of results reported in the thesis with the literature.

	Results reported in the thesis	**Literature reported values**
Chapter 3 Superhydrophobic coatings	WCA – 157.3° Transmittance (88 %)	WCA range (150° - 165°) Transmittance (70 to 92 %) [References: 175,227]
Chapter 4 Amphiphobic coatings	WCA – 116° Transmittance (91 %)	WCA range (110°- 123°) Transmittance (80 to 93 %) [References: 159,160]
Chapter 5 Superamphiphobic coatings (TiO_2)	WCA – 166.3° SCA (hexadecane) – 138.5 ° Transmittance (74 %)	WCA range (150°- 165°) SCA range (hexadecane) (130° - 156°) Transmittance (70 to 90 %) [References: 156,226]
Chapter 6 Superamphiphobic coatings (SiO_2)	WCA – 161.3° SCA (hexadecane) – 146.5 ° Transmittance (85 %)	

2. Future work

2.1. Research

- In this research work, Superamphiphobic coatings with transmittance of around 85% have been fabricated successfully. This work can be further extended in future to develop superamphiphobic surfaces with transmittance over 90% by using much lower refractive index materials like MgF_2 (Refractive Index: 1.37).
- As discussed before, for non-metallic substrates, metal oxide based coatings may not be suitable as these coatings have to be heat treated to over 400 ºC. In such cases, PFPE based coatings will be highly suitable. However, in this research, the surface contact angle achieved using PFPE is < 120º. In future, this work can be further extended to develop superamphiphobic coating (SCA > 150º) using PFPE by introducing roughness in micro/nano scale regimes.
- Furthermore, liquid repellent self-cleaning surfaces coupled with Anti-reflective properties can also be fabricated by introducing sub-wavelength structures using low surface energy materials.
- Humidity plays a vital role in electrospinning process. As the humidity increases, water may condense on the fibers affecting the fiber morphology and also increases the pores. Reduced humidity will result in the formation of less porous nanofibers. In this research, the humidity is maintained between 50 and 60%. In future, works can be conducted to

study the wettability of nanofibers fabricated at low humidity (< 15 %). Furthermore, potential areas including wettability studies of core-shell nanofibers, core-sheath nanofibers and hollow fibers can also be explored.

- In addition to self-cleaning, future works can also focus on studies like Anti-icing/Anti-fogging and Corrosion resistant coatings which may have potential impact in the growing automobile, architectural, marine, photovoltaic, optical industrial sectors and household applications.

2.2. Scalability

- Future research works can also focus on developing electrospinning/electrospraying set-ups capable of coating larger substrates by employing multiple nozzle jets. In this way, the scalability of the process along with parameters like coating speed and time can be improved significantly and larger substrates can be coated effectively in less time.

Bibliography

1. P. Kim, M. J. Kreder, J. Alvarenga and J. Aizenberg, *Nano Lett.*, **2013**, 13, 1793-1799.
2. The global market for anti-fingerprint, anti-bacterial, anti-fouling, easy-to-clean and self-healing nanocoatings, in: Future Markets Technology Report, Future Markets, Inc., Rockville, MD USA, **2012**.
3. X. Chen and S. S. Mao, *Chem. Rev*., **2007**, 107, 2891-2959.
4. A. Fujishima, X. Zhang and D. Tryk, *Surf. Sci. Rep*., **2008**, 63, 515-582.
5. U. Beck, D. T. Smith, G. Reiners and S .J. Dapkunas, *Thin Solid Films*, **1998**, 332, 164-171.
6. T. Tolke, A. Heft and A. Pfuch, *Thin Solid Films*, **2008**, 516, 4578-4580.
7. C. Battaglin, F. Caccavale, A. Menelle, M. Montecchi, E. Nichelatti, F. Nicoletti and P. Polato, *Thin Solid Films*, **1999**, 351, 176-179.
8. S. H. Jeong, J. K. Kim, B. S. Kim, S. H. Shim and B. T. Lee, *Vacuum*, **2004**, 76, 507-515.
9. S. Beibwenger, G. Brauer, W. Dicken and J. Szczyrbowski, *Surf. Coat. Technol*., **1993**, 60, 624-628.
10. Q. Xu, D. V. Wellia, M. A. Sk, K. H. Lim, J. S. Loo, D. W. Liao, R Amal and T. T. Tan *J. Photochem. Photobiol. A*, **2010**, 210, 181-187.
11. C. Euvananont, C. Junin, K. Inpor, P. Limthongkul and C. Thanachayanont, *Ceram. Int.*, **2008**, 34, 1067-1071.
12. O. Kesmez, H. Erdem C¸ amurlu, E. Burunkaya and E. Arpac¸ *Sol. Energy Mater. Sol. Cells*, **2009**, 93, 1833-1839.

13. K. L. Choy, *Prog. Mater. Sci*., **2003**, 48, 57-170.

14. W. E Teo and S. Ramakrishna, *Nanotechnology*, **2006**, 17, R89.

15. D. Byun, J. Hong, Saputra, J. H. Ko, Y. J. Lee, H. C. Park, B. Byun and J. R. Lukes, *J. Bionic Eng.*, **2009**, 6, 63-70.

16. (a) X. Li, D. Reinhoudt and M. Crego-Calama, *Chem. Soc. Rev.*, **2007**, 36, 1350-1368; (b) A. Marmur, *Ann. Rev. Mater. Res.*, **2009**, 39, 473-489;
(c) K.J. Stout, P.J. Sullivan, W.P. Dong, E. Mainsah, N. Luo, T. Mathia and H. Zahouani, "The development of methods for the characterization of roughness in three dimensions", **1993**; (d) [ISO25178] Geometrical product specifications (GPS) – Surface texture: Areal-Part 2: Terms, definitions and surface texture parameters.

17. R. N. Wenzel, *Ind. Eng. Chem.*, **1936**, 28, 988-994;

18. A. B. D. Cassie, S. Baxter, *Trans. Faraday Soc.*, **1944**, 40, 546-551.

19. C. Dorrer and J. Ruhe, *Soft Matter*, **2009**, 5, 51-61.

20. A. Solga, Z. Cerman, B. F. Striffler, M. Spaeth and W. Barthlott, *Bioinspir. Biomimetics*, **2007**, 2, S126-134.

21. A. R. Parker and C. R. Lawrence, *Nature*, **2001**, 414, 33-34.

22. S. Herminghaus, *Europhys. Lett*., **2000**, 52, 165-170.

23. P. Ball, *Nature*, **1999**, 400, 507-509.

24. Z. Guo and W. Liu, *Plant Sci.*, **2007**, 172, 1103-1112.

25. A. Otten and S. Herminghaus, *Langmuir*, **2004**, 20, 2405-2408.

26. M. T. Khorasani, H. Mirzadeh and Z. Kermani, *Appl. Surf. Sci.*, **2005**, 242, 339-345.

27. M. Jin, X. Feng, J. Xi, J. Zhai, K. Cho, L. Feng and L. Jiang, *Macromol. Rapid Commun.,* **2005**, 26, 1805-1809.

28. J. Zhang, J. Li and Y. Han, *Macromol. Rapid Commun.*, **2004**, 25, 1105-1108.

29. M. Morra, E. Occhiello and F. Garbassi, *Langmuir*, **1989**, 5, 872-876.

30. X. Lu, C. Zhang and Y. Han, *Macromol. Rapid Commun.*, **2004**, 25, 1606-1610.

31. L. Jiang, Y. Zhao and J. Zhai, *Angew. Chem., Int. Ed.*, **2004**, 43, 4338-4341.

32. R. Mohammadi, J. Wassink and A. Amirfazli, *Langmuir*, **2004**, 20, 9657-9662.

33. N. Zhao, J. Xu, Q. Xie, L. Weng, X. Guo, X. Zhang and L. Shi, *Macromol. Rapid Commun.*, **2005**, 26, 1075-1080.

34. J. Zhang, X. Lu, W. Huang and Y. Han, *Macromol. Rapid Commun.*, **2005**, 26, 477-480.

35. X. Feng, L. Feng, M. Jin, J. Zhai, L. Jiang and D. Zhu, *J. Am. Chem. Soc.*, **2003**, 126, 62-63.

36. Z. G. Guo, W. M. Liu and B. L. Su, *Appl. Phys. Lett.*, **2008**, 92, 63104.

37. T. C. Lee, W. J. Wang and T. Y. Han, *J. Adhes. Sci. Technol.*, **2009**, 23, 1799-1810.

38. H. Liu, S. Szunerits, M. Pisarek, W. Xu and R. Boukherroub, *ACS Appl. Mater. Interfaces*, **2009**, 1, 2086-2091.

39. S. Wang, L. Feng and L. Jiang, *Adv. Mater.*, **2006**, 18, 767-770.

40. M. Qu, B. Zhang, S. Song, L. Chen, J. Zhang and X. Cao, *Adv. Funct. Mater.*, **2007**, 17, 593-596.

41. M. Li, J. Xu and Q. Lu, *J. Mater. Chem.*, **2007**, 17, 4772-4776.

42. Z. Guo, J. Fang, L. Wang and W. Liu, *Thin Solid Films*, **2007**, 515, 7190-7194.

43. Q. M. Pan, H. Z. Jin and H. B. Wang, *Nanotechnology*, **2007**, 18, 355605.

44. J. Liang, Z. G. Guo, J. Fang and J. C. Hao, *Chem. Lett.*, **2007**, 36, 416-417.

45. Y. Zhu, J. Li, M. Wan and L. Jiang, *Macromol. Rapid Comm.*, **2008**, 29, 239-243.

46. P. Jiang, J. J. Zhou, H. F. Fang, C. Y. Wang, Z. L. Wang and S. S. Xie, *Adv. Funct. Mater.*, **2007**, 17, 1303-1310.

47. H. Li, Z. Bian, J. Zhu, D. Zhang, G. Li, Y. Huo, H. Li and Y. Lu, *J. Am. Chem. Soc.*, **2007**, 129, 8406-8407.

48. S. Srinivasan, V. K. Praveen, R. Philip and A. Ajayaghosh, *Angew. Chem., Int. Ed.*, **2008**, 47, 5750-5754.

49. D. Wang, Z. Guo, Y. Chen, J. Hao and W. Liu, *Inorg. Chem.*, **2007**, 46, 7707-7709.

50. L. Zou, X. Xiang, J. Fan and F. Li, *Chem. Mater.*, **2007**, 19, 6518-6527.

51. Z. G. Guo and W. M. Liu, *Appl. Phys. Lett.*, **2007**, 90, 193108.

52. X. Feng, L. Feng, M. Jin, J. Zhai, L. Jiang and D. Zhu, *J. Am. Chem. Soc.*, **2003**, 126, 62-63.

53. M. Guo, P. Diao and S. Cai, *Thin Solid Films*, **2007**, 515, 7162-7166.

54. X. Hou, F. Zhou, B. Yu and W. Liu**,** *Mater. Sci. Eng. A*, **2007**, 452-453, 732-736.

55. A. Safaee, D. K. Sarkar and M. Farzaneh, *Appl. Surf. Sci*., **2008**, 254, 2493-2498.

56. N. Vourdas, A. Tserepi, A. G. Boudouvis and E. Gogolides, *Microelectron. Eng*., **2008**, 85, 1124-1127.

57. H. Shin and M. Liu, *Chem. Mater*., **2004**, 16, 5460-5464.

58. X. Zhang, F. Shi, X. Yu, H. Liu, Y. Fu, Z. Wang, L. Jiang and X. Li, *J. Am. Chem. Soc.*, **2004**, 126, 3064-3065.

59. E. Hosono, S. Fujihara, I. Honma and H. Zhou, *J. Am. Chem. Soc.*, **2005**, 127, 13458-13459.

60. J. T. Han, Y. Jang, D. Y. Lee, J. H. Park, S. Song, D. Ban and K. Cho, *J. Mater. Chem.*, **2005**, 15, 3089-3092.

61. I. A. Larmour, S. E. J. Bell and G. C. Saunders, *Angew. Chem., Int. Ed.*, **2007**, 46, 1710-1712.

62. S. T. Wang, Y. L. Song and L. Jiang, *Nanotechnology*, **2007**, 18, 015103.

63. Y. Li, W. Jia, Y. Song and X. Xia, *Chem. Mater*., **2007**, 19, 5758-5764.

64. M. Ma, Y. Mao, M. Gupta, K. K. Gleason and G. C. Rutledge, *Macromolecules*, **2005**, 38, 9742-9748.

65. P. Favia, M. V. Stendardo and R. d'Agostino, *Polymer*, **1996**, 1, 91.

66. A. Satyaprasad, V. Jain and S. K. Nema, *Appl. Surf. Sci.*, **2007**, 253, 5462-5466.

67. A. Ruiz, A. Valsesia, G. Ceccone, D. Gilliland, P. Colpo and F. Rossi, *Langmuir*, **2007**, 23, 12984-12989.

68. N. Vourdas, A. Tserepi, and E. Gogolides, *Nanotechnology*, **2007**, 18, 125304.

69. R. P. Garrod, L. G. Harris, W. C. E. Schofield, J. McGettrick, L. J. Ward, D. O. H. Teare and J. P. S. Badyal, *Langmuir*, **2006**, 23, 689-693.

70. L. Cao, H. Hu and D. Gao, *Langmuir*, **2007**, 23, 4310-4314.

71. K. Teshima, H. Sugimura, Y. Inoue, O. Takai and A. Takano, *Appl. Surf. Sci.*, **2005**, 244, 619-622.

72. X. Yan, B. Tay, Y. Yang and W. Y. K. Po, *J. Phys. Chem. C*, **2007**, 111, 17254-17259.

73. L. Ci, R. Vajtai and P. M. Ajayan, *J. Phys. Chem. C*, **2007**, 111, 9077-9080.

74. S. Li, H. Xie, S. Zhang and X. Wang, *Chem. Commun.*, **2007**, 4857-4859.

75. W. Y. Gan, S. W. Lam, K. Chiang, R. Amal, H. Zhao and M. P. Brungs, *J. Mater. Chem.*, **2007**, 17, 952-954.

76. X. Zhang, H. Kono, Z. Liu, S. Nishimoto, D. A. Tryk, T. Murakami, H. Sakai, M. Abe and A. Fujishima, *Chem. Commun.*, **2007**, 4949-4951.

77. W. Hou and Q. Wang, *Langmuir*, **2007**, 23, 9695-9698.

78. X. Zhang, M. Jin, Z. Liu, D. A. Tryk, S. Nishimoto, T. Murakami and A. Fujishima, *J. Phys. Chem. C*, **2007**, 111, 14521-14529.

79. J. Wang, Y. Wen, J. Hu, Y. Song and L. Jiang, *Adv. Funct. Mater.*, **2007**, 17, 219-225.

80. Z. Huang, Y. Zhu, J. Zhang and G. Yin, *J. Phys. Chem. C*, **2007**, 111, 6821-6825.

81. Y. Li, W. Cai and G. Duan, *Chem. Mater.*, **2007**, 20, 615-624.

82. N. J. Shirtcliffe, G. McHale, M. I. Newton, C. C. Perry and P. Roach, *Chem. Commun.*, **2005**, 3135-3137.

83. M. Hikita, K. Tanaka, T. Nakamura, T. Kajiyama and A. Takahara, *Langmuir*, **2005**, 21, 7299-7302.

84. H. M. Shang, Y. Wang, S. J. Limmer, T. P. Chou, K. Takahashi and G. Z. Cao, *Thin Solid Films*, **2005**, 472, 37-43.

85. F. Wang, S. Song and J. Zhang, *Chem. Commun.*, **2009**, 4239-4241.

86. E. Burkarter, C. K. Saul, F. Thomazi, N. C. Cruz, L. S. Roman and W. H. Schreiner, *Surf. Coat. Techno*l., **2007**, 202, 194-198.

87. Z. Guo, J. Liang, J. Fang, B. Guo and W. Liu, *Adv. Eng.Mater.*, **2007**, 9, 316-321.

88. R. Menini and M. Farzaneh, *Surf. Coat. Techno*l., **2009**, 203, 1941-1946.

89. D. K. Sarkar and M. Farzaneh *J. Adhes. Sci. Technol.*, **2009**, 23, 1215-1237.

90. S. A. Kulinich and M. Farzaneh, *Appl. Surf. Sci.*, **2004**, 230, 232-240.

91. S. A. Kulinich and M. Farzaneh, *Langmuir*, **2009**, 25, 8854-8856.

92. S. A. Kulinich and M. Farzaneh, *Appl. Surf. Sci.*, **2009**, 255, 8153-8157.

93. B. Na and R. L. Webb, *Int. J. Heat Mass Transfer*, **2003**, 46, 3797-3808.

94. L. Cao, A. K. Jones, V. K. Sikka, J. Wu and D. Gao, *Langmuir*, **2009**, 25, 12444-12448.

95. P. Brunet, F. Lapierre, V. Thomy, Y. Coffinier and R. Boukherroub, *Langmuir*, **2008**, 24, 11203-11208.

96. F. Lapierre, V. Thomy, Y. Coffinier, R. Blossey and R. Boukherroub, *Langmuir*, **2009**, 25, 6551-6558.

97. B. Kakade, R. Mehta, A. Durge, S. Kulkarni and V. Pillai, *Nano Lett.*, **2008**, 8, 2693-2696.

98. Z. Han, B. Tay, C. Tan, M. Shakerzadeh and K. Ostrikov, *ACS Nano*, **2009**, 3, 3031-3036.

99. J. L. Campbell, M. Breedon, K. Latham and K. Kalantar-zadeh, *Langmuir*, **2008**, 24, 5091-5098.

100. T. N. Krupenkin, J. A. Taylor, T. M. Schneider and S. Yang, *Langmuir*, **2004**, 20, 3824-3827.

101. D. L. Herbertson, C. R. Evans, N. J. Shirtcliffe, G. McHale and M. I. Newton, *Sens. Actuators, A*, **2006**, 130-131, 189-193.

102. M. S. Dhindsa, N. R. Smith, J. Heikenfeld, P. D. Rack, J. D. Fowlkes, M. J. Doktycz, A. V. Melechko and M. L. Simpson, *Langmuir*, **2006**, 22, 9030-9034.

103. N. Verplanck, E. Galopin, J.C. Camart, V. Thomy, Y. Coffinier and R. Boukherroub, *Nano Lett.*, **2007**, 7, 813-817.

104. T. N. Krupenkin, J. A. Taylor, E. N. Wang, P. Kolodner, M. Hodes and T. R. Salamon, *Langmuir*, **2007**, 23, 9128-9133.

105. J.C. Baret, M. M. J. Decré and F. Mugele, *Langmuir*, **2006**, 23, 5173-5179.

106. R. G. Picknett and R. Bexon, *J. Colloid Interface Sci.*, **1977**, 61, 336-350.

107. K. S. Birdi, D. T. Vu and A. Winter, *J. Phys. Chem.*, **1989**, 93, 3702-3703.

108. C. Poulard, G. Guéna, A. M. Cazabat, A. Boudaoud and M. Ben Amar, *Langmuir*, **2005**, 21, 8226-8233.

109. Y. Takata, S. Hidaka, J. M. Cao, T. Nakamura, H. Yamamoto, M. Masuda and T. Ito, *Energy*, **2005**, 30, 209-220.

110. G. McHale, S. Aqil, N. J. Shirtcliffe, M. I. Newton and H. Y. Erbil, *Langmuir*, **2005**, 21, 11053-11060.

111. X. Zhang, S. Tan, N. Zhao, X. Guo, X. Zhang, Y. Zhang and J. Xu, *ChemPhysChem*, **2006**, 7, 2067-2070.

112. M. L. McLauchlin, D. Yang, P. Aella, A. A. Garcia, S. T. Picraux and M. A. Hayes, *Langmuir*, **2007**, 23, 4871-4877.

113. S. Boduroglu, M. Cetinkaya, W. J. Dressick, A. Singh and M. C. Demirel, *Langmuir*, **2007**, 23, 11391-11395.

114. Z. G. Guo and W. M. Liu, *Appl. Phys. Lett.*, **2007**, 90, 223111.

115. L. T. Qu and L. M. Dai, *Adv. Mater.*, **2007**, 19, 3844-3849.

116. C. Duez, C. Ybert, C. Clanet and L. Bocquet, *Nat. Phys.*, **2007**, 3, 180-183.

117. D.G. Lee and H.Y. Kim, *Langmuir*, **2007**, 24, 142-145.

118. D. Quere and A. Ajdari, *Nat. Mater*., **2006**, 5, 429-430.

119. H. Linke, B. J. Aleman, L. D. Melling, M. J. Taomina, M. J. Francis, C. C. Dow-Hygelund, V. Narayanan, R. P. Taylor and A. Stout, *Phys. Rev. Lett*., **2006**, 96, 154502.

120. M. Elbahri, D. Paretkar, K. Hirmas, S. Jebril and R. Adelung, *Adv. Mater.*, **2007**, 19, 1262-1266.

121. A. Mills, A. Lepre, N. Elliott, S. Bhopal, I. P. Parkin and S. A. O'Neill, *J. Photochem. Photobiol., A*, **2003**, 160, 213-224; I. P. Parkin and R. G. Palgrave, *J. Mater. Chem.*, **2005**, 15, 1689-1695.

122. K. E. Karakitsou and X. E. Verykios, *J. Phys. Chem.*, **1993**, 97, 1184-1189.

123. S. E. Park, H. Joo and J. W. Kang, *Sol. Energy Mater. Sol. Cells*, **2004**, 83, 39-53.

124. V. Subramanian, E. E. Wolf and P. V. Kamat, *J. Am. Chem. Soc.*, **2004**, 126, 4943-4950.

125. H. Tada, A. Kokubu, M. Iwasaki and S. Ito, *Langmuir*, **2004**, 20, 4665-4670.

126. R. Harrop, *Surf. Technol.*, **1978**, 6, 385-393.

127. J. Yu, X. Zhao, Q. Zhao and G. Wang, *Mater. Chem. Phys.*, **2001**, 68, 253-259.

128. X. Zhang, O. Sato, M. Taguchi, Y. Einaga, T. Murakami and A. Fujishima, *Chem. Mater.*, **2005**, 17, 696-700.

129. X. Zhang, A. Fujishima, M. Jin, A. V. Emeline and T. Murakami, *J. Phys. Chem. B*, **2006**, 110, 25142-25148.

130. H. Yaghoubi, N. Taghavinia and E. K. Alamdari, *Surf. Coat. Technol.*, **2010**, 204, 1562-1568.

131. R. Prado, G. Beobide, A. Marcaide, J. Goikoetxea and A. Aranzabe, *Sol. Energy Mater. Sol. Cells*, **2010**, 94, 1081-1088.

132. Q. Xu, D. V. Wellia, M. A. Sk, K. H. Lim, J. S. C. Loo, D. W. Liao, R. Amal and T. T. Y. Tan, *J. Photochem. Photobiol.*, **2010**, 210, 181-187.

133. L. K. Verma, M. Sakhuja, J. Son, A. J. Danner, H. Yang, H. C. Zeng and C. S. Bhatia, *Renew Energ.*, **2011**, 36, 2489-2493.

134. S. Nishimoto, A. Kubo, X. Zhang, Z. Liu, N. Taneichi, T. Okui, T. Murakami, T. Komine and A. Fujishima, *Appl. Surf. Sci.*, **2008**, 254, 5891-5894.

135. K. Katsumata, C. E. J. Cordonier, T. Shichi and A. Fujishima, *Mater. Sci. Eng., B*, **2010**, 173, 267-270.

136. A. Fujishima and X. Zhang, *C. R. Chim.*, **2006**, 9, 750-760.

137. S. Nishimoto, A. Kubo, K. Nohara, X. Zhang, N. Taneichi, T. Okui, Z. Liu, K. Nakata, H. Sakai, T. Murakami, M. Abe, T. Komine and A. Fujishima, *Appl. Surf. Sci.*, **2009**, 255, 6221-6225.

138. K. Nakata, K. Udagawa, T. Ochiai, H. Sakai, T. Murakami, M. Abe and A. Fujishima, *Mater. Chem. Phys.*, **2011**, 126, 484-487.

139. A. Fujishima, T. N. Rao and D. A. Tryk, *J. Photochem. Photobiol. C*, **2000**, 1, 1-21.

140. Y. Li, T. Sasaki, Y. Shimizu and N. Koshizaki, *J. Am. Chem. Soc.*, **2008**, 130, 14755-14762.

141. Y. Li, T. Sasaki, Y. Shimizu and N. Koshizaki, *Small*, **2008**, 4, 2286-2291.

142. C. Pan, C. Sun, H. Wei, G. Han, J. Zhang, A. Fujishima and Z. Gu, *Mater. Res. Bull.*, **2007**, 42, 1395-1401.

143. Q. Xie, J. Xu, L. Feng, L. Jiang, W. Tang, X. Luo and C. C. Han, *Adv. Mater.*, **2004**, 16, 302-305.

144. X. Wang, X. Liu, F. Zhou and W. Liu, *Chem. Commun.*, **2011**, 47, 2324-2326.

145. Z. He, M. Ma, X. Lan, F. Chen, K. Wang, H. Deng, Q. Zhang and Q. Fu, *Soft Matter*, **2011**, 7, 6435-6443.

146. X. Wang, H. Hu, Q. Ye, T. Gao, F. Zhou and Q. Xue, *J. Mater. Chem.*, **2012**, 22, 9624-9631.

147. V. A. Ganesh, S. S. Dinachali, H. K. Raut, T. M. Walsh, A. S. Nair and S. Ramakrishna, *RSC Adv.*, **2013**, 3, 3819-3824.

148. D. Xiong, G. Liu, L. Hong and E. J. S. Duncan, *Chem. Mater.*, **2011**, 23, 4357-4366.

149. A. Tuteja, W. Choi, M. L. Ma, J. M. Mabry, S. Mazzella, G. C. Rutledge, G. H. McKinley, R. E. Cohen, *Science*, **2007**, 318, 1618-1622.

150. A. Tuteja, W. Choi, J. M. Mabry, G. H. McKinley, R. E. Cohen, *Proc. Natl. Acad. Sci. U.S.A.*, **2008**, 105, 18200-18205.

151. L. Cao, T. P. Price, M. Weiss and D. Gao, *Langmuir*, **2008**, 24, 1640-1643.

152. R. T. Rajendra Kumar, K. B. Mogensen and P. Bøggild, *J. Phys. Chem. C*, **2010**, 114, 2936-2940.

153. W. Wu, X. Wang, D. Wang, M. Chen, F. Zhou, W. Liu and Q. Xue, *Chem. Commun.*, **2009**, 1043-1045.

154. H. Butt, C. Semprebon, P. Papadopoulos, D. Vollmer, M. Brinkmann and M. Ciccotti, *Soft Matter*, **2013**, 9, 418-428.

155. A. Steele, I. Bayer and E. Loth, *Nano Lett.*, **2008**, 9, 501-505.

156. X. Deng, L. Mammen, H. Butt and D. Vollmer, *Science*, **2012**, 335, 67-70.

157. T. Wong, S. H. Kang, S. K. Y. Tang, E. J. Smythe, B. D. Hatton, A. Grinthal, J. Aizenberg, *Nature*, **2011**, 477, 443-447.

158. D. F. Cheng, C. Urata, M. Yagihashi, A. Hozumi, *Angew. Chem., Int. Ed.*, **2012**, 51, 2956-2959.

159. P. Kim, M. J. Kreder, J. Alvarenga, J. Aizenberg, *Nano Lett.*, **2013**, 13, 1793-1799.

160. W. Ma, Y. Higaki, H. Otsuka, A. Takahara, *Chem. Commun.*, **2013**, 49, 597-599.

161. S. Pan, A. K. Kota, J. M. Mabry and A. Tuteja, *J. Am. Chem. Soc.*, **2012**, 135, 578-581.

162. V. A. Ganesh, H. K. Raut, A. S. Nair and S. Ramakrishna, *J. Mater. Chem.*, **2011**, 21, 16304-16322.

163. Z. Guo, W. Liu and B. L. Su, *J. Colloid Interface Sci.*, **2011**, 353(2), 335-355.

164. A. Vilčnik, I. Jerman, A. Šurca Vuk, M. Koželj, B. Orel, B. Tomšič, B. Simončič and J. Kovač, *Langmuir*, **2009**, 25, 5869-5880.

165. S. S. Chhatre, A. Tuteja, W. Choi, A. l. Revaux, D. Smith, J. M. Mabry, G. H. McKinley and R. E. Cohen, *Langmuir*, **2009**, 25, 13625-13632.

166. W. Choi, A. Tuteja, S. Chhatre, J. M. Mabry, R. E. Cohen and G. H. McKinley, *Adv. Mater.*,**2009**, 21, 2190-2195.

167. L. Feng, Z. Zhang, Z. Mai, Y. Ma, B. Liu, L. Jiang and D. Zhu, *Angew. Chem., Int. Ed.*, **2004**, 43, 2012-2014.

168. J. Li, J. Fu, Y. Cong, Y. Wu, L. Xue and Y. Han, *Appl. Surf. Sci.*, **2006**, 252, 2229-2234.

169. H. Y. Kwong, M. H. Wong, Y. W. Wong and K. H. Wong, *Appl. Surf. Sci.*, **2007**, 253, 8841-8845.

170. K. Wang, N. X. Hu, G. Xu and Y. Qi, *Carbon*, **2011**, 49, 1769-1774.

171. X. Wang, B. Ding, J. Yu and M. Wang, *Nano Today*, **2011**, 6, 510-530.

172. J. Wu and P. Mather, *Polym. Rev.*, **2009**, 49, 25-63.

173. S. H. Phillips, T. S. Haddad and S. J. Tomczak, *Curr. Opin. Solid State Mater. Sci.*, **2004**, 8, 21-29.

174. J. M. Mabry, A. Vij, S. T. Iacono and B. D. Viers, *Angew. Chem.*, **2008**, 120, 4205-4208.

175. Y. Xue, H. Wang, D. Yu, L. Feng, L. Dai, X. Wang and T. Lin, *Chem. Commun.*, **2009**, 6418-6420.

176. J. R. Hottle, H. J. Kim, J. Deng, C. E. Farmer-Creely, B. D. Viers and A. R. Esker, *Macromolecules*, **2004**, 37, 4900-4908.

177. A. S. Nair, Y. Shengyuan, Z. Peining and S. Ramakrishna, *Chem. Commun.*, **2010**, 46, 7421-7423.

178. Y. Shengyuan, Z. Peining, A. S. Nair and S. Ramakrishna, *J. Mater. Chem.*, **2011**, 21, 6541-6548.

179. P. Zhu, A. S. Nair, Y. Yang, S. Peng and S. Ramakrishna, *J. Mater. Chem.*, **2011**, 21, 12210-12212.

180. I.-D. Kim, A. Rothschild, B. H. Lee, D. Y. Kim, S. M. Jo and H. L. Tuller, *Nano Lett.*, **2006**, 6, 2009-2013.

181. R. Ravichandran, S. Sundarrajan, J. R. Venugopal, S. Mukherjee and S. Ramakrishna, *Macromol. Biosci.*, **2012**, 12, 286-311.

182. J. Xu, X. Li, C. M. Cho, C. L. Toh, L. Shen, K. Y. Mya, X. Lu and C. He, *J. Mater. Chem.*, **2009**, 19, 4740-4745.

183. D. K. Owens and R. C. Wendt, *J. Appl. Polym. Sci.*, **1969**, 13, 1741-1747.

184. F. M. Fowkes, M. B. Kaczinski and D. W. Dwight, *Langmuir*, **1991**, 7, 2464-2470.

185. J. M. Deitzel, J. Kleinmeyer, D. Harris and N. C. Beck Tan, *Polymer*, **2001**, 42, 261-272.

186. P. K. Baumgarten, *J. Colloid Interface Sci.*, **1971**, 36, 71-79.

187. A. Singh, L. Steely and H. R. Allcock, *Langmuir*, **2005**, 21, 11604-11607.

188. S. V. Fridrikh, J. Yu, M. P. Brenner and G. C. Rutledge, *Phys. Rev. Lett.*, **2003**, 90, 144502.

189. R. Misra, B. X. Fu and S. E. Morgan, *J. Polym. Sci., Part B: Polym. Phys.*, **2007**, 45, 2441-2455.

190. P. Muthiah, S. H. Hsu and W. Sigmund, *Langmuir*, **2010**, 26, 12483-12487.

191. Y. Y. Yan, N. Gao and W. Barthlott, *Adv. Colloid Interface Sci.*, **2011**, 169, 80-105.

192. K. Rykaczewski, S. Anand, S. B. Subramanyam and K. K. Varanasi, *Langmuir*, **2013**, 29, 5230-5238.

193. L. Mishchenko, B. Hatton, V. Bahadur, J. A. Taylor, T. Krupenkin and J. Aizenberg, *ACS Nano*, **2010**, 4, 7699-7707.

194. A. J. Meuler, G. H. McKinley and R. E. Cohen, *ACS Nano*, **2010**, 4, 7048-7052.

195. W. Chen, A. Y. Fadeev, M. C. Hsieh, D. Öner, J. Youngblood and T. J. McCarthy, *Langmuir*, **1999**, 15, 3395-3399.

196. P. Roach, N. J. Shirtcliffe and M. I. Newton, *Soft Matter*, **2008**, 4, 224-240.

197. K. Honda, M. Morita, H. Masunaga, S. Sasaki, M. Takata and A. Takahara, *Soft Matter*, **2010**, 6, 870-875.

198. V. A. Ganesh, A. S. Nair, H. K. Raut, T. T. Yuan Tan, C. He, S. Ramakrishna and J. Xu, *J. Mater. Chem.*, **2012**, 22, 18479-18485.

199. J. M. Xi, L. Feng, and L. Jiang, *Appl. Phys. Lett.*, **2008**, 92, 053102.

200. C. Hsieh, J. Chen, R. Kuo, T. Lin, C. Wu, *Appl. Surf. Sci.*, **2005**, 240, 318-326.

201. Z. Xue, M. Liu, and L. Jiang, *J. Polym. Sci., Part B: Polym. Phys.*, **2012**, 50, 1209-1224.

202. L. Cao, and D. Gao, *Faraday Discuss.*, **2010**, 146, 57-65.

203. J. Zhang, and S. Seeger, *Angew. Chem., Int. Ed.*, **2011**, 50, 6652-6656.

204. R. G. Karunakaran, C.-H Lu, Z. Zhang, and S. Yang, *Langmuir*, **2011**, 27, 4594-4602.

205. H. Yabu, and M. Shimomura, *Chem. Mater.*, **2005**, 17, 5231-5234.

206. M. M. Bergshoef, and G. J. Vancso, *Adv. Mater*., **1999**, 11, 1362-1365.

207. P. A. Levkin, F. Svec, and J. M. J. Fréchet, *Adv. Funct. Mater.*, **2009**, 19, 1993-1998.

208. J. W. Krumpfer, and T. J. McCarthy, *Faraday Discuss.*, **2010**, 146, 103-111.

209. N. Bock, M. A. Woodruff, D. W. Hutmacher, and T. R. Dargaville, *Polymers*, **2011**, 3, 131-149.

210. A. Jaworek and A. T. Sobczyk, *J. Electrostat.*, **2008**, 66, 197-219.

211. P. A. V. O'Rourke-Muisene, J. T. Koberstein and S. Kumar, *Macromolecules*, **2003**, 36, 771-781.

212. D. H. K. Pan and W. M. Prest, *J. Appl. Phys.*, **1985**, 58, 2861.

213. D. E. Suk, G. Chowdhury, T. Matsuura, R. M. Narbaitz, P. Santerre, G. Pleizier and Y. Deslandes, *Macromolecules*, **2002**, 35, 3017-3021.

214. *J. Phys. Chem.*, Ref. Data 1982, 11 (Supplement 2).

215. N. M. Bedford and A. J. Steckl, *ACS Appl. Mater. Interfaces*, **2010**, 2, 2448-2455.

216. Z. Z. Luo, Z. Z. Zhang, L. T. Hu, W. M. Liu, Z. G. Guo, H. J. Zhang and W. J. Wang, *Adv. Mater.*, **2008**, 20, 970-974.

217. A. S. Nair, R. Jose, Y. Shengyuan and S. Ramakrishna, *J. Colloid Interface Sci.*, **2011**, 353, 39-45.

218. Z. Peining, A. S. Nair, P. Shengjie, Y. Shengyuan and S. Ramakrishna, *ACS Appl. Mater. Interfaces*, **2012**, 4, 581-585.

219. S. S. Dinachali, M. S. M. Saifullah, R. Ganesan, E. S. Thian and C. He, *Adv. Funct. Mater.*, **2013**, 23, 2201-2211.

220. V. A. Ganesh, A. S. Nair, H. K. Raut, T. M. Walsh and S. Ramakrishna, *RSC Adv.*, **2012**, 2, 2067-2072.

221. V. A. Ganesh, S. S. Dinachali, A. S. Nair and S. Ramakrishna, *ACS Appl. Mater. Interfaces*, **2013**, 5, 1527-1532.

222. H. K. Raut, A. S. Nair, S. S. Dinachali, V. A. Ganesh, T. M. Walsh and S. Ramakrishna, *Sol Energ Mat Sol.*, **2013**, 111, 9-15.

223. W. Stober, A. Fink and E. Bohn, *J. Colloid Interface Sci.*, **1968**, 26, 62-69.

224. M. Chen, L. Wu, S. Zhou and B. You, *Adv. Mater.*, **2006**, 18, 801-806.

225. X. Deng, L. Mammen, Y. Zhao, P. Lellig, K. Mullen, C. Li, H.J. Butt and D. Vollmer, *Adv. Mater.*, **2011**, 23, 2962-2965.

226. S. G. Lee, D. S. Ham, D. Y. Lee, H. Bong and K. Cho, *Langmuir*, **2013**, 29, 15051-15057.

227. L. Xu and J. He, *Langmuir*, **2012**, 28, 7512-7518.